Communications Research Centre

EQUATIONS GOVERNING THE CRC SOFTWARE-BASED SYNTHETIC APERTURE RADAR SIGNAL PROCESSOR

by

M.R. Vant

This work was sponsored by the Department of National Defence, Research and Development Branch under Project No. 33C74

DEPARTMENT OF COMMUNICATIONS
MINISTÈRE DES COMMUNICATIONS

CRC REPORT NO. 1342

CANADA

OTTAWA, JUNE 1981

COMMUNICATIONS RESEARCH CENTRE

DEPARTMENT OF COMMUNICATIONS
CANADA

EQUATIONS GOVERNING THE CRC SOFTWARE-BASED SYNTHETIC APERTURE RADAR SIGNAL PROCESSOR

by

M.R. Vant

(Radar and Communications Technology Branch)

CRC REPORT NO. 1342

June 1981

OTTAWA

This work was sponsored by the Department of National Defence, Research and Development Branch under Project No. 33C74

TABLE OF CONTENTS

EQUATIONS GOVERNING THE CRC SOFTWARE-BASED SYNTHETIC APERTURE RADAR SIGNAL PROCESSOR

by

M.R. Vant

ABSTRACT

A novel software-based synthetic-aperture radar (SAR) processor is described. The processor is capable of routinely producing a variety of data products from data acquired by either the SEASAT-A satellite-borne SAR or the Environmental Research Institute of Michigan (ERIM) airborne, dual frequency/dual polarization, SAR. The SAR processor described is adaptable in that it can be configured to process imagery from any SAR system that maintains the range coding constant from pulse-to-pulse. A description of the equations that were used to implement the SAR processor is given as are details of the processor configuration. It is shown that the processor consists of two main subsystems: a very general SAR processing subsystem; and a radar data product-specific support subsystem. It is described how the processor can be reconfigured by changes to parameter files, and how the processor modules communicate with each other by means of a data file structure. The hardware upon which the processor was programmed is briefly described, and timings for the various production products; generated using this hardware, are given. Examples of the image data products are also included in the description. Finally, specific comments are made with respect to extending the capabilities of the processor.

1. INTRODUCTION

The purpose of this report is to present a description of the equations used to implement the CRC software-based, synthetic-aperture radar (SAR) digital processor and also to present a brief overview of the processor itself. The CRC processor is capable of producing imagery from any SAR system that maintains the range coding constant from pulse-to-pulse. It has been used to produce a full (7.4m) azimuth resolution product, as well as the normal 25m, 4-look product from the SEASAT-A L-band SAR. In addition, data have been processed from the Environmental Research Institute of Michigan (ERIM) X/L-band SAR.

The theory upon which the processor is based has been described elsewhere[1,2,3]. In this report the various processing steps and the equations used to implement these steps in software are described.

Airborne and satellite-borne synthetic-aperture radars are used to produce pseudo-photographic two-dimensional radar images of terrain and targets of civilian or military interest. The radar transmits radio pulses that are reflected by the targets of interest and then received back at the radar. In order to convert the received data into an image, it is generally required that a two-dimensional signal processing operation be performed. Conventionally, this operation is segmented into two, one-dimensional operations where the radar return signals along the slant-range (r_1) (measured along the antenna pointing direction) and azimuth (along-track), (s) coordinates (see Figure 1) are independently cross-correlated with their respective reference functions. Provided the range and azimuth signals are orthogonal, and provided the extents of these signals are small, this approach works well.

For certain types of SAR systems the antenna is not pointed perpendicular to track and therefore the range and azimuth signals are not orthogonal. In the SEASAT-A case the SAR antenna is pointed in a direction nominally perpendicular to the spacecraft's ground-track. However, the effect of spacecraft yaw combined with the yaw caused by earth rotation causes the antenna to be 'squinted' at an angle with respect to the perpendicular to track. The complement of the squint angle is angle α, the squint angle itself is therefore $(90-\alpha)°$ as shown in Figure 1. The squint angle, $(90-\alpha)°$ is typically only a few degrees for satellite systems such as SEASAT. For airborne systems the antenna is sometimes deliberately 'squinted' for tactical reasons. In such airborne systems the magnitude of the squint can approach 90°.

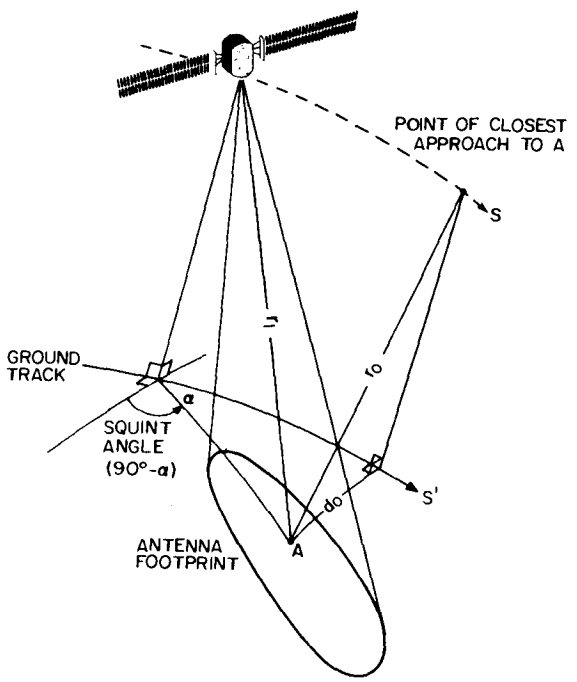

Figure 1. Radar-target geometry

If the SAR antenna is 'squinted' or if the azimuth time-bandwidth product is large the range and azimuth signals are coupled; i.e., they are not independent. The signal processing, required to produce a high quality distortion-free image, then becomes more complicated than the conventional, unsquinted low azimuth time-bandwidth product case.

The CRC software-based SAR processor produces an image by means of true two-dimensional matched filtering[4,5]. The matched filtering is implemented using two-dimensional fast-convolution[4,6]. The range variation of the parameters of the SAR signal causes a mismatch between the filter and the data at the edges of the processing block[1]. The range swath over which a single matched filter is applied is determined solely by the requirement that the image produced for this swath be in focus[1]. In most cases this requirement is lax enough that the fast convolution operation is efficient, i.e., the range swath can usually be made much wider than the width of the matched filter in range, but it is not so stringent as to prevent a geometric distortion of the image. This geometric distortion must be removed as a final step in the processing.

The software-based SAR processor has been implemented as two major subsystems: the SAR Processing subsystem and the support subsystem. The former subsystem is very general in nature; it can be used, with only minor changes, to process data from any SAR that maintains the range coding constant from pulse to pulse over the processing block length. The latter subsystem is more specific in application; it provides the necessary scheduling, parameter computation, look overlaying and sub-swath merging, for the automated running of the SAR Processing subsystem. At present the support subsystem can handle data from the ERIM X/L-band, and the SEASAT-A L-band SARs.

In the following sections the theoretical concepts embodied in the processor design are described briefly, then a detailed description of the equations that were used in designing the processor software is given. No attempt is made to derive the equations in this report, the reader is referred to Reference 1 for the derivation. A brief description of the equipment upon which the processor was programmed is also given, as are some representative times for processing image scenes on this equipment.

2. THEORY

In this section a simple model of the SAR is presented, the two-dimensional natures of the radar signal and the signal processing are discussed, and a conceptual description of the image formation process is given. It is described how the received radar signal can be considered to be two-dimensional in nature, and then it is pointed out that, with the signal described in this form, it is natural to think of forming the SAR image by means of a two-dimensional matched filtering operation[1]. The properties of the radar signal are briefly discussed and it is shown pictorially that the signal characteristics vary with range. The effect of using a range-invariant matched filter over a wide range swath is also shown by means of diagrams. It is important to be aware of the effect of using a single matched filter over a wide range swath because in many cases wide range swaths can be digitally processed more efficiently than narrow swaths.

2.1 THE TWO-DIMENSIONAL SAR SIGNAL

As the first step in the understanding of the properties of the SAR signal, it is useful to examine how the signal is acquired. The radar signal is gathered as the target passes through the azimuth antenna pattern of the radar. A general point on the earth's surface, such as A in Figure 2, is first illuminated by the antenna beam when the radar is located at S_1 in its orbit. The illumination continues until the spacecraft reaches S_2, at which time the target at A leaves the beam. The maximum length of the synthetic-aperture is the arc-length S_1S_2. The two-dimensional signal is formed by segmenting the signal received during the time the spacecraft is moving from S_1 to S_2 into sections, each section being of duration equal to the radar interpulse period. Then, a stack is formed out of the segments. The resulting stack forms the two-dimensional signal. The transit time t' (from radar to target and back) is a measure of target position within a segment (range position). The interpulse period number or segment number 'm', when multiplied by the ground velocity, is a measure of along-track or azimuth position. The maximum azimuth resolution that can be achieved with a given radar is proportional to the number of segments or the height of the stack, which is in turn proportional to the synthetic-aperture length S_1S_2.

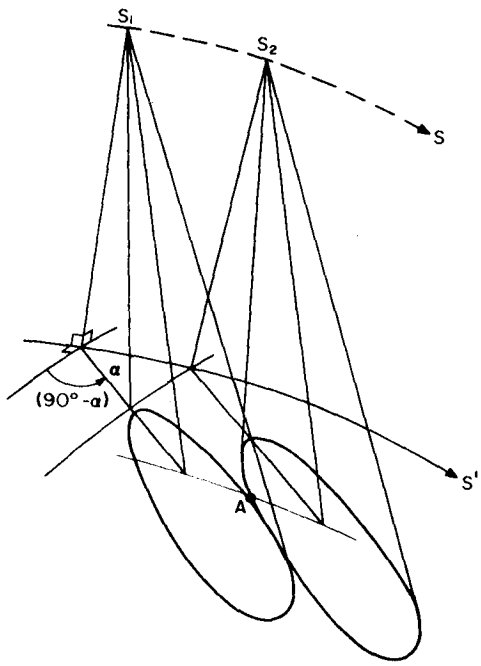

Figure 2. The maximum length of the synthetic-aperture is arc-length S_1S_2

Often the antenna beam is so broad that the arc length S_1S_2 exceeds the synthetic-aperture length required to produce a specific azimuth resolution. Rather than merely stacking up fewer segments, i.e., truncating the signal, and thereby wasting energy and information, it is common practice to filter the data into several stacks, each of the appropriate height for the desired azimuth resolution. Each of these two-dimensional signals, or stacks, can be processed to form a separate image. These separate images or azimuth 'looks' can then be registered with each other, and non-coherently summed together to produce what is commonly known as a 'multilook' image. 'Multilook' processing, or non-coherent integration as it is sometimes called, produces an image with less speckle. Speckle, which is a phenomenon that causes SAR images to look grainy, is due to scintillation of the signal reflected from the target complex during formation of the synthetic-aperture. By forming a 'multilook' image from several 'looks', each 'look' acquired from a different aspect angle α, one can make use of angular diversity to reduce the effect of scintillation.

The form of the received SAR signal for three point targets located at different ranges and azimuth positions is illustrated in Figure 3. At some particular instant targets (1) and (2) lie in the same direction but are at different ranges. Target (3) lies at the same ground-range distance d_o from ground-track (see Figure 1) as target (1) but appears at the centre of the antenna beam at a higher pulse number than does target (1). The horizontal thick solid lines in Figure 3 bound the approximately trapezoidal envelopes of each of the received signals and are determined by the pulse number at which the point enters and exits from the antenna illumination. Since the antenna pattern broadens with range, so too does the signal extent in the m-direction. The curved lines, limiting the slant-range extent of the signal, are the limits of the envelope of the transmitted pulse. The curvature of the envelope is caused by the variation in range of the target from the radar as the point target is traversed by the antenna beam. The solid lines inside the two-dimensional envelope represent phase contours of the signal. In Figure 3, it has been assumed that the SAR is employing linear FM pulse compression in order to achieve fine range resolution.

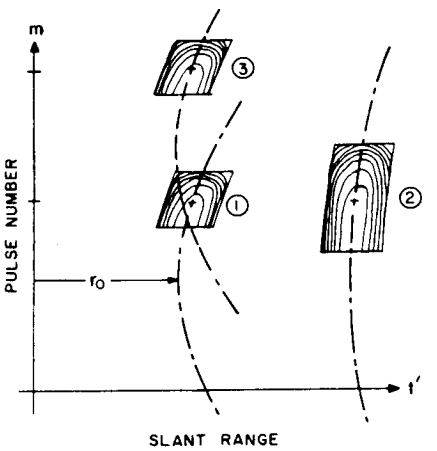

Figure 3. The shape of the envelope of the phase peaks of the SAR receiver output for three point targets

The signals shown in Figure 3 can be thought of as the SAR receiver's impulse response, $h_1(m,t')$ for three different values of (m,t'). If the radar scene is considered to be composed of many individual point scatterers the output $g(m,t')$ of the receiver is simply the convolution of the input with $h_1(m,t')$, i.e.,

$$g(m,t') = \sum_{t'_o=-\infty}^{\infty} \sum_{m_o=-\infty}^{\infty} [\delta(m-m_o, t'-t'_o) * h_1(m,t')] \qquad (1)$$

(see Figure 4). It is then possible to generate a matched filter[1] for $h_1(m,t')$ that will produce a SAR image.

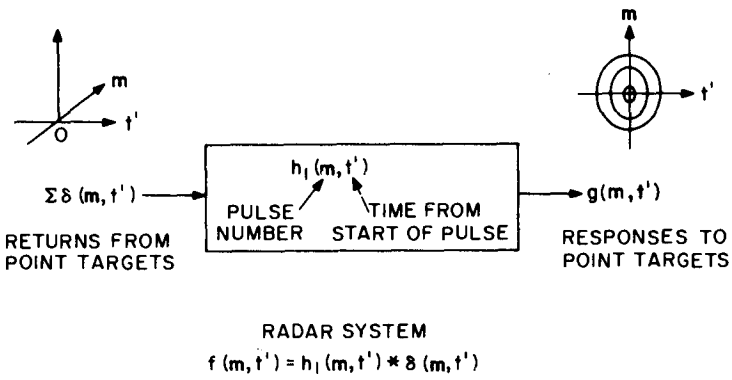

Figure 4. Point target response of SAR receiver

2.2 TWO-DIMENSIONAL MATCHED FILTERING

It has been shown heuristically in Section 2.1 that, at the output of the SAR receiver, the SAR signal can be modelled by the two-dimensional function $g(m,t')$. It is assumed[1] that the signal processing required to produce an image takes the form of a two-dimensional matched filtering operation. It remains to describe how the matched filter needed to produce the SAR image is defined.

The impulse response of the matched filter is just the time and pulse-number reversed, complex conjugate of the receiver impulse response $h_1(m-m_o, t'-t'_o)$ for a particular m_o and t'_o. The output of the matched filter is the two-dimensional convolution of the signal $g(m,t')$ with the impulse response of the shift variant matched filter $h_1^*(m-m_o, t'-t'_o)$ (see Figure 5). The SAR image is obtained by taking the magnitude of the output of the matched filter. The values of m_o and t'_o are chosen such that the match point is in the middle of the range swath to be processed.

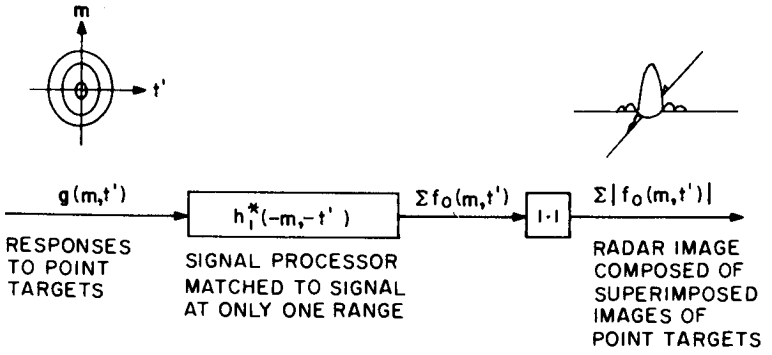

$$f_o(m,t') = h_1(m,t') * h_1^*(-m,-t')$$

$$F_o(fm,f_{t'}) = H_1(fm,f_{t'})\,\mathcal{F}\left\{h_1^*(-m,-t'_o)\right\}$$

Figure 5. Two-dimensional matched filtering of the SAR signal

2.3 GEOMETRICAL DISTORTIONS

In a two-dimensional SAR signal processor it may be more efficient to implement the two-dimensional convolution via the fast-convolution technique. In terms of the SAR signal processing problem, greatest efficiency is achieved by match-filtering a block of signal data that is large in both range and pulse number extent with respect to the two-dimensional matched filter. However, as was seen in Section 2.1, the SAR signal properties vary as a function of range; i.e., the filter is truly matched to the signal at only one range. When a block of SAR data with large range extent is convolved with the impulse response of the matched filter, the range variation of the matched filter causes a defocussing and geometrical distortion at ranges far away from the centre of the swath. Provided the range extent of the block of SAR data is not excessive (i.e., depth of focus criteria are not violated), the resulting image will be adequately focussed[1]. However, the mismatch between signal and filter occurring at the edges of the range swath will produce shifts in both range and pulse number of the imaged points. (Note, for sidelooking SARs no geometric distortion occurs.)

The image distortion phenomena can be explained by reference to Figure 6, where SAR signal responses from three points located at different ranges are shown. The filter is matched to the middle signal, where the rate of change of phase in the pulse number direction for both the signal and filter are identical. The image produced by the filtering process will be correctly located at D. This is not the case for the signal located at a nearer range. Rather than placing the image point at the correct location E, the filter selects that portion of the signal that has the same rate of change of phase in the pulse number direction as itself, and places the image point at F. In comparing F with the correct location E, one observes that both a pulse number (azimuth) and range placement error has been introduced by the processing.

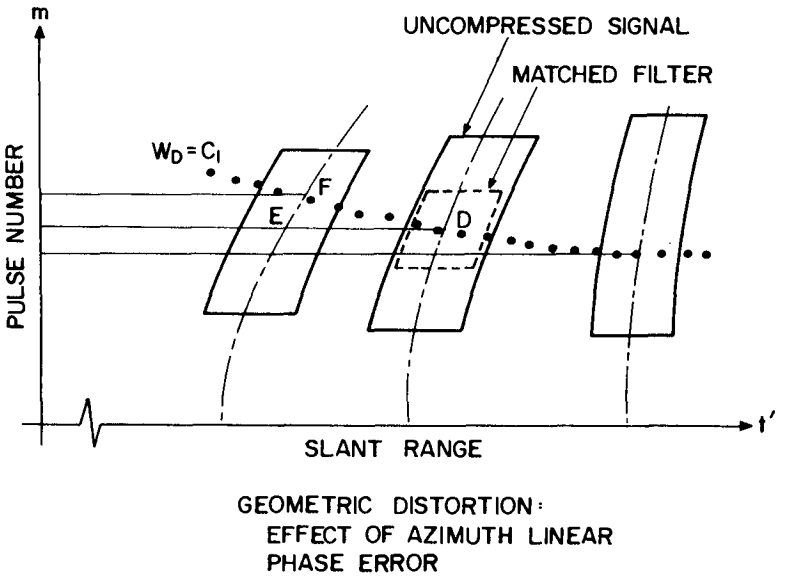

Figure 6. The form of the geometric distortion

Normally the final SAR image is required in the (d_o,s') coordinate system (see Figure 1) whereas the processor operates in the (t',m) or (r_1,s) coordinates as shown in Figures 3-6. A coordinate transformation must be done to convert from (t',m) to (d_o,s'). This transformation converts the image from a squinted slant-range $(\frac{ct'}{2})$ to sidelooking ground-range (d_o) presentation. The slant-range to ground-range conversion part of the transformation consists of a nonlinear resampling of the range data. The remainder of the transformation consists of a set of range dependent range and azimuth shifts, which have the same effect as writing the range lines $(\frac{ct'}{2})$, which were acquired by an antenna pointing at an angle α to ground-track, onto the final image at an angle α to s'.

In most cases the geometrical distortions introduced by the processing do not seriously degrade image quality. If left uncorrected the distorted image cannot be directly overlaid on a map, even after the coordinate transformation described above is done. If a capability to register various SAR images is required, as in multilook SAR processing, the geometrical distortions must be corrected. Since both the distortions produced by the processor, and the shifts required to do the coordinate transformation are deterministic, they can be precomputed and combined into a single set of range and azimuth shifts. This single set of shifts can then be applied to the output of the two-dimensional fast convolution to produce the required SAR image.

3. SYSTEM OVERVIEW

In this section a description of the current production modes and a brief overview of the processor are given.

3.1 CURRENT PRODUCTION MODES

The current production system generates the following data products for the SEASAT-A satellite-borne L-band SAR:

1. 7m azimuth x 25m ground-range resolution, single-look, geometrically correct images, 4.1m x 4.1m pixels; images usually contain ~3600 pixels ground-range x ~3600 pixels azimuth;

2. 12.2m azimuth x 25m ground-range resolution, two azimuth-looks, geometrically correct images, 8.2m x 8.2m pixels; images usually contain ~2400 pixels ground range x ~6000 pixels azimuth;

3. 25m azimuth x 25m ground-range resolution, four azimuth-looks, geometrically correct images, 16.4m x 16.4m pixels; images usually contain ~2400 pixels ground range x ~2900 pixels azimuth;

4. SEASAT Survey-Mode 100m azimuth x 100m ground-range resolution, single-look, no azimuth corrections, 65.6m x 65.6m pixels; images usually contain 2048 pixels ground-range x 2048 pixels azimuth;

and for the ERIM (SAR-580) airborne X/L-band SAR:

1. X-band, 2.1m azimuth x 1.5m slant-range resolution, single-look, geometrically correct images, 1.42m x 1.42m pixels; images usually contain >4000 pixels ground-range x 2000 pixels azimuth;

2. L-band, 2.1m azimuth x 2.3m slant-range resolution, single-look, geometrically correct images, 1.42m x 1.42m pixels; images usually contain >4000 pixels ground-range x 2000 pixels azimuth.

All the above data products except the SEASAT Survey-Mode imagery are generated as a set of blocks. These blocks are concatenated in azimuth to form a range sub-swath. The range sub-swaths, if there are more than one, are merged to form the final image. The width of the range sub-swath is determined by three factors:

1) the range dimension of the two-dimensional matched filter;

2) the slant-range increment over which a single two-dimensional matched filter can produce an image which is in focus in azimuth; and

3) the available disc file space.

The length of the block in azimuth is determined by:

1) the azimuth dimension of the two-dimensional matched filter;

2) the available disc file space.

The dimensions of the processing blocks must be at least the range dimension x the azimuth dimension of the two-dimensional matched filter. When they are this minimum size one valid output point is produced.

The SEASAT data set consists of 8 1600 BPI 9-track tapes of 4096 records, each containing 13,680 real slant-range samples. In the SEASAT survey mode the range record is augmented with zeroes to length 16,384, then it is low pass filtered and resampled by a factor of 4 so that the 16,384 range sample record becomes length 4096. The 32,768 azimuth records are low-pass filtered and resampled by a factor of 16 in azimuth to produce 2048 azimuth records. The 2048 azimuth x 4096 range sample block is processed to produce a single look 100m x 100m resolution image. This survey image is then used to pick an area over which the angle α is to be estimated using the Doppler centroid estimator (see following explanation); and to locate, in the tape set, scenes of interest to be processed at higher resolution. A special program is used to locate the starting range sample and starting azimuth record, of each block to be processed.

The value of angle α that is used in the production of the Survey-Mode image is calculated from information in the orbit and attitude files contained on the SEASAT data tapes. This calculated value of α is accurate enough for the Survey-Mode image, but is not accurate enough for the higher resolution products. The low accuracy of the calculated value necessitates the use of the Doppler centroid estimator to obtain a better value of α.

The ERIM (SAR 580) data set consists of single tapes of two sets of 2048 records x 4096 baseband slant-range samples. The sets of data on the tape can be any pair of:

- X-band, vertical/vertical polarization,
- X-band, vertical/horizontal polarization,
- L-band, vertical/horizontal polarization,
- L-band, vertical/vertical polarization;

or any pair of:

- X-band, horizontal/horizontal polarization,
- X-band, horizontal/vertical polarization,
- L-band, horizontal/vertical polarization,
- L-band, horizontal/horizontal polarization.

Each of the sets on the tape is processed separately. The set is processed in one operation by breaking the 4096 range samples up into sub-swaths which contain all the azimuth samples. The starting sample positions for the sub-swaths are found using a special sub-swath location program. Once all the sub-swaths in the set are processed they are merged into a single image.

3.2 THE SAR PROCESSOR

The SAR processor is composed of two subsystems: the SAR processing subsystem, which performs the actual image generation; and the support subsystem, which generates the input parameters and the control information and thereby provides the necessary command files so that the SAR processing subsystem can produce a large number of images routinely, with a minimum of human intervention required.

3.2.1 The SAR Processing Subsystem

The SAR processing subsystem is very general in nature. As presently implemented it can be used to process data from any SAR that uses Linear Frequency Modulation (LFM) coding in range. Only the tape unpacking subroutine must be rewritten for each new radar type. With minor changes in the software it can be further generalized so that it can be used to process data from any SAR that maintains the range coding constant from pulse-to-pulse over the processing block length.

3.2.1.1 General Description of Processing

As discussed in Section 2, the processing consists of a two-dimensional (2-D) convolution of the received radar signal with the impulse response of an appropriate matched filter. In the technique described here the 2-D convolution is implemented in the frequency domain using fast convolution[4-6].

As the first step in the processing, the two-dimensional impulse response of the matched filter for each of the looks is computed (see Figure 7). The 2-D impulse responses are stored as range lines; i.e., the word number in a record is a measure of 'squinted' slant-range, and the record number in a file is a measure of ground-track (azimuth) position. The size of each of the impulse responses, in numbers of words and records, is determined by the time-bandwidth products and sample spacings of the SAR signal data in range and azimuth respectively. Each record is augmented with zero-valued words so that it is length N_R, where N_R is the processing swath size. Similarly, each file of records has zero valued records added to it so that there are N_{AZ} records in the file, where N_{AZ} is the processing block size. (N_R and N_{AZ} are chosen to be integer powers of two to allow the straightforward use of the fast Fourier transform (FFT).) Next the 2-D frequency-domain transfer function of each of the matched filters is computed by performing a 2-D FFT on each impulse response. The steps involved in calculating the 2-D FFT are shown in Figure 8. An FFT is performed on each data record; then the matrix or filter containing the data records is transposed[4], and an FFT is performed on each new data record (the former columns of the matrix). The 2-D frequency-domain matched filters are stored on a disc file for use later during the processing.

After computation of the matched filters the processing of the signal can proceed. Figure 9 is a block diagram of the major processing steps. The SAR signal data are input on computer compatible tape (CCT) and the data are unpacked into an appropriate computer word format. At this stage each data record consists of the signal received at the SAR at the time of the particular azimuth pulse; i.e., the record is a range line. The data block to be processed normally consists of $N_L N_{AZ}$ such records of length N_R, where N_L is the number of azimuth 'looks'.

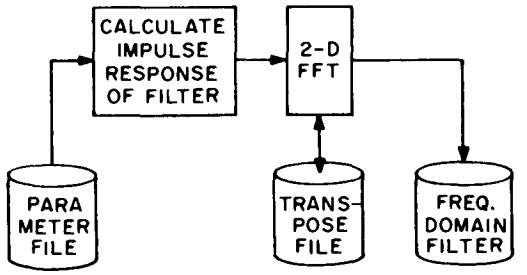

Figure 7. The generation of the two-dimensional frequency-domain matched filter

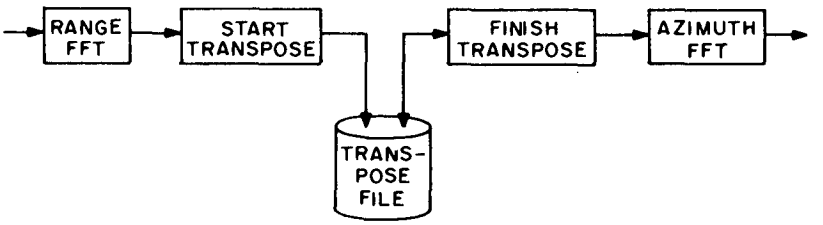

Figure 8. The two-dimensional fast Fourier transform, row-column method

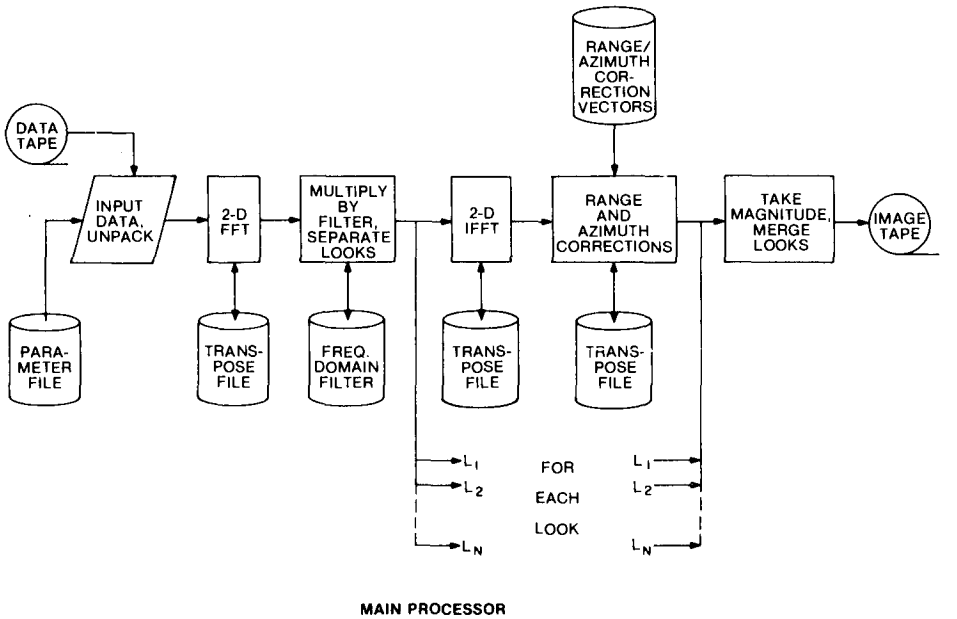

Figure 9. The two-dimensional software-based SAR digital processor

Once the data have been unpacked from the CCT, a 2-D FFT is performed on them to put the data in the frequency domain. The procedure followed is identical to that used to compute the matched filter. Then the 2-D FFT of the signal is separated into 'looks' by extracting or filtering out sections of the 2-D FFT along the azimuth-frequency coordinate. Each of the extracted sections is multiplied by the frequency-domain matched filter appropriate for that 'look'. The multiplication is done point-by-point; i.e., data point (n,m) is multiplied by filter point (n,m). It is not a matrix multiplication[4].

After the multiplication, a 2-D inverse fast Fourier transform (FFT) is performed on each of the looks. At this stage of processing, i.e., after the 2-D IFFT, one could compute the magnitude of the data to produce an image. However, the image would be in the 'squinted' slant-range, azimuth plane, and as described in Section 2.3 it would contain distortions caused by mismatch between the 'matched' filter and the data. To remove the distortions an additional processing step is incorporated prior to taking the magnitude. The additional step consists of the application of a set of range and azimuth corrections, and a conversion from 'squinted', slant-range, azimuth coordinates to orthogonal, ground-range, azimuth coordinates. The range and azimuth corrections for each range cell are precomputed at the time of calculation of the 2-D matched filter. The corrections are known to have the same precision as that of the mismatch between the data and filter. For example, given a set of parameters for the extracted data and the matched filter, the corrections required to place the dotted line in Figure 6 along the middle horizontal line can be precomputed. The precomputed range and azimuth correction vectors also include the coordinate transformation outlined above. At the time of processing the vectors are read from a file and applied to the data. The range corrections are applied first; then the data matrix is transposed and the azimuth corrections are applied.

The final step of the processing consists of computing the magnitude of each of the corrected 'looks', registering the 'looks' with respect to each other, and summing them together point-by-point. The image, which consists of a single range swath, is then stored on a CCT. If a multi-swath image is required the entire procedure is repeated for each range swath and then the swaths are aligned and merged together to form the final image.

3.2.1.2 General Description of Programs Used

The processing subsystem consists of the following programs (see Figure 10): the filter generation program (J7SE30), the sub-task monitor (J7SEA0), and the image generation programs (J7SE00,J7RE00,ZER0128,J7SE01, J7SE02,J7IG02,J7SE80).

The following functions are performed by the filter generation program (J7SE30) for each of the azimuth looks to be processed; the generation of a two-dimensional, frequency-domain filter matched to the radar signal at a particular range, the computation of the range and azimuth correction vectors, which are used to correct the SAR image produced by the two-dimensional fast-convolution (the correction is applied in (J7SE02)), the calculation of the centre line numbers used for azimuth look extraction and demodulation in J7SE01, and the generation of a file of information used by the merge support program (J7MS00) in merging adjacent range swaths.

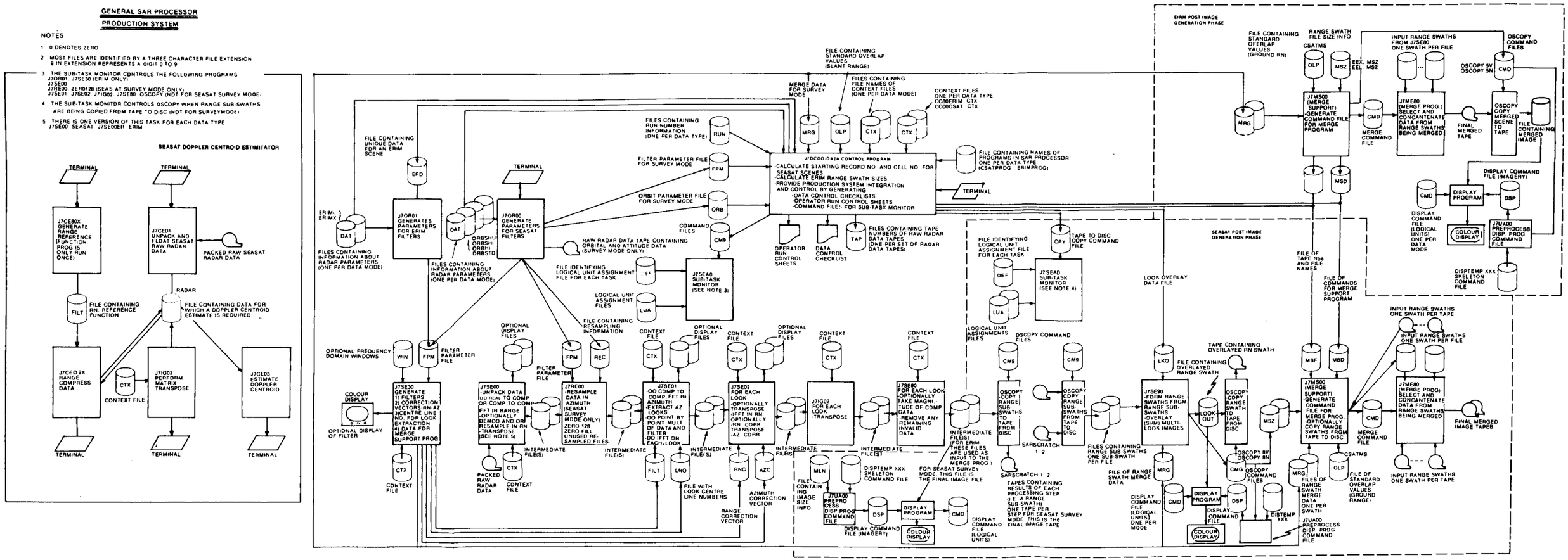

Figure 10. System block diagram

The sub-task monitor (J7SEA0) is used to control all the stages of the image generation phase of the SAR processing for the ERIM data, and is used to control all but the filter generation program for the SEASAT data. It is also used to control some of the processing in the post-image generation phase. The sub-task monitor has the following capabilities: it can load and start execution of a sub-task and monitor the progress of a sub-task until it has finished execution; it can allocate and delete files; it can modify an indexed file's contents by adding, subtracting, multiplying, dividing, or replacing entries; it can perform operations on tapes (or files) e.g., forward file, forward record, and rewind; it can prompt for operator assistance or provide operator information by performing Input/Output (I/O) to the operator's console; and it can also loop through and execute a set of commands.

The image generation program package consists of seven main programs. The first program (J7SE00), unpacks a block of data from magnetic tape, converts the data from its particular tape format to floating-point format, performs either a real-to-complex (e.g., SEASAT) or a complex-to-complex (e.g., ERIM) fast Fourier transform (FFT) on the data in range, demodulates and/or resamples the range data (e.g., SEASAT) if necessary, and finally transposes the data block.

The next program (J7RE00) is only run when azimuth resampling and/or demodulation is required, e.g., SEASAT survey.

The program ZER0 128 is a special program used only for the SEASAT Survey-Mode. If not enough tape records, and therefore range lines, are available, so that a full data block would remain after the azimuth resampling in J7RE00 is performed, ZER0 128 adds zero valued elements to complete the block.

In the normal processing mode J7SE01 is executed immediately following J7SE00. The program J7SE01 performs an FFT in azimuth, extracts a section of the FFT for each azimuth look being processed, writes the extracted data to a separate file and in the process demodulates the azimuth signal to baseband. The data in each of the look files is then multiplied point-by-point with the filter. The filter for each look is generated using J7SE30. The program J7SE01 then inverse fast Fourier transforms each of the azimuth records in the look files.

The next program in the processor is J7SE02. This program performs the following functions for each of the azimuth looks: it transposes the data block; it inverse fast Fourier transforms the data in range; it applies the range corrections and squint slant-range to sidelooking ground-range conversions; it then transposes the data, and applies the azimuth corrections and azimuth coordinate transformation.

The final program in the image generation subsystem of the processor is J7SE80. This program computes the magnitude of the complex data, removes any invalid data before the image is written to the final output file, and when required, e.g., for special types of multilook imagery, sums the looks. It is not normally used for summing the looks for ERIM and SEASAT-A production runs.

3.2.2 The Support Subsystem

The support subsystem is more specific in application than the SAR processing subsystem. Most of the programs in the package are designed to be executed as part of either an ERIM or a SEASAT-A production run. There are two major sub-divisions in the support subsystem: the pre-image generation support programs, and the post-image generation programs.

3.2.2.1 The Pre-Image Generation Support Programs

The pre-image generation support programs are all specific to either the ERIM or SEASAT-A production runs. The package of programs consists of the following (see Figure 10): the data control program (J7DC00), the radar compression filter parameter generation programs (J70R00,J70R01), and the Doppler centroid estimator programs (J7CE00X, J7CE01, J7CE02X, J71G02, J7CE03).

The data control program (J7DC00) is the first program run when processing either ERIM or SEASAT-A data. It generates the operator run control sheets, i.e., lists of all the procedures the computer operator must perform and of all the tapes that are required by each procedure. It also generates the data control checklist, which contains a list of tasks (programs) that must be executed before the operator can start a production run. In addition, the data control program creates the command files for the sub-task monitor (J7SEA0). These command files are used to control the image generation phase and the tape to disc, disc to tape copies. The data control program also contains the SEASAT location subroutine and the ERIM sub-swath location subroutine. The SEASAT location program is used to calculate, from coordinates on the SEASAT Survey-Mode image, the starting range and azimuth position for each SEASAT image sub-swath in terms of the element numbers within a record, and record numbers within a tape. The ERIM swath location program calculates the starting positions of each of the range sub-swaths and minimizes the overlap required between sub-swaths.

The radar filter parameter generation programs (J70R00, J70R01) are used to create the files of parameters used as input to the filter generation program (J7SE30).

The Doppler centroid estimation[7] package is used to estimate the complement of the squint angle α for the SEASAT data.

3.2.2.2 The Post-Image Generation Support Programs

The post-image generation support programs are not data-type specific. The package consists of the look overlay program (J7SE90), the merge support program (J7MS00), and the merge program (J7ME00) (see Figure 10).

The look overlay program (J7SE90) is used to overlay (sum) the looks together to form a multilook image. The program reads the multiple input files which contain the imagery for each look (several files may be used for the image of a single look), and it sums the data for all the looks on a point-by-point basis. If no data exist for a look at a particular point then zero is added to the sum. Some ancillary data such as record length and number of records for the multilook image are also calculated for use by the merge support program.

The merge support program (J7MS00) reads input data created by several different programs. This data contains the information necessary to merge together the range swaths to make the final image. The merge support program generates a command file, which is used as input to the merge program.

The merge program (J7ME00) reads the data from each range swath and selects the section of data from each swath that is to be combined with the data from the other range swaths being merged. The final merged image is written out to tape.

4. DETAILED PROCESSOR DESCRIPTION

In this section detailed descriptions of the equations and signal processing algorithms used in the processor are given. The reader is referred to the program documentation and processor user's manual for detailed descriptions of each of the programs used in the system. The material in this section is not intended to prove or derive the equations used in the system, the reader is referred to Ref. 1 for a derivation of the theory.

The description of the equations roughly follows the order of execution of the programs that contain them, i.e., the radar matched filter parameter generation programs (J70R00, J70R01), the data control program (J7DC00), the first part of the SAR processor (J7SE00, J7RE00, J7SE01), the filter generation program (J7SE30), the last part of the SAR processor (J7SE02, J7IG02, J7SE80, J7SE90), the merge support program (J7MS00), and finally the Doppler centroid estimation programs (J7CE0X, J7CE01, J7CE02X, J7CE03).

4.1 FILTER PARAMETER GENERATION

A standard set of parameters describing the radar characteristics, and the radar-target geometry is required by the program that generates the two-dimensional matched-filter (compression filter) (J7SE30). The programs J70R00 (SEASAT) and J70R01 (ERIM) compute these parameters from the information provided with the radar data. They are specific to either SEASAT or ERIM data and act as an interface between the information provided with the radar data and the inputs required by the general SAR processor.

Both programs generate the following set of parameters for each look 'q' to be processed:

1. r_e - the radius of the earth, (m)
2. λ - the radar wavelength, (m)
3. $\rho_{az_{1q}}$ - the parameter governing azimuth look spacing, (m)
4. $\rho_{az_{2q}}$ - the azimuth resolution for an unweighted aperture, (m)
5. Δx_q - the azimuth sample spacing on the surface of the Earth, (m), measured along ground-track

6. $\tilde{r}_1$ - slant range to the centre of the processing swath, all looks, (m), measured in the direction of angle α_o
7. τ_{p_1} - radar pulse length after range look extraction, (μs)
8. $\Delta t'_p$ - time interval between the range samples, (μs)
9. $\tilde{\alpha}$ - the aspect angle, or the complement of the squint angle (degrees), for the full antenna beam
10. $K' = \frac{K}{2} \times 10^{-12}$ - linear frequency modulation rate in (MHz/μs)
11. Δa_{1q} - error in the azimuth linear phase term, a_{1q}
12. Δa_{2q} - error in the azimuth quadratic phase term, a_{2q} (1/m)
13. h_s - height of vehicle carrying the radar, (m)
14. h_t - height of terrain above sea level, (m)
15. Δd_o - ground range sample spacing, (m), measured perpendicular to ground track
16. NN_R - length of FFT used for range resampling
17. Δf_R - range offset frequency, (Hz), to be used for range multilooking (not implemented, August 1980)
18. V_{eq} - velocity of the sub-satellite (aircraft) point (m/s)
19. PRF - the reciprocal of the azimuth input record spacing (s)
20. f_{oA} - azimuth-offset frequency, (Hz), (not implemented, August 1980)

The parameters are output to a file which has the filename extension .FPM, e.g., SSV00010.FPM (SEASAT Survey-Mode, run 0001, swath 0).

The two filter parameter calculation programs differ in complexity. The SEASAT parameter calculation program is the more complicated of the two; it must include the calculation of certain orbital and attitude parameters that are used to obtain r_e, Δx_o, $\tilde{r}_1$, $\tilde{\alpha}$, h_s and V_{eq}.

Certain parameters are fixed for each radar type and production mode; these fixed values are input from files that have the filename extension .DAT, e.g., ERIMX.DAT. The other parameters are either entered by the operator, read off files on the input data tape header, or in the case of ERIM, read from a file defined by the Data Control Program (J7DC00), i.e., a file with the filename extension .EFD.

The .EFD file contains the following parameters:

n_{1st} - the range cell at which to start unpacking for this swath; n_{1st} is specified in real samples for range-offset data and in complex samples for azimuth-offset or baseband data; the terms range-offset, azimuth-offset and baseband are defined in Section 4.3.1;

t'_D - the time delay to the edge of the recorded data (μs),

h_s - height of the vehicle carrying the radar, (m),

N_{LKS_A} - the number of azimuth-looks,

N_{LKS_R} - the number of range-looks (not implemented, August 1980).

The parameter n_{1st} is updated for each subsequent swath. The updating is done by the sub-Task Monitor (J7SEA0) program, which reads a command file generated by the Data Control Program (J7DC00). The sub-swath location program in J7DC00 calculates a set of n_{1st} values which are inserted in the appropriate place in the command file.

4.1.1 ERIM (J70R01)

The ERIM.DAT files contain the following parameters.

Δx_o - the azimuth sample spacing before look extraction,

Δd_o - the ground-range sample spacing (not implemented, August 1980),

f_{SR} - the range sampling frequency,

λ - previously defined,

$\rho_{az_{1q}}$ - previously defined,

$\rho_{az_{2q}}$ - previously defined,

$N_{SLCELLS/SSW}$ - the number of slant-range samples to unpack from the input tape record; $N_{SLCELLS/SSW}$ is in real samples for range-offset data and in complex samples for azimuth-offset or baseband data;

τ - radar pulse length before range-look extraction,

$(K/2\pi) \times 10^{12}$ - previously defined,

Δa_{1q} - previously defined,

NN_R - previously defined,

Δf_R - previously defined,

r_e - previously defined,

V_{eq} - previously defined,

$\tilde{\alpha}$ - $\pi/2$ rad,

h_t - previously defined,

and

fo_A - previously defined (not implemented, August 1980)

The parameters required for the .FPM file are either transferred directly from the .DAT file, as in the case of r_e, λ, $\rho_{az_{1q}}$, $\rho_{az_{2q}}$, $\tilde{\alpha}$, K', Δa_{1q}, Δa_{2q}, h_s, h_t, NN_R, Δf_R, V_{eq}, and fo_A, or they are calculated using the following equations.

The first parameter to be calculated is the PRF. In the aircraft, the PRF is adjusted to compensate for changes in V_{eq}, and thereby Δx_o is maintained constant. In the processor only the ratio of V_{eq}/PRF is needed, therefore a dummy value of $V_{eq} = 1^m/s$ can be used for the ERIM case, and the *nominal* PRF, to be used in the equations, can be calculated using the following:

$$PRF = \frac{V_{eq}}{\Delta x_o} \tag{2}$$

The processes of azimuth and range-look extraction embody a resampling of the data. After azimuth-look extraction the azimuth sample spacing is either

$$\Delta x_q = \Delta x_o \, N_{LKS_A} \text{ (baseband, range-offset)}, \tag{3}$$

or

$$\Delta x_q = 2\Delta x_o \, N_{LKS_A} \text{ (azimuth-offset)}. \tag{4}$$

Similarly, after range-look extraction the spacing of the range samples in time is either

$$\Delta t'_p = (2/f_{SR}) \, N_{LKS_R} \text{ (range-offset)}, \tag{5}$$

or

$$\Delta t'_p = (1/f_{SR}) \, N_{LKS_R} \text{ (baseband, azimuth-offset)}. \tag{6}$$

The remaining parameters required for the .FPM file are computed as follows: the slant-range (measured in the slant-range plane, but in the direction of $\tilde{\alpha}$), to the edge of the swath is

$$r_{1 \text{ edge}} = \frac{c}{2} t'_D \, , \tag{7}$$

where c is the velocity of light in free space and t'_D is the time delay to the first slant-range sample recorded; the slant range to the middle of the

range swath to be processed is

$$\tilde{r}_1 = r_{1\ \text{edge}} + \left(n_{1_{ST}} + \frac{N_{SLCELLS/SSW}}{2}\right) \frac{c}{2f_{SR}} \ ; \tag{8}$$

the ground-range sample spacing Δd_o is equal to the azimuth sample spacing, i.e.,

$$\Delta d_o = \Delta x_q ; \tag{9}$$

and the pulse length, after range-look extraction is

$$\tau_p = \frac{\tau}{N_{LKS_R}} \ . \tag{10}$$

NOTE: It is planned to change the action performed for parameter Δd_o, so that in the future (9) will not be used, but instead Δd_o will be transferred directly from the .DAT file to the .FPM file.

4.1.2 SEASAT (J70R00)

There are four .DAT files for SEASAT, i.e., one for each mode. Survey, 25m 4-look, 12.5m 2-look, and 7.4m 1-look. These files contain values of the following parameters appropriate to the particular mode:

- θ_i - the angle of inclination of the orbit,
- PRF - previously defined,
- t'_{REF} - the time delay from the edge of the digitization window to the start of the data,
- f_{SR} - previously defined,
- N_{RRS} - input data slant-range resampling factor,
- N_{AZRS} - input data azimuth resampling factor, (does not include resampling done by look extraction),
- N_{PULS} - the number of pulses elapsed between the times of transmission and reception of the radar pulses returned from the range swath illuminated by the real antenna,
- h_t - previously defined,
- $\Omega_{ASC_{REF}}$ - spacecraft reference right ascension node,
- $N_{REV_{REF}}$ - spacecraft revolution number for which $\Omega_{ASC_{REF}}$ is the right ascension node,

T_{orb} - period of orbit in degrees/rev,

λ - previously defined,

ρaz_{1q} - previously defined,

ρaz_{2q} - previously defined,

N_{LKS_A} - previously defined,

N_{LKS_R} - (to be added, July 1980),

$N_{SLCELLS/SSW}$ - previously defined,

τ - previously defined,

$\frac{K}{2\pi}$ - previously defined,

Δa_{1_q} - previously defined,

Δa_{2_q} - previously defined,

NN_R - FFT length for range resampling during slant/ground range conversion,

Δf_R - range-look spacing parameter (Hz),

L_{az} - azimuth FFT length before look extraction and azimuth resampling,

f_{o_A} - azimuth-offset frequency (not implemented, August 1980).

Most of these parameters are used to compute the standard set of parameters used in the .FPM file, others like $\Omega_{ASC_{REF}}$, T_{orb} and $N_{REV_{REF}}$ are only used to compute image location parameters, which are not used in the processing itself.

The SEASAT data tape also contains attitude and orbit information. Sets of values for the satellite's position (X,Y,Z), and velocity (V_X,V_Y,V_Z), expressed in an earth-centred inertial coordinate system defined as[8],: X, true of date of vernal equinox; Y, right-hand system; and Z, true of date of earth rotation axis (North). The time and frequency of the orbit points are one per minute with points provided on even-minute marks. The attitude information consists of sets of pitch, roll and yaw data measured at five-second intervals. Each data point of determined satellite attitude is expressed at a time coupled with a set of Euler angle rotations. The Euler angle rotations can be used to convert any vector expressed in the geocentric orbital reference axes to the Satellite Alignment Reference Axes[8]. The geocentric orbital reference axes are defined as: the X-axis in the inertial direction of flight (derived from Y and Z), the Y-axis parallel to the negative of the orbit normal, and the Z-axis toward the earth centre of mass[8]. The Euler angle

rotations are in the Z, X, Y order of axes, which correspond to satellite yaw, roll, and pitch ($\theta_Y, \theta_R, \theta_P$).

There is also a set of ancillary data at the beginning of each SEASAT record, this data contains such information as the delay N_{DELAY}, an integer which when divided by 64 gives the location of the start of the digitization window, expressed as a fraction of 1/PRF, from the start of interpulse period N_{PULS}. The ancillary data record also contains the time of day for the data record.

In addition to the above data the computer operator must input the following information specific to the run: the run number, the estimate of $\tilde{\alpha}$ produced by the Doppler centroid estimator (for all but the Survey-Mode), the SEASAT data type record number to be used in the calculation of the .FPM parameters, the range cell number in the range-offset data at which to start unpacking ($n_{1_{ST}}$), and the SEASAT revolution number (I_{REV}). For the Survey-Mode a value for α is calculated using the attitude and orbit data (see also (29)).

From all this information the necessary parameters for the .FPM can then be calculated. First, the approximate right ascension node Ω_{ASC} is calculated, i.e.,

$$\Omega_{ASC} = \Omega_{ASC_{REF}} + (N_{REV_{REF}} + I_{REV})T_{orb}, \tag{11}$$

and then Ω_{ASC} is normalized to the interval $0 \leq \Omega_{ASC} < 2\pi$. The Ω_{ASC} can be used in conjunction with the SEATRAK* calculator and the spacecraft latitude to locate the radar scene on the surface of the earth. Next, the file of values of: X, Y, and Z; V_X, V_Y, V_Z, and θ_Y, θ_P and θ_R are read from the SEASAT data tape and the pairs of values, which bracket the time of acquisition of the record selected for the orbit computation, are extracted, converted to appropriate units, and then the values of: X, Y, Z; V_X, V_Y, V_Z; and θ_Y, θ_P, θ_R at the selected time are found by linear interpolation. From these basic parameters the ground-track velocity V_{eq}, the altitude and latitude of the satellite h_s, and ϕ_{LAT}, and the radius of the Earth r_e are calculated.

The calculation of the ground-track velocity involves many steps, which produce as by-products all of the other above-mentioned parameters. The spacecraft velocity in inertial coordinates (X, Y, Z) is

$$V_s = (V_X^2 + V_Y^2 + V_Z^2)^{\frac{1}{2}}. \tag{12}$$

This velocity must be combined with the tangential velocity of the surface of the earth in order to obtain V_{eq}.

The computation of the earth's tangential velocity involves the calculation of: the spacecraft latitude ϕ_{LAT}, the radius of the Earth at

---

* The SEATRAK calculator is a circular sliderule used to find the satellite track over the Earth's surface.

this latitude, the angular position (ϕ_o) of the satellite in its orbit (see Figure 11), and the angle that the velocity vector V_s makes with the north vector at the satellite point. The spacecraft latitude is

$$\phi_{LAT} = \tan^{-1}\left(\frac{Z}{(X^2+Y^2)^{\frac{1}{2}}}\right). \tag{13}$$

The radius of the Earth at this latitude is

$$r_e = \sqrt{\frac{a_e^2 b_e^2}{a_e^2\cos^2\phi_{LAT} + b_e^2\sin^2\phi_{LAT}}}, \tag{14}$$

where a_e = 6378388.0, the semi-minor axis of the Earth; and b_e = 6356912.0[9], the semi-major axis of the Earth. The angular position of the satellite is

$$\phi_o = \sin^{-1}\left(\frac{\sin\phi_{LAT}}{\sin\theta_i}\right). \tag{15}$$

The components of the Earth's tangential velocity normal and parallel to V_s can then be calculated using the following equations:

$$V_{en} = \omega_e r_e \cos\phi_{LAT} = \frac{\sin\theta_i\cos\phi_o}{(1 - \sin^2\theta_i\sin^2\phi_o)^{\frac{1}{2}}}, \tag{16}$$

and

$$V_{ep} = \omega_e r_e \cos_{LAT}\ 1 - \left[\frac{\sin^2\theta_i\cos^2\phi_o}{1 - \sin^2\theta_i\sin^2\phi_o}\right]^{\frac{1}{2}}, \tag{17}$$

where, ω_e is the radial velocity of the Earth. The ground-track velocity V_{eq} is then

$$V_{eq} = \left[V_{en}^2 + \left(\frac{|V_s|}{c_a} + |V_{ep}|\right)^2\right]^{\frac{1}{2}}, \tag{18}$$

where

$$c_a = 1 + \frac{h_s}{r_e}, \tag{19}$$

and

$$h_s = (X^2+Y^2+Z^2)^{\frac{1}{2}} - r_e \tag{20}$$

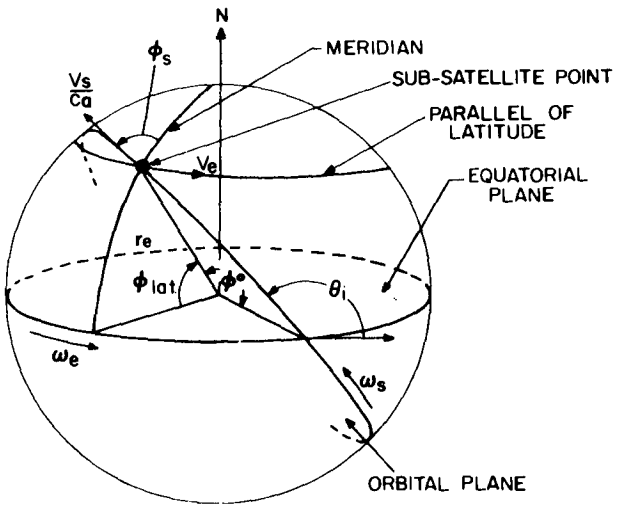

Figure 11. Angles that define orbit. $\underline{V_s}/c_a$ and $\underline{V_{eq}}$ are tangential to the planet surface.

The slant-range to the middle of the range sub-swath to be processed is given by

$$\tilde{r}_1 = r_{1_{edge}} + \left(n_{1_{ST}} + \frac{N_{SLCELLS/SSW}}{2}\right)\frac{c}{2f_{SR}} \quad , \tag{21}$$

where,

$$r_{1_{edge}} = \frac{c}{2}\left[\left(N_{PULS} + \frac{N_{DELAY}}{64}\right)\frac{1}{PRF} - t'_{REF}\right]. \tag{22}$$

The calculation of a very approximate value of angle $\tilde{\alpha}$, (as opposed to the value measured by the Doppler centroid estimator), requires the computation of several other values. First, the equivalent yaw of the spacecraft θ_{ye} (see Figure 12) must be found. For a descending orbit, i.e., $V_Z > 0$,

$$\theta_{ye} = \tan^{-1}\left(\frac{|V_{en}|}{\left|\frac{V_s}{c_a}\right| + |V_{ep}|}\right) \quad , \tag{23}$$

and for an ascending orbit, i.e., $V_Z \leq 0$,

$$\theta_{ye} = \tan^{-1}\left(\frac{-|V_{en}|}{\frac{|V_s|}{c_a} - |V_{ep}|}\right) . \tag{24}$$

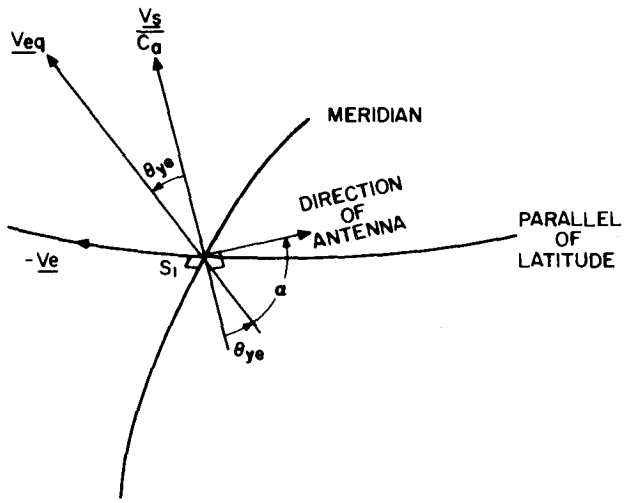

Figure 12. Vehicle equivalent velocity

Then the ground-range, d_o, measured perpendicular to track, to the middle of the total 100 km ground-range swath must be calculated. The distance is

$$d_o = d_{1\ edge} \cos\left(\frac{\pi}{2} - \alpha_y\right) + 50000, \tag{25}$$

where

$$d_{1\ edge} = r_e \cos^{-1}\left[\frac{\left(\frac{r_{1\ edge}}{r_e}\right)^2 - c_a^2 - c_b^2}{-2c_a c_b}\right] , \tag{26}$$

$$c_b = 1 + \frac{h_t}{r_e} , \tag{27}$$

and

$$\alpha_y = \left(\frac{\pi}{2} - \theta_{ye}\right) - \theta_y \quad . \tag{28}$$

Finally, the calculated value of $\tilde{\alpha}$, denoted by $\tilde{\alpha}_{yp}$, is

$$\tilde{\alpha}_{yp} = \tan^{-1}\left(\frac{\tan\alpha_y}{1 + \frac{h_s}{d_o}\tan(-\theta_p)\tan\alpha_y}\right) . \tag{29}$$

Angle $\tilde{\alpha}_{yp}$ must be normalized to the range $-\pi/2 \leq \alpha_{yp} < \pi/2$. If no centroid estimate ($\tilde{\alpha}$) is available, $\tilde{\alpha}_{yp}$ is transferred to the .FPM file in place of $\tilde{\alpha}$.

The remaining parameters for the .FPM file: $\Delta t'$, τ_p, Δx_q and Δd_o, are found by using the following equations:

$$\Delta t'_p = \frac{2}{f_{SR}} N_{RRS} N_{LKS_R} \quad , \tag{30}$$

$$\tau_p = \frac{\tau}{N_{RRS} N_{LKS_R}} \quad , \tag{31}$$

and

$$\Delta x_q = \frac{V_{eq}}{PRF} N_{LKS_A} N_{AZR_S} \quad , \tag{32}$$

$$\Delta d_o = \Delta x_q \quad . \tag{33}$$

For azimuth-offset data (not implemented as of August 1980), eqn. (32) becomes

$$\Delta x_q = \frac{2V_{eq}}{PRF} N_{LKS_A} N_{AZRS} \quad . \tag{34}$$

The real azimuth-offset data are converted to complex baseband data during azimuth-look extraction, therefore an extra factor of 2 must be used in (32) to obtain eqn. (34). The range sample spacing $\Delta t'$ is the spacing of the complex baseband samples, therefore a factor of 2 must also be used in (30) to convert from $1/f_{SR}$, the spacing of the real range-offset samples, to the spacing of the complex baseband samples. The ground-range sample spacing Δd_o is set equal to the azimuth sample spacing in the individual azimuth-looks so that square pixels are produced in the final image.

It is not necessary to run all of program J70R00 for each new scene or mode to be processed from the same set of input data. The values calculated by J70R00 particular to a specific orbit are stored in a file that has the filename extension .0RB. The parameters, relevant to this discussion, that are stored in the .0RB file are:

- the record number at which the orbital data is computed,
- r_e - previously defined,
- $r_{1\ edge}$ - previously defined,
- V_{eq} - previously defined,
- $\tilde{\alpha}_{yp}$ - previously defined,

and

- h_s - previously defined.

A further set of calculations is performed for the *SEASAT Survey-Mode only*. The data used to produce a Survey-Mode image undergoes a sampling rate reduction by a factor of 4 in range and a factor of 16 in azimuth. The range sampling rate reduction is straightforward and is done in J7SE00 as part of the range-offset to baseband demodulation (see Section 4.3.2.3). The azimuth sample rate reduction is more complicated because the azimuth data are modulated on a carrier, f_α, the frequency of which changes with α. The azimuth sampling rate reduction (see Section 4.3.4)(J7RE00), involves a demodulation, a low-pass filtering operation, and a sampling rate reduction by an integer factor. The program J7RE00 that does the azimuth sampling rate reduction requires as input the FFT line number ($LNOM_{SM}$) that corresponds to azimuth-frequency, f_α. For all data types except azimuth-offset (defined in Section 4.3.1), this line number, $LNOM_{SM}$ is calculated using one of the following equations.

$$LNOM_{SM} = \underset{PART}{INTEGER} \left[\frac{L_{az}(f_\alpha - N_\alpha\ PRF)}{PRF} + L_{az} \right], \qquad \alpha_{yp} \leq \frac{\pi}{2}, \tag{35}$$

or

$$LNOM_{SM} = \underset{PART}{INTEGER} \left[\frac{L_{az}(f_\alpha - N_\alpha\ PRF)}{PRF} \right], \quad (\alpha_{yp} > \frac{\pi}{2}), \tag{36}$$

where

$$f_\alpha = -\frac{2V_{eq}}{\lambda}\frac{r_e}{r_1}c_a\frac{\sin\theta_r}{\tan\alpha_{yp}} \quad , \tag{37}$$

$$\theta_r = \sin\alpha_{yp}\left\{1 - \left[\frac{\left(\frac{r_1}{r_e}\right)^2 - c_a^2 - c_b^2}{-2c_a c_b}\right]^2\right\}^{\frac{1}{2}} \quad , \tag{38}$$

and,

$$N_\alpha = \underset{\text{PART}}{\text{INTEGER}}\left(\frac{f_\alpha}{PRF}\right) . \tag{39}$$

The value of $LNOM_{SM}$ is written out to a file, which has the filename extension .REC. This file is used by J7RE00 (see Figure 10).

For azimuth-offset data (37) is changed to

$$f_\alpha = f_{o_A} \quad , \tag{40}$$

where f_{o_A} is the azimuth-offset frequency. This modified value of f_α is then used in (39) and either (35) or (36) to find $LNOM_{SM}$.

4.2 DATA CONTROL PROGRAM (J7DC00)

The data control program generates: the operator run control sheets, i.e., lists of all the procedures the computer operator must perform and of all the tapes which are required by each procedure; the data control checklist which contains a list of tasks (programs) that must be executed before the operator can start a production run; and the command files for the sub-task monitor (J7SEA0). The command files are used to control the image generation phase and the tape-to-disc, disc-to-tape copies. In addition to the above functions, the Data Control Program also provides a capability for calculating ERIM subswath sizes and start-cell positions, as well as a capability for calculating SEASAT sub-swath start-record and start-cell numbers.

As shown in Figure 10, the Data Control Program has associated with it numerous input and output files. The files and their uses are as follows:

1. {CSAT, ERIM}.RUN - contains a list of previously designated run numbers and range swaths; it is used in preparing run control sheets, data control checklists, and command files;

2. DC00 {CSAT, ERIM}.CTX - configuration parameters for J7DC00 itself, i.e., buffer sizes, etc.;

3. S {SV, LR, IR, HR} NAMES.CTX - file of filenames, used in selection of the appropriate task .CTX files when doing Logical Unit assignments, it is also used in command files;

4. {CSAT, ERIM} 9999.TAP - file of tape numbers for run 9999, it is used in creating run control sheets;

5. {CSAT, ERIM}.PROG - file of the names of the programs that must be run for each data type; it is used in creating the command files;

6. ERIM {X, L}.DAT - used to update $\tilde{r}_1$ in the ERIM {X, L} .FPM file. *(NOTE: ERIM data is run as group of sub-swaths and between each sub-swath $\tilde{r}_1$ must be updated)*

7. ORBSUR.DAT - set of fixed orbit and radar parameters for SEASAT Survey-Mode, it is used in SEASAT scene location program;

8. SSV99990.FPM - file containing input to filter generation program for SEASAT Survey-Mode, run 9999, it is used in SEASAT scene location program;

9. SSV99990.ORB - file containing basic orbit information for SEASAT run 9999, it is output by J70R00 at the time the set-up operations are performed for the Survey-Mode image of run 9999, and is used in the SEASAT scene location program for the other SEASAT modes;

10. SSV99990.MRG - file merge data for Survey-Mode; it is output by the filter generation program (J7SE30) at the time of processing of the SEASAT Survey-Mode image of run 9999, and is used in the SEASAT scene location program;

11. CSAT.OLP - file containing the standard values of slant-range overlap to be used when designating either SEASAT or ERIM range sub-swaths;

12. E {EX, EL} 9999A.EFD - file containing range delay, start-cell number and altitude for ERIM run 9999, swath A; it is output by J7DC00;

13. S {SV, LR, IR, HR} 9999A.CM2 - command file for azimuth block-group 2, for run 9999, sub-swath A; each group of azimuth blocks has associated with it, its own command file, which is used by the sub-task monitor; the number of azimuth blocks per group is determined by the processing mode; the command file is output by the Data Control Program;

14. S {SV, LR, IR, HR} 9999A.MSD - file containing command input to be used by the merge-support program, i.e., the number of sub-swaths to be merged to form the final scene, the data mode, the run number, sub-swath numbers of the sub-swaths being merged and whether complex or real data is to be output;

15. S {SV, LR, IR, HR} 9999A.MSF - file containing information about the files and tape drives to be used during tape-to-disc copy operations and during subsequent merging operations;

E {EX, EL} 9999A.MSF

16. S {SV, LR, IR, HR} 9999A.LKO - the look overlay displacement file; it contains the number of looks to overlay, the number of elements in each record, the number of records to read from each input file for each look, the total number to read for each look, and the number of records to skip on the first input file before reading data for this look.

E {EX, EL} 9999A.LKO

The description given in this document is mainly concerned with the ERIM and SEASAT location equations. The operator run control sheet, data control checklist, and command file generation functions are described in details in Refs. 10, 11.

4.2.1 SEASAT Location Program

Early in the development of the CRC SAR processor SEASAT processing modes, the need for a facility that would allow one to easily locate targets about which high (7m azimuth resolution), intermediate (12m azimuth resolution), and low (25m azimuth resolution) images were to be centred was recognized. In particular, a precision location capability minimizes the size of the scene that must be processed to contain a desired target or feature. This capability is especially useful when processing 7m azimuth resolution

images. It was decided that the best method was to produce a quick-look or Survey-Mode (100m x 100m resolution - 1 look) image of the entire data set contained on the input tapes (100 km x 100 km), then to measure the position of targets of interest on this image, and finally to use the measured position to locate the desired size and mode of scene, i.e., find the starting record and starting cell within the input tape set.

In the following discussion it is assumed that a Survey-Mode image has already been processed and that all of the files necessary to produce a Survey-Mode image have been set up.

The following parameters are required for operation of the location program:

1. from the operator's terminal:

Z_x - the measured horizontal distance, to the target being located, on the photograph of the Survey-Mode image;

Z_w - the measured total width of the photograph of the Survey-Mode image (the zero-filled areas are not included);

Z_y - the measured vertical distance, to the target being located, on the photograph of the Survey-Mode image;

Z_h - the measured total height of the photograph of the Survey-Mode image (the zero-filled areas are not included);

$\tilde{\alpha}$ - the complement of the squint angle, as measured using the Doppler centroid estimator;

N_{SSW} - the number of slant-range sub-swaths in the scene to be located;

$N_{REC/LAST\ TAPE}$ - the number of records on the last tape of the SEASAT input data tape set; and,

N_{BLK} - the number of azimuth blocks in the scene to be located.

2. from the DC00CSAT.CTX file:

$N_{SLCELLS/REC}$ - the number of real slant-range samples per tape record;

$N_{SLCELLS\ ADV}$ - the number of real slant-range cells to advance per range sub-swath (after sub-swath overlap is taken into account); the value is selected on the basis of the width in slant-range of the two-dimensional matched filter; the width of the filter depends in turn on the mode of the image to be processed;

$N_{REC/TAPE}$ - the number of records per SEASAT input data tape;

$N_{l_{SUR}}$ - the approximate length in azimuth of the two-dimensional matched filter that was used to process the SEASAT Survey-Mode image;

$N_{REC_{ADV}}$ - the number of records to advance per azimuth block for the scene being located; the value of $N_{REC_{ADV}}$ is selected on the basis of the length in azimuth of the two-dimensional matched filter; the length depends in turn on the processing mode;

N_{LKS} - the number of azimuth looks in the scene being located (depends on the data mode);

N_{OV_B} - the number of records, for the mode being located, to be removed at the bottom of the processed image; during the azimuth corrections a certain number of records are wrapped around in azimuth on the processing block; these wrapped around records must be removed;

$N_{l_{MODE}}$ - the approximate length, in resampled azimuth samples, of the two-dimensional matched filter, for the mode of the scene being located ($N_{l_{MODE}}$ must be multiplied by the number of azimuth-looks N_{LKS_A} to get the actual length, in input data records, of the azimuth filter);

$N_{SLCELLS/SSW}$ - the number of real slant-range samples per sub-swath for the mode being processed; and,

$N_{REC/BLK}$ - the number of records processed per azimuth block for the scene being located.

3. from the SSV99990.MRG file:

$n^*_{o_{SUR}}$ - the edge of the vector containing the Survey-Mode image range data; $n^*_{o_{SUR}}$ is zero at the ground-track and is and is measured perpendicular to the ground-track;

$FNZRCV_{SUR}$ - the first non-zero element of the vector containing the Survey-Mode image range data; and,

$LNZRCV_{SUR}$ - the last non-zero element of the vector containing the Survey-Mode image range data.

4. from the SSV99990.FPM file:

$\Delta d_{o_{SUR}}$ - the ground-range sample spacing (in the Survey-Mode image);

r_e - the radius of the Earth;

h_s - the height of the satellite above sea level;

h_t - the height of the terrain above sea level;

$\tilde{r}_{1_{SUR}}$ - the slant-range to the centre of the swath for the Survey-Mode image; $\tilde{r}_{1_{SUR}}$ is measured along the squint direction α_{yp};

V_{eq} - the velocity along ground-track of the sub-satellite point; and,

PRF - the pulse repetition frequency of the radar.

5. from the ORBSUR.DAT file:

f_{SR} - the range sampling frequency; and

N_{AZRS} - the azimuth resampling factor for the Survey-Mode image.

6. from the CSAT.OLP file:

$N_{OVL_{MODE}}$ - the overlap, for the mode of scene being located, to be allowed on the left side of each range sub-swath; $N_{OVL_{MODE}}$ is specified in complex slant-range samples; in azimuth multilook images the looks are offset from each other in range (see Section 4.7), this offset means that at the edges of the image a step wedge effect is produced, i.e., zones of one look, two looks, three looks, etc., exist (see Figure 36); these zones, which do not contain the full number of looks, must be removed, hence the sub-swaths must be overlapped by $N_{OVL_{MODE}}$.

7. from SSV99990.ORB file:

$r_{1\ edge}$ - the slant-range to the edge of the full range-swath; and

8. from CSAT9999.TAP file:

N_{TAPES} - the number of tapes in the SEASAT input data set.

The preceding information is used in conjunction with the tape numbers in the CSAT9999.TAP file during the production of the operator run control sheets, and the generation of the command files. In addition, the starting range sample number for each sub-swath is placed in the .CTX file for J7SE00 via the sub-task monitor.

The starting and ending range samples are calculated by: 1) finding the ground-range to the target, measured perpendicular to ground-track, from the distance measured on the Survey-Mode image photograph; 2) converting the ground-range perpendicular to track, to the ground-range measured in the squint direction; 3) calculating the slant-range in the squint direction from the ground-range in the squint direction; 4) converting the slant-range in the squint direction into a slant-range sample number; and 5) using the slant-range sample number at mid-scene to find the starting and ending slant-range samples for each sub-swath (see Figures 13, 14). The ground-range to the target, measured perpendicular to ground-track, is

$$d_{o_x} = \frac{Z_x}{Z_w} (d_{o_R} - d_{o_L}) + d_{o_L} \quad , \tag{41}$$

where d_{o_R}, the ground-range distance to the far edge measured perpendicular to track, is

$$d_{o_R} = [n^*_{o_{SUR}} + (LNZRCV_{SUR} - 1)]\Delta d_{o_{SUR}} \quad , \tag{42}$$

and d_{o_L}, the ground-range distance to the near edge measured perpendicular to track, is

$$d_{o_L} = [n^*_{o_{SUR}} + (FNZRCV_{SUR} - 1)]\Delta d_{o_{SUR}} \quad . \tag{43}$$

The ground-range d_{1_x}, measured in the squint direction is found from the ground-range d_{o_x} using the following equation:

$$d_{1_x} = r_e \sin^{-1}\left[\frac{\sin(d_{o_x}/r_e)}{\sin\tilde{\alpha}}\right] \quad . \tag{44}$$

Ground-range d_{1_x} is then converted to slant-range r_{1_x}, where

$$r_{1_x} = r_e \left[c_a^2 + c_b^2 - 2c_a c_b \cos\left(\frac{d_{1_x}}{r_e}\right)\right]^{\frac{1}{2}} \quad . \tag{45}$$

The slant-range r_{1_x} is then used to compute the slant-range sample $n_{1_{MID}}$ which corresponds to the middle of the scene, i.e.,

$$n_{1_{MID}} = \frac{r_{1_x} - r_{1_{edge}}}{\frac{c}{2f_{SR}}} + \frac{N_{SLCELLS/REC}}{2} \quad . \tag{46}$$

From $n_{1_{MID}}$, the starting and ending sample numbers $n_{1_{ST}}$ and $n_{1_{END}}$, for each of the N_{SSW} sub-swaths can be calculated using the following algorithm (see Figure 14);

1. Repeat for j=1, N_{SSW}

$$\text{i)} \quad n_{1_{ST}}(j) = \text{INTEGER PART} \left(n_{1_{MID}} - \frac{N_{SSW}}{2} \left(N_{SLCELLS_{ADV}} - 2N_{OV_{L\ MODE}} \right) + (j-1) \left(N_{SLCELLS_{ADV}} - 2N_{OV_{L\ MODE}} \right) \right)$$

$$\text{ii)} \quad n_{1_{check}}(j) = n_{1_{ST}}(j) \Bigg) \; ; \tag{47}$$

2. if $n_{1_{ST}}(1) \leq 0$, then repeat for all j=1, N_{SSW}

$$\text{i)} \quad n_{1_{ST}}(j) = n_{1_{check}}(j) - n_{1_{check}}(1) + 1,$$

and

$$\text{ii)} \quad n_{1_{check}}(j) = n_{1_{ST}}(j); \tag{48}$$

3. If $[n_{1_{ST}}(N_{SSW}) + N_{SLCELLS/SSW}] > N_{SLCELLS/REC}$, then repeat for all j=1, N_{SSW}

i) $$n_{1_{ST}}(j) = n_{1_{CHECK}}(j) - \left[n_{1_{CHECK}}(N_{SSW}) - N_{SLCELLS/REC} + N_{SLCELLS/SSW} \right];$$ (49)

4. if $n_{1_{ST}}(1) \leq 0$, then set $n_{1_{ST}}(1) = 1$; and, (50)

5. repeat for all j=1, N_{SSW}:

$$n_{1_{END}}(j) = n_{1_{ST}}(j) + N_{SLCELLS/SSW}$$ (51)

The algorithm assumes that one will not try to locate more swaths than is possible in $N_{SLCELLS/REC}$.

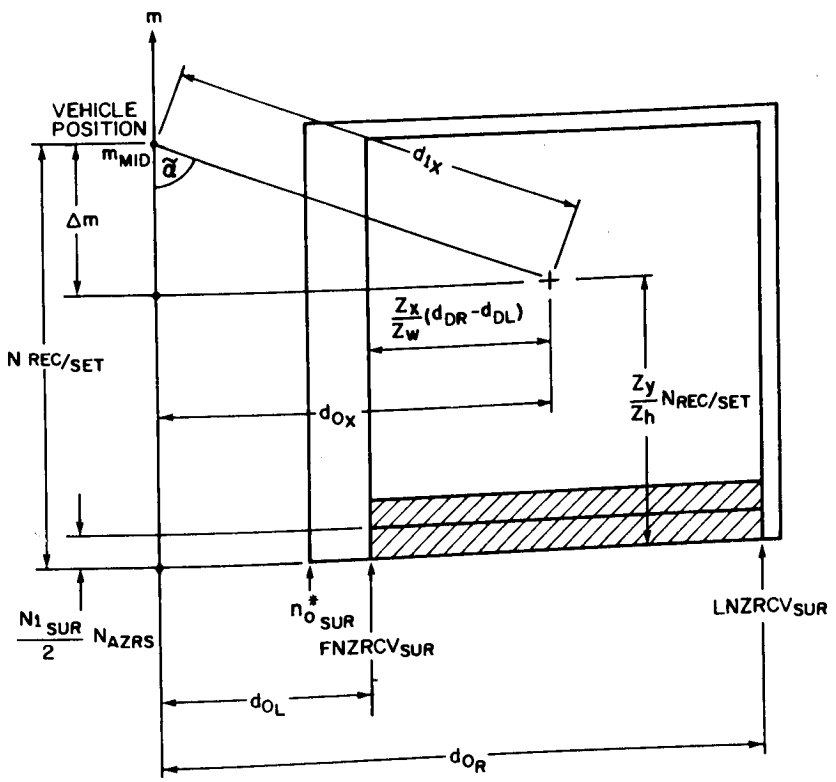

Figure 13. Location on survey-image of SEASAT scenes to be processed

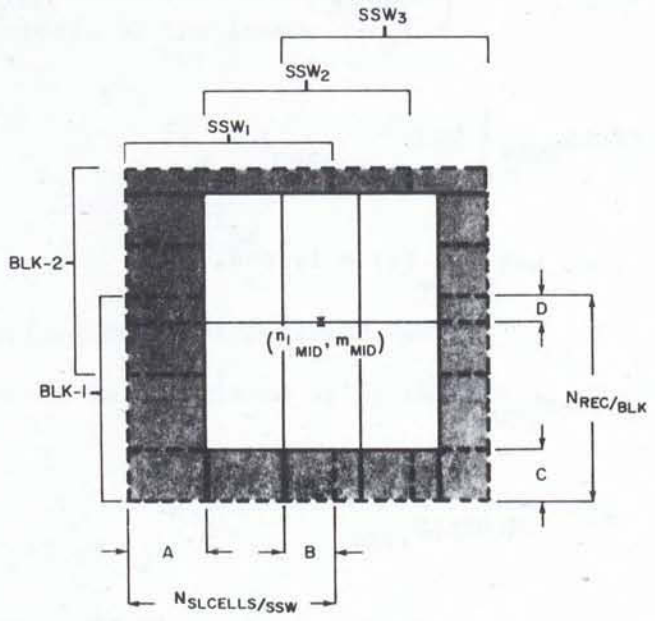

$$A = B + 2\ NOV_{L_{MODE}}$$

$$B = \frac{N_{SLCELLS/SSW} - N_{SLCELLS\ ADV}}{2}$$

$$C = D + NOV_{B_{MODE}}$$

$$D = \frac{N_{REC/BLK} - N_{REC\ ADV}}{2}$$

Figure 14. Overlap of swaths and blocks for located scene

The values of $n_{1_{ST}}$ (j) are passed by the Data Control Program, via the sub-task monitor, to the .CTX file for J7SE00, the program that does the unpacking. In addition the values of both $n_{1_{ST}}$ (j) and $n_{1_{END}}$ (j) are printed out on the data control forms.

The starting and ending tape and record numbers are calculated by:

1) finding the shift in records that exists between the record number calculated from the position measured on the photograph of the Survey-Mode image and the record number at which the data, from the centre of the azimuth phase history for that target, was actually acquired;

2) converting the vertical distance measured off the photograph of the Survey-Mode image into a record number in the data set;

3) finding the absolute starting and ending record numbers in the data set; and

4) converting these record numbers into relative starting and ending records and absolute starting and ending tape numbers. The relative

starting and ending record numbers are measured from the beginning of the starting and ending tape.

The absolute record numbers are measured from the beginning of the total tape set. There is a shift between the measured record number and the record number at which the data was acquired because the Survey-Mode image (as are all the other images) has been corrected so that the imagery will look as if it was acquired by a sidelooking SAR. However, the data is really acquired by a squinted SAR and therefore the data associated with a given position on the Survey-Mode image either occurs before or after the measured record number in the data set (see Figure 13). The shift is negative (data occurs after) if $0 \leq |\alpha| \leq \pi/2$, and is positive (data occurs before) if $\pi/2 < |\alpha| \leq \pi$. The record shift Δm is

$$\Delta m = -\frac{r_e}{\Delta x_o} \sin^{-1}\left\{\tan\left\{\cos^{-1}\left[\frac{\left(\frac{r_{1_x}}{r_e}\right)^2 - c_a^2 - c_b^2}{-2c_a c_b}\right]\right\} \Big/ \tan\tilde{\alpha}\right\} \tag{52}$$

This shift is used to correct the measured value of m as follows:

$$m_{MID} = \frac{Z_y}{Z_h} N_{REC/SET} + \Delta m - \frac{N_{1_{SUR}}}{2} N_{AZRS}, \tag{53}$$

where,

$$N_{REC/SET} = N_{REC/TAPE} (N_{TAPES} - 1) + N_{REC/LAST\ TAPE} \quad . \tag{54}$$

The shift $(N_{1_{SUR}}/2)N_{AZRS}$ is necessary to compensate for the wrap-around of $N_{1_{SUR}}/2$ Survey-Mode azimuth samples that occurs during the processing of the Survey-Mode imagery (see Section 4.4.5). The absolute starting and ending record numbers (m_{ST} and m_{END}) can then be found using the following algorithm:

1. $$m_{ST} = m_{MID} - \frac{N_{BLK}}{2} (N_{REC_{ADV}} - N_{OV_{B\ MODE}} N_{LKS_A}) \quad , \tag{55}$$

2. if $m_{ST} \leq 0$, set $m_{ST} = 1$, (56)

$$3.\quad m_{END} = m_{ST} + (N_{BLK}-1)N_{REC_{ADV}} + N_{REC/BLK} ,$$

and

$$4.\quad \text{if } m_{END} > N_{REC/SET}, \text{ set } m_{END} = N_{REC/SET} . \tag{58}$$

The values of m_{ST} and m_{END} are then used to find the starting and ending tape TP_{ST} and TP_{END}, and the starting record m'_{ST} relative to the start of TP_{ST} and the ending record m'_{END} relative to the start of TP_{END}. The starting tape number is

$$TP_{ST} = \underset{PART}{INTEGER}\left(\frac{m_{ST}-1}{N_{REC/TAPE}}\right) + 1 , \tag{59}$$

and the ending tape number is

$$TP_{END} = \underset{PART}{INTEGER}\left(\frac{m_{END}-1}{N_{REC/TAPE}}\right) + 1 . \tag{60}$$

The relative starting record m'_{ST} is

$$m'_{ST} = m_{ST} - N_{REC/TAPE}(TP_{ST}-1) , \tag{61}$$

and the relative ending record m'_{END} is

$$m'_{END} = m_{END} - N_{REC/TAPE}(TP_{END}-1) . \tag{62}$$

The values m'_{ST}, m'_{END}, TP_{ST} and TP_{END} are used by the Data Control Program in forming the operator run control sheets and the command files. The operator run control sheets are lists used by the operator. The command files are read by the sub-task Monitor, which has the capability of loading and starting tasks, assigning logical units, and outputting messages, such as 'MOUNT TAPE XXXX ON MT XX'. The combination of the sub-task Monitor and command files allows the automated running of the processor, and the automatic control of tape motion.

4.2.2 ERIM Sub-Swath Location Program

In some modes of operation the ERIM radar views the ground at a steeper angle (i.e., $\pi/2$ rad) than the SEASAT radar. This steep viewing angle causes the number of ground-range samples per slant-range sample to change very rapidly with ground-range. It was found that a fixed-overlap sub-swath location technique, such as that used for SEASAT was inadequate for the ERIM data. Instead, a variable overlap was used. The ERIM sub-swath location program calculates these overlaps so that a multiple sub-swath ERIM image can be processed with a minimum number of operations and with no gaps between the sub-swaths. File size limitations restrict the number of ground-range cells that can be output per sub-swath. The maximum number of slant-range cells that can be advanced per sub-swath is the lessor of: the number of slant-range cells advanced when the maximum number of ground-range cells that can be accommodated are produced; and the number of valid slant-range samples produced per sub-swath. The number of valid samples is defined as the number that remain when the range filter length is subtracted from the sub-swath width. The program must establish the maximum number of slant-range cells to advance, find the start of each sub-swath, and check that all the sub-swaths are completely contained within the data set.

The following parameters are required by the sub-swath location program:

1. From the operator's terminal:

h_s - the height of the aircraft,

t_D' - the time delay to the first slant-range sample,

$n_{1_{ST}}$ - the slant-range cell, in the input data, at which to start unpacking, and

MODE - X- or L-band;

2. From the DC00ERIM.CTX file:

$N_{GCELLS/SSW_{MAX}}$ - maximum number of ground-range samples per sub-swath, and

$N_{SLCELLS_{/REC}}$ - the total number of slant-range cells per record;

3. From the ERIM{MODE}.DAT file:

Δd_o - ground-range sample spacing, measured perpendicular to ground-track,

f_{SR} - range data sampling rate, and

τ - the transmitted pulsewidth;

4. From an internal data statement:

$N_{OV_{MODE}}$ - the sub-swath overlap for this mode.

The first step in finding the range sub-swath starting cells is the calculation of the length, N_R of the 2-D matched filter in range, i.e.,

$$N_R = \tau \, f_{SR} \quad . \tag{63}$$

Then, the slant-ranges to the start of the record and to the edge of the scene are found, i.e.,

$$r_{1_{ST_0}} = \frac{c}{2} t_D' \quad , \tag{64}$$

and,

$$r_{1_{edge}} = r_{1_{ST_o}} + n_{1_{ST}} \frac{c}{2f_{SR}} \quad . \tag{65}$$

If the distance to the edge of the scene is less than the aircraft height, i.e., if the digitization window has been set incorrectly, the start cell $n_{1_{ST}}$ must be adjusted to force $r_{1\ edge}$ to h_s, i.e., if $r_{1\ edge} < h_s$, then

$$n_{1_{ST}} = \left(h_s - \frac{c}{2} t_D' \right) \frac{2f_{SR}}{c} \quad , \tag{66}$$

and (65) is used to find $r_{1\ edge}$ again.

One more parameter, the maximum number of slant-range cells to be advanced per sub-swath, $N_{SLCELLS_{ADV}}$, must be calculated before the sub-swath location can begin. The parameter $N_{SLCELLS_{ADV}}$ is computed as follows:

$$N_{SLCELLS_{ADV}} = N_{GCELLS/SSW_{MAX}} - N_R - N_{OV_{MODE}} \tag{67}$$

The location of the range sub-swaths can now be done. Three arrays and one variable are computed:

$r_{1_{ST}}(i)$ - the slant range to the start of the sub-swath 'i';

$N_{SLCELLS/SSW}(i)$ - the number of slant-range cells contained in sub-swath 'i';

$N_{GCELLS/SSW}(i)$ - the number of ground-range cells contained in sub-swath 'i';

N_{SSW} - the number of sub-swaths required for the scene.

The calculation proceeds from near range to far range. The slant- and ground-ranges to the edge of the first swath are calculated, then for each swath in turn the values of $r_{1_{ST}}(i)$, $N_{SLCELLS/SSW}(i)$, and $N_{GCELLS/SSW}(i)$ are found. The algorithm used is as follows:

1. Reset the cumulative number of slant and ground-range cells per scene

$$N_{SLCELLS_{CUM}} = 0, \text{ and}$$

$$N_{GCELLS_{CUM}} = 0;$$

2. Set the value of

$$r_{1_{ST}}(1) = r_{1\ edge}\ ; \tag{68}$$

3. then, for each swath 'i' starting with i=2 and continuing up to i=100, unless the loop is exitted, do the following calculations:

   a) find the ground-range to the start of the next sub-swath with the assumption that $N_{GCELLS/SSW\ MAX}$ are advanced per swath, i.e.,

$$d_{1_{TEMP}} = \sqrt{r_{1_{ST}}^2(i-1) - h_s^2} + N_{GCELLS/SSW\ MAX}\ \Delta d_o; \tag{69}$$

b) use $d_{1_{TEMP}}$ to find $r_{1_{ST}}(i)$, allowing for an overlap,

$$r_{1_{ST}}(i) = \sqrt{d^2_{1_{TEMP}} + h_s^2} - N_{OV_{MODE}} \frac{c}{2f_{SR}} \tag{70}$$

c) check if

$$r_{1_{ST}}(i) > [r_{1_{ST_o}} + (N_{SLCELLS/REC} - N_{GCELLS/SSW_{MAX}})\frac{c}{2f_{SR}}] ,$$

i.e., check to see if the starting slant-range is beyond the last permissible starting slant-range, and if it is, set the starting slant-range to the maximum allowable,

$$r_{1_{ST}}(i) = r_{1_{ST_o}} + (N_{SLCELLS/REC} - N_{GCELLS/SSW_{MAX}})\frac{c}{2f_{SR}} , \tag{71}$$

and then set a flag IEND=1 to indicate that an end condition has been reached;

d) calculate the number of slant-range cells in the sub-swath

$$N_{SLCELLS/SSW}(i-1) = (r_{1_{ST}}(i) - r_{1_{ST}}(i-1)) \Big/ \frac{c}{2f_{SR}} ; \tag{72}$$

e) save this value of $N_{SLCELLS/SSW}(i-1)$, i.e.,

$$N_{SLCELLS/SSW} = N_{SLCELLS/SSW}(i-1) ; \tag{73}$$

f) check if the number of slant-range cells is greater than the maximum number allowed, if so, set $N_{SLCELLS/}(i-1)$ to the maximum allowed, i.e., if $N_{SLCELLS/SSW}(i-1) > N_{SLCELLS/SSW\ MAX}$, then

$$N_{SLCELLS/SSW}(i-1) = N_{SLCELLS/SSW\ MAX} ; \tag{74}$$

g) check if the number of cells has been modified; if it has adjust $r_{1_{ST}}(i)$, i.e., if $N_{SLCELLS/SSW} \neq N_{SLCELLS/SSW}(i-1)$, then

$$r_{1_{ST}}(i) = N_{SLCELLS/SSW}(i-1)\,\frac{c}{2f_{SR}} + r_{1_{ST}}(i-1)\ . \tag{75}$$

h) calculate the ground-range to the start of this sub-swath,

$$d_{1_{ST}}(i) = \sqrt{\left[r_{1_{ST}}(i) + \frac{c}{2f_{SR}}\,N_{OV_{MODE}}\right]^2 - h_s^2}\ ; \tag{76}$$

i) calculate the number of ground-range samples advanced for sub-swath 'i-1',

$$N_{GCELLS/SSW}(i-1) = \frac{d_{1_{ST}}(i) - d_{1_{ST}}(i-1)}{\Delta d_o}\ ; \tag{77}$$

j) reset $d_{1_{ST}}(i-1)$ to $d_{1_{ST}}(i)$;

k) calculate the cumulative numbers of slant- and ground-range cells for the sub-swaths located thus far, i.e.,

$$N_{SLCELLS/CUM}(i) = N_{SLCELLS/CUM}(i-1) + N_{SLCELLS/SSW}(i-1)\ , \tag{78}$$

and

$$N_{GCELLS/CUM}(i) = N_{GCELLS/CUM}(i-1) + N_{GCELLS/SSW}(i-1)\ ; \tag{79}$$

l) update the number of swaths,

$$N_{SSW} = i-1\ ; \tag{80}$$

and

m) check if an end condition has occurred, i.e., if lEND=1 exit loop, otherwise go to a);

4. Output a table of values of i, $r_{1_{ST}}(i)$, $N_{SLCELLS/SSW}(i)$, $N_{GCELLS/SSW}(i)$, $N_{SLCELLS/CUM}(i)$, $N_{GCELLS/CUM}(i)$; and

5. Pass the values, $r_{1_{ST}}(i)$, $N_{SLCELLS/SSW}(i)$, $N_{GCELLS/SSW}(i)$ and N_{SSW} back to J7DC00.

The value $r_{1_{ST}}(1)$ is used by J7DC00 in the creation of the $E\begin{Bmatrix}EX\\EL\end{Bmatrix}$.9999A.EFD file which contains t'_D, $n_{1_{ST}}$, and h_s. The array $r_{1_{ST}}(i)$ is used to calculate an array of slant-range increments $[r_{1_{ST}}(i) - r_{1_{ST}}(i-1]$ which in turn is used to update the slant-range to the middle of the sub-swath, $\tilde{r}_1$ contained in the ERIM.FPM file, produced by J70R01. The updating is done after each sub-swath in the scene is processed.

4.3 THE SAR PROCESSOR PART 1 (J7SE00, J7RE00, J7SE01)

This section describes the portion of the SAR processor that performs the data unpacking, the two-dimensional FFT, the optional range-offset to base-band demodulation, the look extraction, and the multiplication of the frequency-domain data for each look by the frequency-domain filter for that look. During an actual processing run the filter generation (J7SE30) is done before the above steps. In the following, the order of description has been reversed so that J7SE00, J7RE00 and J7SE01 are described first. This has been done so that the reader can more easily understand, by following the processing steps the radar data goes through before the filter is applied, why the two-dimensional reference function has the form it does. The section begins with a description of the received radar signal, and then continues with the range FFT, the optional range-offset to baseband demodulation, the azimuth FFT and look extraction, and ends with the filter multiply.

4.3.1 The Form of the Input Data

As was explained in Section 2.1 the received signal can be considered to be two-dimensional. The range signal characteristics are determined by the modulation on the transmitted signal, and the azimuth characteristics are determined by the modulation induced on the coherent carrier signal by the Doppler effect.

The transmitted signal is pulsed at the PRF, which in effect samples the azimuth signal at the PRF and causes the Doppler (azimuth) spectrum to be repeated with the multiples spaced at the PRF. The radar squint causes the centre of the azimuth spectrum to be shifted away from zero Doppler frequency to some other value, possibly several multiples of the PRF away. Therefore, the signal contained between +PRF and -PRF is sometimes a multiple of the basic spectrum.

In the radar receiver the signal is converted to one of three forms: baseband, range-offset or azimuth-offset. The two-dimensional signal spectrum for each of the three signal types is shown in Figure 15. The range-offset and the baseband spectra are similar in form, whereas the azimuth-offset spectrum is different in that the effect of squint has been removed. The RF-signal used to form the azimuth-offset spectrum is shown in Figure 16. The signal undergoes a demodulation along the f_m (Doppler) axis before it is collapsed to the azimuth-offset form. This demodulation shifts sidebands of the Doppler spectrum by $f_D - f_{o_A}$ and $f_D + f_{o_A}$ so that the centres of the upper and lower Doppler spectrum sidebands lie at $+f_{o_A}$ and $-f_{o_A}$. The demodulation also shifts the spectrum in range so that it is centred about zero range frequency.

The SAR processor requires the data to be in complex format. For certain data types such as ERIM, the data is recorded as a baseband signal and therefore no further conversion is necessary. For SEASAT data, which is recorded as a range-offset signal, a conversion to baseband must be done. The processor has a parameter in the .CTX file for J7SE00, which can be set to turn on the range-offset to baseband conversion. If the parameter is not set, no conversion is done and that part of the processor software is skipped. A second parameter in the .CTX file provides the line number (the equivalent of the range-offset frequency f_{o_R} in Figure 15(b) about which the demodulation must be done.

If the data is in azimuth-offset format a real-to-complex FFT is still used for the range signal and a complex-to-complex FFT is still used for the azimuth signal. However, the range FFT is half the length used for range-offset data and the azimuth FFT is twice the length used for the range-off-set data.

In order to illustrate the demodulation process the equations for the radar signal, returned from a unity reflection coefficient point target are given. The antenna weighting is assumed to be rectangular and of length $N_1 \Delta x_o$ at range r_1. The signal modulation is assumed to be linear FM. For a target at range r_1 the received range-offset signal $g_{RO}(t)$ is

$$g_{RO}(t',m) = \mathrm{Re}\left\{ \mathrm{Rect}\left(\frac{t'-t_1'(m) - \frac{\tau}{2}}{\tau}\right) \mathrm{Rect}\left(\frac{m}{N_1}\right) \right.$$

$$\left. \exp\left\{ j\left[2\pi f_{o_R} t' - 2\pi \frac{c}{\lambda} t_1'(m) \right] \right\} \right.$$

$$\exp\left\{j\left[\phi_\Gamma + \frac{K}{2}\left(t' - t_1'(m) - \frac{\tau}{2}\right)^2\right]\right\}, \tag{81}$$

where ϕ_Γ is the phase of the signal at $t'=0$, and

$$t_1'(m) = \frac{2r_1(m)}{c}, \tag{82}$$

where,

$$r_1(m) = a_0 + a_1\, m\Delta x_o + a_2(m\Delta x_o)^2, \tag{83}$$

and,

$$a_0 = r_1(0), \tag{84}$$

$$a_1 = \frac{r_e}{r_1(o)}\,\frac{c_a \sin\theta_r}{\tan\alpha}, \tag{85}$$

$$a_2 = \frac{1}{2r_1(o)}\left\{\frac{c_b^2+c_a^2}{2} - \frac{1}{2}\left[\frac{r_1(o)}{r_e}\right]^2 - a_1^2\right\}^2, \tag{86}$$

and

$$\sin\theta_r = \sin\alpha\left\{1-\left[\frac{\left(\frac{r_1(o)}{r_e}\right)^2 - c_a^2 - c_b^2}{-2c_a c_b}\right]^2\right\}^{\frac{1}{2}}. \tag{87}$$

The range-offset signal is sampled at a rate f_{SR}, consistent with its bandwidth, to obtain the digital data. This sampling, if done properly, allows one to write t' as $n_{RO}\Delta t'/2$, where n_{RO} is the range-offset (real) sample number measured from the edge of the digitization window t_D', and $\Delta t'$ is twice the sampling interval of the range-offset data. After sampling, (81) can be rewritten as

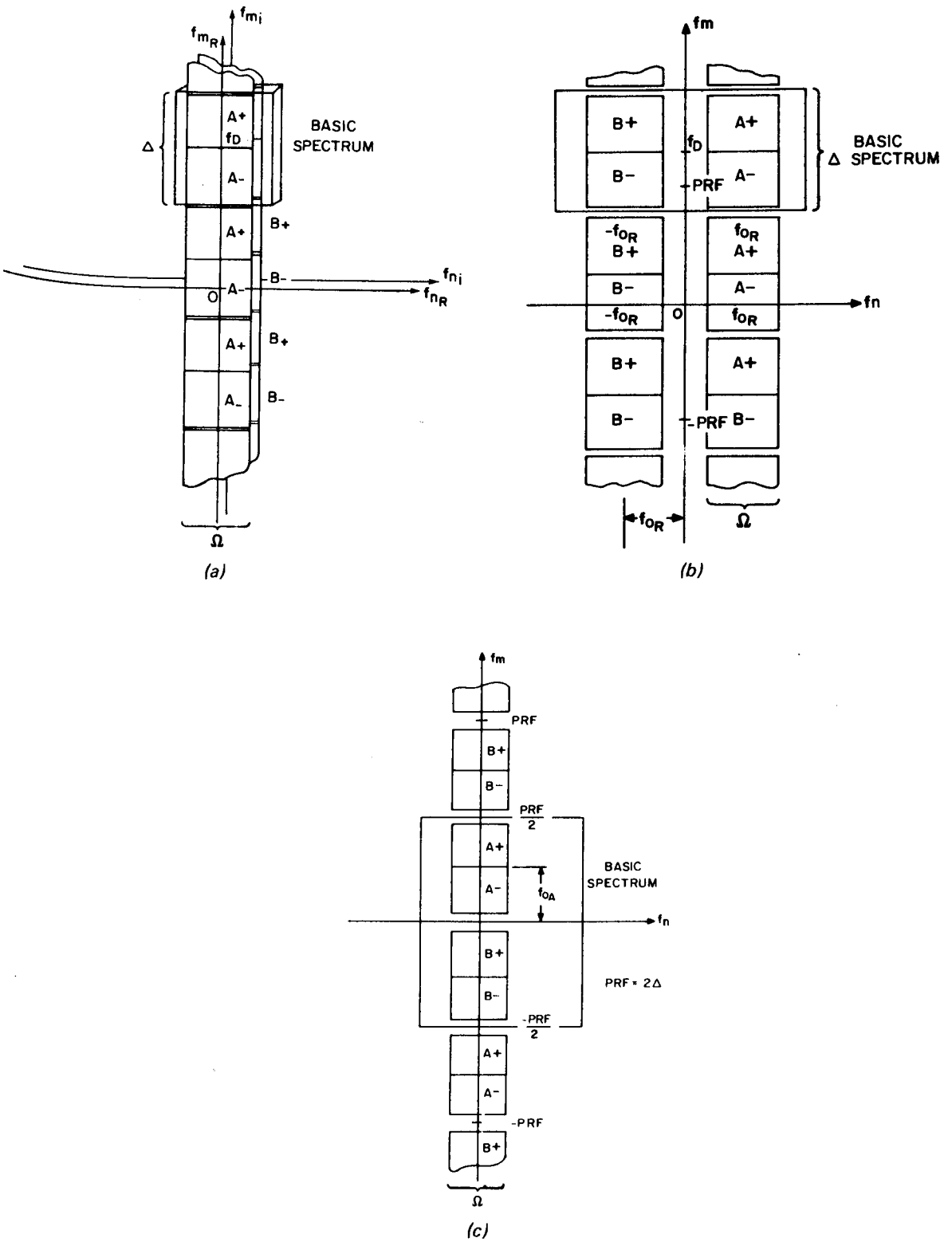

Figure 15. Form of the baseband, range-offset, and azimuth-offset spectra

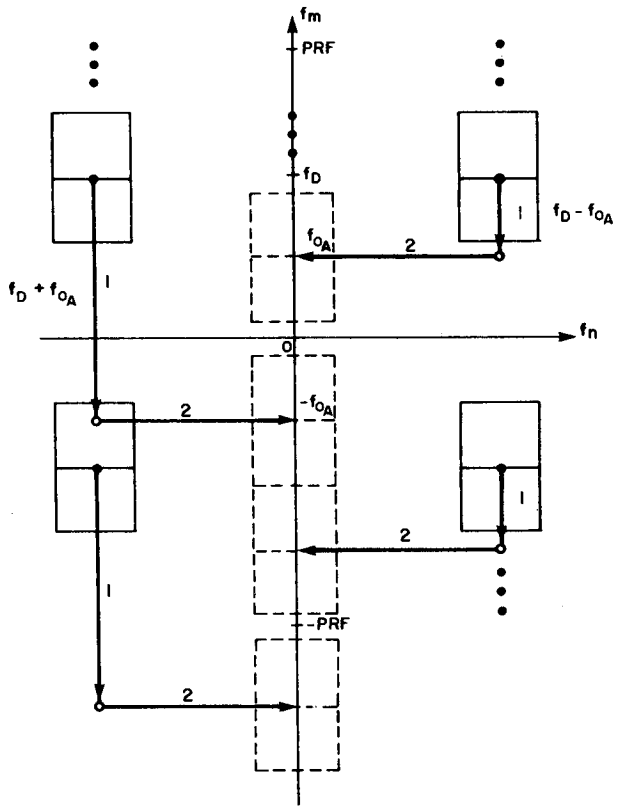

Figure 16. Formation of the azimuth-offset spectrum

$$g_{RO_s}(n_{RO},m) = \mathrm{Re}\left\{\mathrm{Rect}\left(\frac{\frac{n_{RO}\Delta t'}{2} - t_1'(m) - \frac{N_R\Delta t'}{2}}{N_R\Delta t'}\right)\right.$$

$$\mathrm{Rect}\left(\frac{m}{N_1}\right)\exp\left\{j\left[\pi f_{o_R} n_{RO}\Delta t' - 2\pi\frac{c}{\lambda}t_1'(m)\right]\right\}$$

$$\left.\exp\left\{j\left[\phi_\Gamma + \frac{K}{2}\left(\frac{n_{RO}\Delta t'}{2} - t_1'(m) - \frac{N_R\Delta t'}{2}\right)^2\right]\right\}\right\} , \qquad (88)$$

where N_R is given by (63), and $\Delta t'$ by (30) with $N_{RRS}=1$. N_1 is specified in Section 4.4.

For comparison, the baseband equivalent of (88) is

$$g_{BB_S}(n,m) = \text{Rect}\left(\frac{n\Delta t' - t_1'(m) - \frac{N_R\Delta t'}{2}}{N_R\Delta t'}\right)$$

$$\text{Rect}\left(\frac{m}{N_1}\right)\exp\left\{j\left[-2\pi\,\frac{c}{\lambda}\,t_1'(m)\right]\right\}$$

$$\exp\left\{j\left[\phi_\Gamma + \frac{K}{2}\left(n\Delta t' - t_1'(m) - \frac{N_R\Delta t'}{2}\right)^2\right]\right\}, \qquad (89)$$

where n is the baseband (complex) sample number measured from the edge of the digitization window t_D', and $\Delta t'$ is the sampling interval of the complex data.

The azimuth-offset signal, comparable to (88) and (89), is

$$g_{AO_S}(n,m_{AO}) = RE\left\{\text{Rect}\left(\frac{n\Delta t' - t_1'\left(\frac{m_{AO}}{2}\right) - \frac{N_R\Delta t'}{2}}{N_R\Delta t'}\right)\right.$$

$$\text{Rect}\left(\frac{m_{AO}}{2N_1}\right)\exp\left\{j\left[\pi\, f_{o_A}\,\frac{m_{AO}\Delta x_o}{V_{eq}} - \frac{2\pi c}{\lambda}\,t_1'\left(\frac{m_{AO}}{2}\right)\right.\right.$$

$$\left.\left.\left. + \pi f_D\left(\frac{m_{AO}\Delta x_o}{V_{eq}}\right)\right]\right.\right.\exp\left.\left.\left.j\left[\phi_\Gamma + \frac{K}{2}\left(n\Delta t' - t_1'\left(\frac{m_{AO}}{2}\right) - \frac{N_R\Delta t'}{2}\right)^2\right]\right\}\right. \qquad (90)$$

where m_{AO} is the azimuth-offset (real) record number measured from the centre of the synthetic-aperture, Δx_o is twice the azimuth-offset sample spacing on the ground, and f_{o_A} is the azimuth-offset frequency. The frequency f_D is the Doppler centre frequency when the antenna pointing angle is α.

4.3.2 Description of J7SE00

4.3.2.1 Unpacking

For both ERIM and SEASAT the data are provided as packed integer words. The first processing step is to unpack the data and convert them to 32-bit floating-point words.

4.3.2.2 Range FFT

The next processing step is the calculation of the discrete Fourier transform (DFT) of the input range signal. This is done by computing the Fast Fourier transform (FFT) of each record of the input data block. The length of the FFT is specified by L_R, a parameter in the .CTX file for J7SE00. A real-to-complex FFT is used for range-offset and azimuth-offset input data and a complex-to-complex FFT is used for baseband input data. The type of FFT to use is also specified by a parameter in the .CTX file. In equation form, the DFT of (88) is

$$G_{RO_S}(f_{n_{RO}},m) = \sum_{n_{RO}=0}^{2L_R-1} g_{RO_S}(n_{RO},m)\, e^{-j\frac{2\pi n_{RO} f_{n_{RO}}}{2L_R}}, \quad f_{n_{RO}} \neq 0 ,$$

and

$$= 0 \qquad f_{n_{RO}} = 0 , \tag{91}$$

where $f_{n_{RO}}$ is the range-frequency line number in range-offset frequency samples and $2L_R$ is the real-to-complex FFT length (see Figure 17). Similarly, the DFT of the baseband signal is

$$G_{BB_S}(f_n,m) = \sum_{n=0}^{L_R-1} g_{BB_S}(n,m)\, e^{-j\frac{2\pi n f_n}{L_R}}, \quad f_n \neq 0 ,$$

and

$$= 0, \qquad f_n = 0 , \tag{92}$$

where f_n is the baseband frequency line number and L_R is the length of the complex-to-complex FFT. To obtain the DFT of the azimuth-offset signal $G_{AO_S}(f_n,m_{AO})$ simply replace $g_{BB_S}(n,m)$ by $g_{AO_S}(n,m_{AO})$ in (92). Note that in all three cases the dc term in the spectra is set to zero to remove any bias on the input signal.

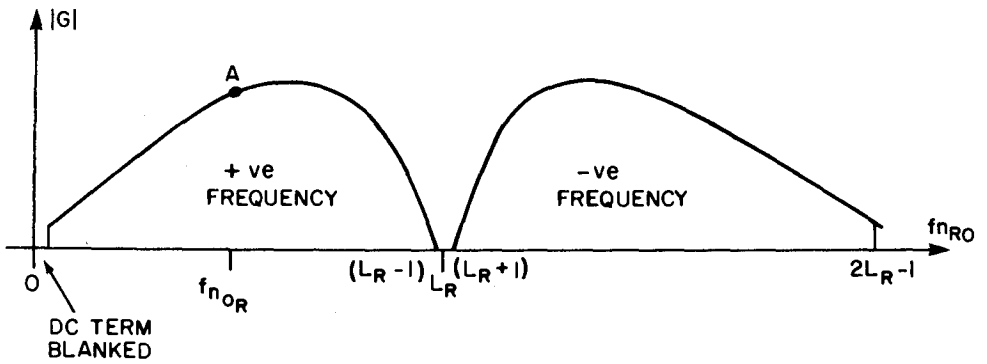

Figure 17. Magnitude of DFT of range-offset signal

4.3.2.3 Range-Offset to Baseband Demodulation and dc Bias Removal

The process used to convert the real, range-offset signal to a complex, baseband signal is described in Ref. 12. The first step is the computation of the pre-envelope $\Psi_{RO}(f_{n_{RO}},m)$ of (91). The pre-envelope is computed by blanking out the upper half of the DFT (see Figure 18), and then doubling the amplitudes of the lower frequencies, i.e.,

$$\Psi_{RO}(f_{n_{RO}},m) = 2\, G_{RO_S}(f_{n_{RO}},m), \quad 1 < f_{n_{RO}} < L_R$$

$$= 0 \qquad\qquad , \quad L_R-1 < f_{n_{RO}} < 2L_R-1 \ . \tag{93}$$

Normally the real-to-complex FFT only computes the first half of the FFT and the blanking step is not actually performed. The baseband signal spectrum $G_{BB_S}(f_n,m)$ is obtained by shifting the pre-envelope as follows (see Figure 19):

$$G_{BB_S}(f_n,m) = \Psi_{RO}(f_{n_{0_R}} + f_{n_{RO}},m) \ , \tag{94}$$

where,

$$f_{n_{0_R}} = \frac{f_{0_R}}{f_{SR}} L_R \ . \tag{95}$$

With the exception that any dc bias on the signal has been removed, (94) is the DFT of (89). Note that the sampling rate has been reduced by a factor of two by blanking the upper frequencies in the original spectrum and retaining only half the samples. No information is lost since the time-domain signal corresponding to (95) now contains L_R complex samples instead of $2L_R$ real samples.

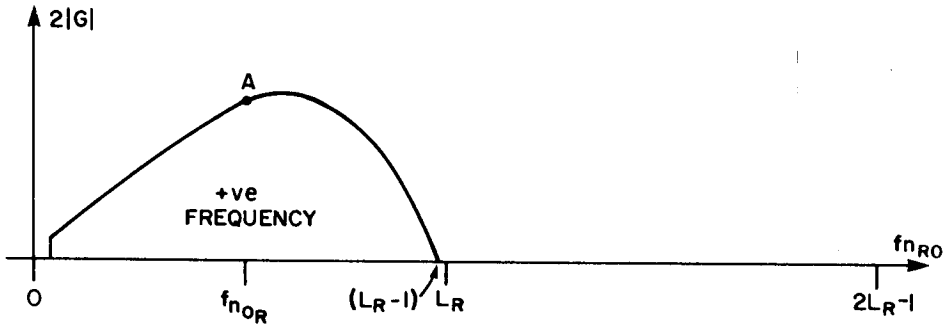

Figure 18. Magnitude of pre-envelope of baseband signal

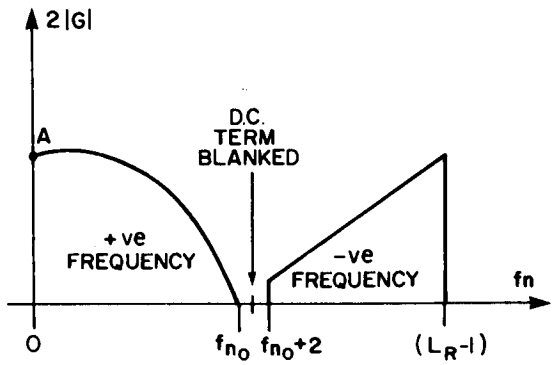

Figure 19. Magnitude of DFT of baseband signal

4.3.2.4 Range Sampling Rate Reduction

For some processing modes, such as the SEASAT Survey-Mode, the range sampling rate is reduced further during the conversion from G_{RO_S} to G_{BB_S}. Any power of 2 reduction is possible. The sampling rate reduction is done by blanking out the centre section of the baseband spectrum and sliding the two ends of the spectrum together to make a new shorter FFT (see Figure 20) (see Section 4.3.4 for comment on appropriateness of this technique).

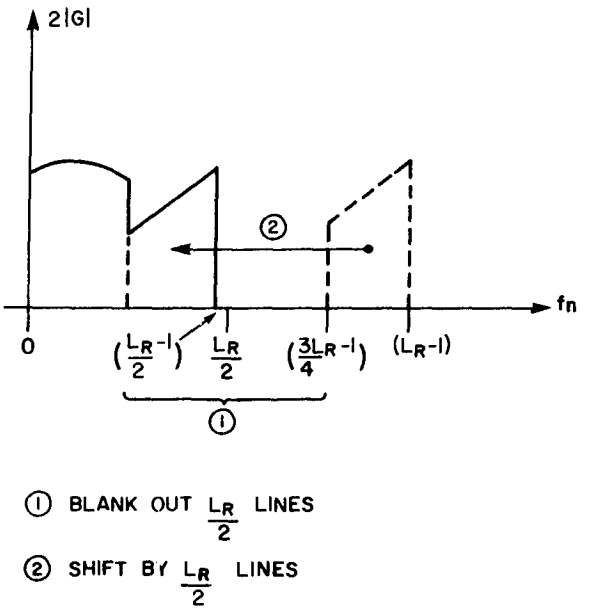

Figure 20. Range sampling rate reduction

4.3.2.5 Range-Look Extraction (not implemented - August 1980)

For each range-look to be processed a different, possible overlapping section of the baseband spectrum vector in Figure 19 is read into a new shorter 'look-vector', (see Figure 21). The line numbers ($LNOM_{R_p}$), which designate the centres of the groups of lines to be extracted for each of the range-looks, are calculated in the filter generation program J7SE30 and passed to J7SE00 via the .LN0 file. Each of the new look-vectors form part of a range-look file. Each range-look file is then sequentially passed through the remaining processing steps. When this feature is actually implemented the shifting required for the range-offset demodulation can be combined with the look extraction (see also comments in Section 4.3.4 and 4.3.5.2 with reference to the appropriateness of this technique).

4.3.3 Transpose

The matrix transpose turns the array so that, for baseband signals,

$$G^{T}_{BB_S}(f_n,m) = G_{BB_S}(m,f_n) \quad . \tag{96}$$

For azimuth-offset signals the appropriate equation is

$$G^{T}_{AO_S}\left(f_n, \frac{m_{AO}}{2}\right) = G_{AO_S}\left(\frac{m_{AO}}{2}, f_n\right) . \tag{97}$$

The transpose used is a modified form of the one described in Refs. 13, 14. All block sizes in the processor are chosen such that their lengths are powers of 2. Non-square blocks are decomposed into square ones. Each square block is transposed separately, and then assembled with other transposed square blocks to form the desired non-square transpose. For further details of the software implementation see Ref. 15.

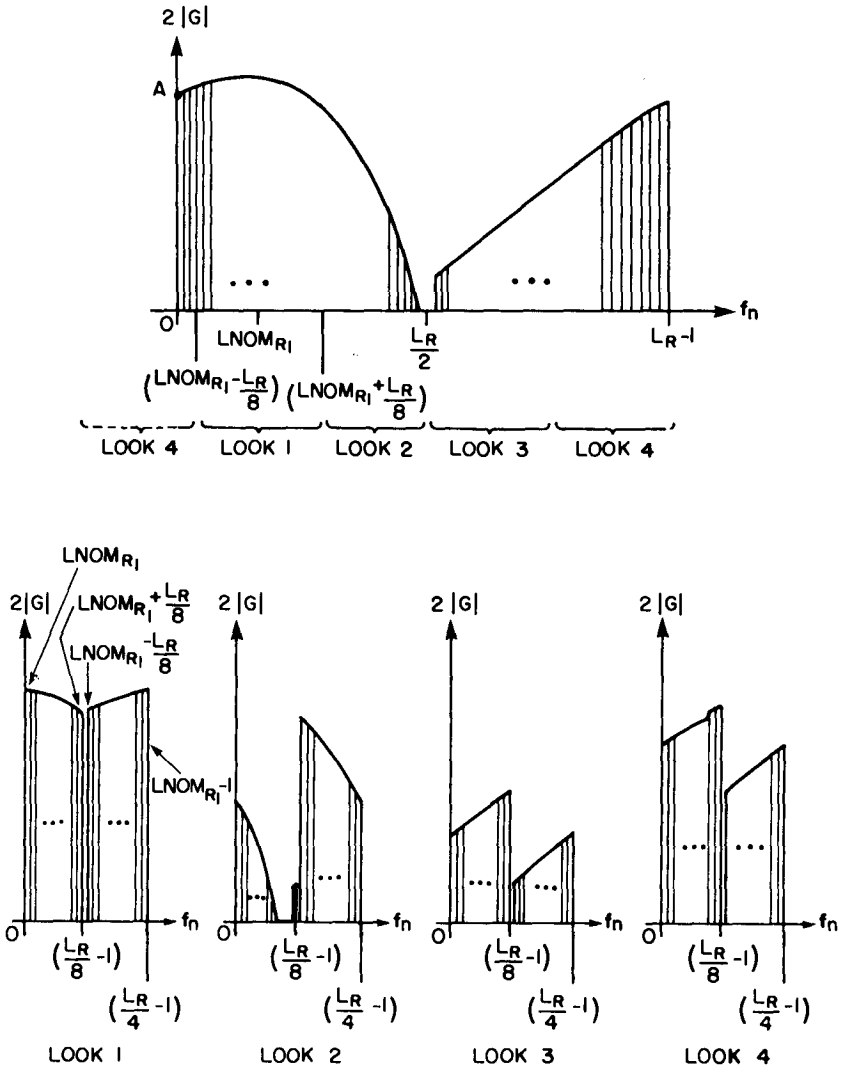

Figure 21. Range-look extraction

4.3.4 Resampling of Azimuth Data (J7RE00) - SEASAT Survey-Mode Only

The SEASAT Survey-Mode is used to produce a low resolution, quick-look, image of a total SEASAT scene, composed of 8 tapes of 4096 azimuth records, each of which is 13680 real, range samples long. Space limitations, and other factors such as processing speed were taken into consideration and it was decided that the Survey-Mode output image would have 100 m x 100m resolution with a pixel size of approximately 65.6m. This meant that the final processing block size could be kept to 4096 (real) range x 2048 azimuth samples. In order to reduce the block of 13680 (real) range x 32768 azimuth samples to the above size, the data had to be resampled. The range sampling, which has already been described in Section 4.3.2.4 is the simpler of the two required operations. The azimuth resampling is more complicated in that the azimuth spectrum is centred about $f_m=f_D$, not $f_m=0$ (see Figure 15(a)); and it is not possible to get all of the azimuth records on the 67 Mbyte disc at once (the maximum number of full length azimuth records that it is possible to store at once is 2048). It is possible to follow the approach used for the range data, but with the low-pass filter replaced by a bandpass filter centred at f_D, however the filter centre frequency would have to be changed whenever f_D changed.

The approach used here is to translate (demodulate) the azimuth spectrum by f_D so that it is centred at zero frequency, and then to low-pass filter the signal by blanking out the higher frequencies in the spectrum. The details of the technique are shown in Figure 22.

1) the FFT of the azimuth signal is computed;

2) the data is demodulated, i.e., the FFT lines are shifted by $LNOM_{SM}$, which is read from the .REC file;

3) the middle lines of the FFT are zeroed;

4) the inverse-FFT is computed; and

5) every $N_{ARS}{}^{th}$ sample is transferred to the output signal vector*.

This type of filter corresponds to a sub-optimum low-pass FIR filter designed by the frequency sampling technique. The transfer function is well defined only at the FFT frequency samples. In between these samples the response is poor and not equal ripple. The group-delay characteristics of the filter are poor and therefore degradation of the phase characteristics of the time-domain signal occurs. This phase degradation can be troublesome, especially since the azimuth signal has to be resampled as 16 blocks of 2048 samples and not as a single large block. Each block of 2048 samples is reduced to 128 samples and the 16 blocks of 128 samples are assembled in the time-domain for input into J7SE01. In addition, if large phase jumps are introduced

---

* A shorter FFT could also be used in place of steps 4) and 5).

are introduced at the block boundaries, they could contribute to the degradation of the Survey-image. However, it was discovered by testing that this was not a problem for the low time-bandwidth products of the Survey-Mode azimuth signals.

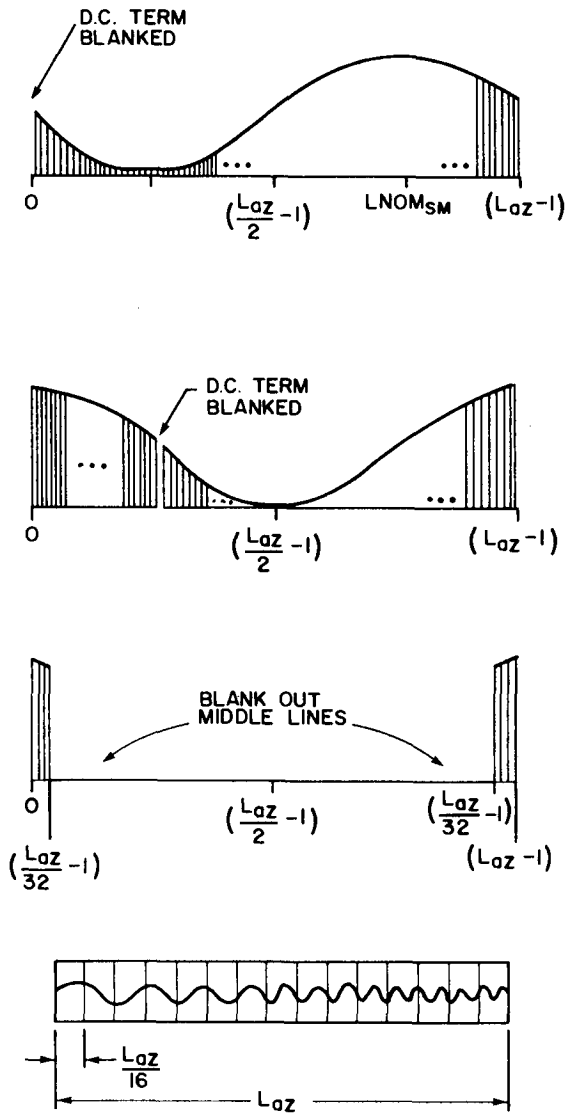

Figure 22. Azimuth sampling rate reduction

For reconstruction of high time-bandwidth product signals it would be advisable to use a finite impulse-response (FIR) low-pass filter with effectively zero response in the stop-band. The low-pass filtered signal could then be resampled by a factor of 16, the invalid samples (i.e., the first M samples, where M is the impulse-response length) removed, and then the next block, which overlaps the one before by M samples, could be processed and concatenated with the previous ones.

If there are insufficient input data tapes to fill the 2048 output resampled data block the procedure ZER0128 is used to fill the remaining space in the block with zeroes. The procedure is run once for every missing output data sub-block of 128 records.

At present (August 1980) there is no provision for resampling in the azimuth-offset dimension. However, it would be relatively easy to replace the lines of code in J7SE00 (Sections 4.3.2.3, and 4.3.2.4) that do the range-offset to baseband conversion, and the range resampling, and to modify the value of $LNOM_{SM}$ so that it is consistent with the azimuth-offset signal, i.e., multiply $LNOM_{SM}$ by two.

4.3.5 Description of J7SE01

In the program J7SE01 the following operations are performed: azimuth FFTs; azimuth-look extraction; multiplication of the frequency-domain data, for each look, by the 2-D FFT of the appropriate reference function (impulse-response of the matched filter); and the azimuth inverse-FFTs for each azimuth-look. Each range-look file is passed through the processor sequentially. As the range-look goes through J7SE01 it is divided into a set of azimuth-looks associated with that range-look. The azimuth-looks are then passed through the remainder of the processor one by one.

4.3.5.1 Azimuth FFTs

Either one of two lengths of azimuth FFTs are required at this stage in the processor. A complex-to-complex FFT of length L_{AZ} is used for the baseband data, whereas a complex-to-complex FFT of length $2L_{AZ}$ is used for the azimuth-offset data. The 2-D DFT of the baseband data for range-look 'p' is calculated from G_{BB_S} as follows:

$$\overline{G}_{BB_{S_p}}(f_m,f_n) = \sum_{m=0}^{L_{AZ}-1} G_{BB_{S_p}}(m,f_n)\, e^{-j\frac{2\pi f_m m}{L_{AZ}}}, \quad f_m \neq 0,$$

and

$$= 0, \quad f_m = 0, \tag{98}$$

where f_m is the baseband azimuth frequency, and L_{AZ} is the length in complex elements of the processing block along the azimuth direction. Similarly, the 2-D DFT of the azimuth-offset data is calculated from G_{AO_S}, i.e.,

$$\overline{G}_{A0_{S_p}}(f_{m_{A0}},f_n) = \sum_{m_{A0}=0}^{2L_{AZ}-1} G_{A0_{S_p}}(m_{A0},f_n)\, e^{-j\frac{\pi f_{m_{A0}} m_{A0}}{L_{AZ}}},$$

and

$$= 0 , \qquad f_{m_{A0}} = 0 , \tag{99}$$

where $2L_{AZ}$ is the length in complex elements of the processing block along the azimuth direction. The dc term in both $\overline{G}_{A0_{S_p}}$ and $\overline{G}_{BB_{S_p}}$ is blanked out to remove any bias on the signal.

4.3.5.2 Azimuth-Look Extraction

The mechanics of the azimuth-look extraction process are the same irrespective of the type of data used. A set of azimuth FFT line numbers, which serve as indices to $\overline{G}_{A0_{S_p}}$ or $\overline{G}_{BB_{S_p}}$, are calculated in the matched filter generation program (J7SE30), (see Section 4.4). These line numbers, denoted by $LNOM_{A_q}$, where 'q' denotes the azimuth look number, are passed from J7SE30 to J7SE01 by means of a .LNO file.

The procedure for azimuth-look extraction is shown in Figure 23. In the example shown in the figure, four azimuth-looks, i.e., $N_{LKS_A}=4$, are extracted from the azimuth dimension of the 2-D FFT of the baseband signal. Starting at $LNOM_{A_1}$, in the f_m dimension of $\overline{G}_{BB_{S_p}}(f_m,f_n)$, $L_{AZ_q}/2$ samples, where L_{AZ} is the length of the processing block in azimuth for a single look, are extracted from the azimuth FFT and written into locations 0 to $(L_{AZ_q}/2 - 1)$ of the multilook vector, then the samples from $LNOM_{A_1} - L_{AZ_q}/2$ to $LNOM_{A_1}-1$ are written into locations $L_{AZ_q}/2$ to $L_{AZ_q}-1$ in the multilook vector. This procedure is repeated for each look. If the look extraction procedure runs out of samples, at either end of the azimuth FFT vector before all L_{AZ_q} samples have been transferred, then the extraction process wraps around the FFT in a circular fashion and the required samples are taken from the other end of the FFT, i.e., if sample $L_{AZ}+2$ is required then sample 2 is read, and if sample -2

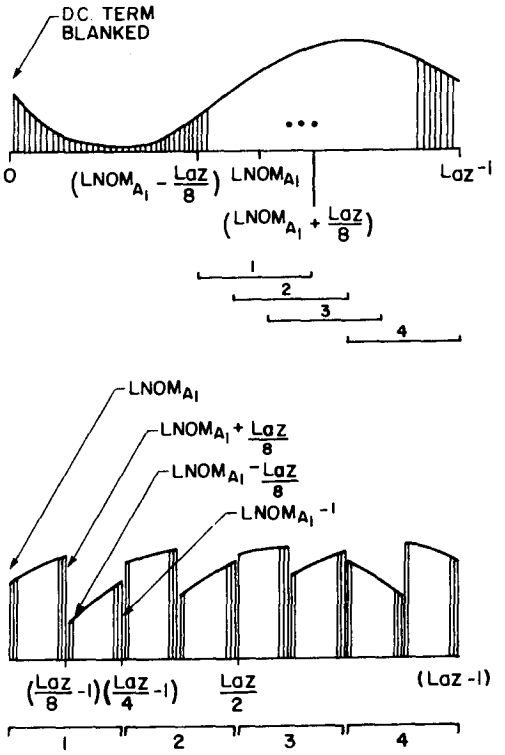

Figure 23. Azimuth-look extraction

is required then sample $L_{AZ}-2$ is read. A window, which is combined with the 2D-FFT of the reference function is later applied to the extracted data to improve the frequency response of the low-pass filter implemente d by means of the FFT (see also comments in Section 4.3.4).

The only restrictions on the process are: 1) the length of each look must be a power of 2, and 2) the product $N_{LKS}L_{AZ_q}$ must be less than or equal to L_{AZ}. In theory each look could be longer than L_{AZ}/N_{LKS_A}, as long as the length was a power of 2, but practical constraints such as the size of the available disc storage have forced the decision to restrict $L_{AZ_q} \leq L_{AZ}/N_{LKS_A}$. The looks do not have to be independent; the $LNOM_{A_q}$'s can be selected by appropriate choice of $\rho_{az_{1q}}$, such that overlapped looks are extracted (see Section 4.4).

The azimuth-offset signal must also be converted to baseband as part of the look extraction process. In a similar fashion as for the range-offset signal (Sections 4.3.2.2 and 4.3.2.3), the upper half of the FFT of the azimuth-offset signal is set to zero, and the amplitude of the lower half is doubled. In equation form the pre-envelope of the baseband signal, derived from the azimuth-offset signal, is

$$\Psi_{AO_p}(f_{m_{AO}},n) = 2\,\overline{G}_{AO_{S_p}}(f_{m_{AO}},n), \qquad 1 < f_{m_{AO}} < L_{AZ}$$

$$= 0 \qquad , \qquad L_{AZ}-1 < f_{m_{AO}} < 2L_{AZ}-1 . \tag{100}$$

If no look extraction were to be done, the baseband signal spectrum would be obtained by shifting the pre-envelope as follows:

$$\overline{G}_{BB_{S_p}}(f_m,f_n) = \Psi_{AO_p}(f_{m_{0_A}} + f_{m_{AO}},f_n) , \tag{101}$$

where

$$f_{m_{0_A}} = \frac{f_{0_A}}{PRF} L_{AZ} . \tag{102}$$

In cases with look extraction, the look extraction and azimuth-offset to baseband demodulation can be combined by merely altering the $LNOM_{A_q}$ values passed via the .LNO file. The values are adjusted so that the group of $LNOM_{A_q}$ line numbers are centred about the line number corresponding to f_{0A} instead of that corresponding to f_D.

4.3.5.3 Filter Multiply

After look extraction there are N_{LKS_A} sets of files containing the 2-D FFTs of the range- and azimuth-looks. Each set corresponds to an azimuth-look and contains the range-looks associated with that azimuth-look. Each of the members of these sets of looks is multiplied by the 2-D FFT of its own reference function (within a set there is only one reference function for all the range-looks). In equation form the product of the multiplication is

$$\overline{F}_{q,p}(f_m,f_n) = \overline{G}_{BB_{q,p}}(f_m,f_n)\overline{H}_{q,p}(f_m,f_n) . \tag{103}$$

where $\overline{G}_{BB_{q,p}}$ is the baseband signal for azimuth-look 'q' and range-look 'p', and $H_{q,p}(f_m,f_n)$ is the 2-D FFT of the reference function appropriate to that azimuth-look.

4.3.5.4 Azimuth Inverse FFT

The products of the filter multiplies, i.e., $\overline{F}_{q,p}(f_m,f_n)$, are inverse fast Fourier transformed in azimuth to complete the execution of J7SE01. The result of the inverse FFT is

$$F_{q,p}(m,f_n) = \frac{1}{L_{AZ_q}} \sum_{f_m=0}^{L_{AZ_q}-1} \overline{F}_{q,p}(f_m,f_n)\, e^{j\frac{2\pi f_m m}{L_{AZ_q}}} . \qquad (104)$$

If possible, part of the invalid azimuth data is dropped after the IFFT, i.e., if there are $BL_{AZ_q}/2^A$ invalid samples, where B and A are integers, these samples may be dropped without violating the restriction that all block dimensions must be a power of 2 (see also Section 4.4.5 and Figure 33).

4.4 FILTER GENERATION PROGRAM (J7SE30)

The organization of the material in this section is as follows: the calculation of the look centre line numbers is described first; then, the form of the ideal signal (90), after it has passed through all the processing steps up to but not including, the filter multiply, is described; this leads into a description of the 2-D reference function itself and a discussion explaining why range and azimuth correction is required; then, the computation of the range- and azimuth-correction vectors is described; and finally a description is given of the calculation of the merge support parameters and look overlay parameters.

Three files are required by J7SE30: 1) a standard set of input parameters, which is provided to J7SE30 by the {ERIM / SEASAT}.FPM file, described in in Section 4.1; 2) a context file, which is used to specify the type of processing done by J7SE30, i.e.: the block sizes, the maximum reference function lengths, whether or not the reference function or its time-reversed conjugate are produced, etc., (for a complete description of the context file see Ref. 10); and 3) the {CSAT / ERIM}.WIN file, which contains weighting vectors, one for each

look (the weighting vectors are multiplied by the frequency-domain matched filter).

Several other files which are used for output, are associated with J7SE30, these are:

1. FILTER - this file contains the 2-D FFT of all the reference functions required to process this sub-swath;

2. S(SV, LR, IR, HR) / E(EX, EL) 9999A.LNO - this file contains the FFT line numbers corresponding to the look centres;

3. S(SV, LR, IR, HR) / E(EX, EL) 9999A.RNC - this file contains the basic range-correction vector;

4. S(SV, LR, IR, HR) / E(EX, EL) 9999A.AZC - this file contains the basic azimuth correction vector; and

5. S(SV, LR, IR, HR) / E(EX, EL) 9999A.MRG - this file contains the parameters necessary for the look overlay, and range sub-swath merging programs.

4.4.1 Calculation of the Azimuth-Look and Range-Look Centre Line Numbers

4.4.1.1 Azimuth-Looks

The spacing of the azimuth-looks is, or at least can be, completely arbitrary. When setting up the .DAT files for the mode, the angular

separation of looks is decided. This angle henceforth denoted as the 'spread-angle' Δn, is defined by

$$\Delta\eta = \frac{\lambda}{2\rho_{az_1}} N_{LKS_A} , \tag{105}$$

where ρ_{az_1} is the look spacing parameter in the .FPM file and N_{LKS_A} is specified in the J7SE30.CTX file. The angle η_o, in the slant-range plane, defining the antenna pointing direction, is related to the corresponding angle α, in the ground-range plane, by

$$\eta_o = \cos^{-1}\left(\frac{r_e \sin\theta_r}{r_1(o)\tan\alpha}\right) , \tag{106}$$

(see Figure 24). The Doppler bandwidth DBW is related to η_o and $\Delta\eta$ by

$$DBW = \frac{2c_a V_{eq}}{\lambda} \Delta\eta \sin\eta_o . \tag{107}$$

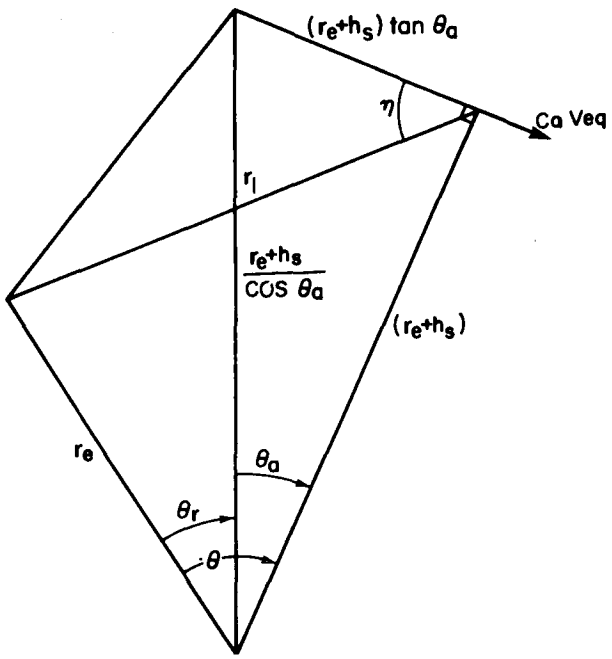

Figure 24. Relationship of η, r, and $\underline{V}_{eq}$

The next step, which is the calculation of the Doppler centre frequency f_D, differs for each of the following cases: 1) baseband and range-offset data, both without azimuth resampling; 2) baseband and range-offset data, both with azimuth resampling; and 3) azimuth-offset data. For the three cases f_D is given by:

$$f_D = - \frac{2c_a V_{eq}}{\lambda} \cos\eta_o \ , \tag{108}$$

or

$$f_D = 0 \ , \tag{109}$$

or

$$f_D = f_{0_A} \tag{110}$$

respectively, where f_{0_A} is the azimuth-offset frequency. Note that case 2) takes precedence over case 3) if azimuth-offset data is resampled in azimuth. In case 2) f_D=0 because the spectrum of the data has been shifted, in J7RE00, from the original f_D, which was defined by (108). In case 3) the spectrum of the data has been shifted in the radar receiver from the original f_D, as described by (108), to the azimuth-offset frequency, f_{0_A}.

The centre frequency f_D is combined with DBW to obtain the look centre frequencies. These frequencies can then be converted to FFT line numbers. The centre frequency for the first look is

$$f_{D_1} = f_D + \frac{DBW}{2} \left(\frac{1}{N_{LKS_A}} - 1 \right) . \tag{111}$$

The centre frequencies for the other looks are found from f_{D_1} as follows:

$$f_{D_q} = f_{D_1} + \frac{DBW}{N_{LKS_A}} (q-1), \qquad q=1,N_{LKS_A} \ . \tag{112}$$

The frequencies f_{D_q} are converted to FFT line numbers $LNOM_{Aq}$ as follows:

$$LNOM_{Aq} = \underset{\text{PART}}{\text{INTEGER}}\left[\frac{L_{AZ}(f_{D_q} - N_q\ PRF)}{PRF} + L_{AZ}\right] ; \qquad \alpha_q \leq \frac{\pi}{2}\ \text{rad}, \tag{113}$$

and

$$LNOM_{Aq} = \underset{\text{PART}}{\text{INTEGER}}\left[\frac{L_{AZ}(f_{D_q} - N_q\ PRF)}{PRF}\right] , \qquad \alpha_q > \frac{\pi}{2}\ \text{rad}. \tag{114}$$

where

$$N_q = \underset{\text{PART}}{\text{INTEGER}}\left[\frac{f_{D_q}}{PRF}\right] . \tag{115}$$

The f_{D_q} are then recomputed so that they will coincide with the available integer FFT line numbers, i.e.

$$f'_{D_q} = \frac{PRF}{L_{AZ}}\ (LNOM_{A_q} - L_{AZ}) + N_q\ PRF ; \qquad \alpha_q \leq \frac{\pi}{2}, \tag{116}$$

and

$$f'_{D_q} = \frac{PRF}{L_{AZ}}\ LNOM_{A_q} + N_q\ PRF , \qquad \alpha_q > \frac{\pi}{2}\ \text{rad}. \tag{117}$$

During the look centre line number calculation, the parameters $\tilde{r}_{1q}$ and $\tilde{\alpha}_q$, (see Figure 25), which are used to define the matched filter, are also generated. The range $\tilde{r}_{1q}$ and angle $\tilde{\alpha}_q$ refer to the geometry that existed when the data point at the middle of the swath, for look q, was collected. The $\tilde{r}_{1q}$ are found from the f'_{D_q} as follows:

$$\tilde{r}_{1q} = \frac{1}{\sqrt{2}}\left[2b - d - \sqrt{(d-2b)^2 + 4(a-b)^2}\right]^{\frac{1}{2}} , \tag{118}$$

where

$$a = 2r_e(r_e+h_s)\cos\tilde{\theta}_r \quad , \tag{119}$$

$$b = r_e^2 + (r_e+h_s)^2 \quad , \tag{120}$$

$$d = \left[2(r_e+h_s)\,\frac{\lambda f'_{D_q}}{Veq}\right]^2 \quad , \tag{121}$$

and

$$\tilde{\theta}_r = \sin^{-1}\left\{\sin\tilde{\alpha}\left\{1-\left[\frac{\left(\frac{\tilde{r}_1(o)}{r_e}\right)^2 - c_a^2 - c_b^2}{-2c_a c_b}\right]^2\right\}^{\frac{1}{2}}\right\} \quad . \tag{122}$$

The α_q are related to f'_{D_q} and $\tilde{r}_{1q}$, by,

$$\tilde{\alpha}_q = \tan^{-1}\left(\frac{-2V_{eq}\, r_e c_a \sin\tilde{\theta}_r}{\lambda \tilde{r}_{1_q}\, f'_{D_q}}\right), \qquad 0 \leq \alpha_q < \pi \; . \tag{123}$$

4.4.1.2 Range-Looks

The calculation for the range-look extraction line numbers is straightforward. The number of looks N_{LKS_R} is read from the .CTX file for J7SE30, and the separation of the looks Δf_R is read from the .FPM file. The available bandwidth as indicated by f_{SR} is divided by N_{LKS_R} to obtain the available range bandwidth per look:

$$RBW_p = \frac{f_{SR}}{N_{LKS_R}} \quad . \tag{124}$$

The centre frequencies f_{n_p} of the looks are then calculated as follows:

$$f_{n_p} = \frac{f_{SR}}{2} - \left[\frac{N_{LKS_R} - 1}{2} + (p-1)\right]\Delta f_R \ , \tag{125}$$

where N_{LKS_R} is constrained to be a power of 2, and $\Delta f_R \leq RBW_p$. These frequencies are then converted into FFT line numbers:

$$LNOM_{R_P} = \underset{\text{PART}}{\text{INTEGER}}\left(\frac{L_R}{f_{S_R}} f_{n_p}\right), \tag{126}$$

for azimuth-offset and baseband; and

$$LNOM_{R_P} = \text{INTEGER PART}\left(\frac{2L_R}{f_{SR}} f_{n_p}\right), \tag{127}$$

for range-offset data. The $LNOM_{R_P}$ are output to the .LNO file for use in J7SE00. This feature is not implemented as of August 1980.

4.4.2 Form of Ideal Signal, after Azimuth-Look Extraction

After azimuth-look extraction the data has a common form regardless of the data-type from which it originated. The purpose of this section is to illustrate this common form by means of the example of the ideal signal described in Section 4.3.1.

The azimuth-look extraction procedure demodulates and, for the multi-look case, resamples the data. The resampling is done by the extraction process itself, i.e., each look contains only L_{AZ}/N_{LKS_A} samples. This resampling should not be confused with that done by J7RE00. The effect of the demodulation can be seen by examining what happens to the azimuth phase term in (89). Equation (89) describes only the baseband signal, but as was stated above, all the data types have a common form at this stage in the processing. The azimuth phase term is

$$\Phi_A = -\frac{2\pi c}{\lambda} t_1'(m) = -2k[a_0 + a_1 m\Delta x_o + a_2(m\Delta x_o)^2] \ , \tag{128}$$

where,

$$k = \frac{2\pi}{\lambda} \quad , \tag{129}$$

The Doppler frequency shift is the product of V_{eq} and the derivative of Φ_A with respect to $m\Delta x_o$, evaluated at m=0, i.e.,

$$2\pi f_D = -2k\ V_{eq}\ a_1 \ . \tag{130}$$

For a target at A in Figure 25 viewed from angle $\tilde{\alpha}_q$, the Doppler frequency shift is

$$2\pi f_{D_q} = -2k\ V_{eq}\ a_{1_q} \ . \tag{131}$$

where a_{1_q} is calculated using (85) with $\tilde{r}_{1_q}(0)$ and $\tilde{\alpha}_q$ substituted for $r_1(0)$ and α. The '~' denotes a reference value. The $\tilde{r}_{1_q}(0)$ are calculated using (118) and (123), with $\tilde{r}_1(0)$ and $\tilde{\alpha}$ substituted for $r_1(0)$ and α in equations (118), (122), and (123). The values of $\tilde{r}_1(0)$ and $\tilde{\alpha}$ are those contained in the .FPM file. The demodulation process (or processes, if the data is azimuth-offset or is azimuth resampled by J7RE00), shifts the spectrum of the look by f_{D_q}.

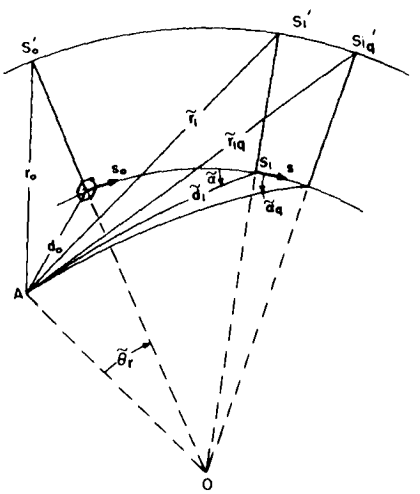

Figure 25. Relationship of r_o, $\tilde{r}_{1q}$, and $\tilde{\alpha}_q$

For a general point target, not necessarily at A, but viewed by look 'q' at α_q, the azimuth phase function is

$$\Phi_{A_q} = -2k[a_{0_q} + a_{1_q} m\Delta x_q + a_{2_q} (m\Delta x_q)^2] , \tag{132}$$

where the sample spacing Δx_q is

$$\Delta x_q = \frac{\Delta x_o}{N_{LKS_A}} \tag{133}$$

and a_{0_q}, a_{1_q} and a_{2_q} are found by substituting r_{1_q} and α_q for $\tilde{r}_1$ and $\tilde{\alpha}$ in (84)-(86).

The shift in Doppler frequency caused by the demodulation for the target at A changes (132) to

$$\Phi_{A_q} = -2k[a_{0_q} + (a_{1_q} - \tilde{a}_{1_q}) m\Delta x_q + a_{2_q} (m\Delta x_q)^2] . \tag{134}$$

The residual Doppler frequency component caused by the incomplete cancellation of the a_{1_q} and a_{1_q} terms will cause a shift in the position of the processor output. This shift will necessitate both range and azimuth corrections, which will be described in Section 4.4.5.

4.4.3 Form of the 2-D Matched Filter (reference function)

The 2-D FFT of each look of the input data must be multiplied by the 2-D FFT of the reference function (i.e., the matched filter, appropriate to that look) and then the 2-D IFFT of the product must be calculated to produce the uncorrected radar image in complex number format. This process is called matched filtering.

The time-domain reference function for each look, i.e., the impulse response of the matched filter for that look, is calculated using the parameters specified in the .FPM file, as well as the calculated values of $\tilde{r}_{1_q}$ and $\tilde{\alpha}_q$. The impulse response of the matched filter for look 'q' is the time-reversed conjugate of (89), with the appropriate parameters replaced by the reference sub'p' and sub'q' parameter, and with the constants $\tilde{a}_{o_q}$ and ϕ_p dropped, i.e.,

$$h_{p,q}(n,m) = \text{Rect}\left\{\frac{1}{N_{R_p}}\left[-n - \frac{2}{c\Delta t'_p}\left(-\tilde{a}_{1_q} m\Delta x_q + \tilde{a}_{2_q} m^2\Delta x_q^2\right) - \frac{N_{R_p}}{2}\right]\right\}\text{Rect}\left(\frac{-m}{N_{1_q}}\right)$$

$$\exp\left\{-j\,\frac{K}{2}\,\Delta t'^2_p\left[-n - \frac{2}{c\Delta t'_p}\left(-\tilde{a}_{1_q} m\Delta x_q + \tilde{a}_{2_q} m^2\Delta x_q^2\right) - \frac{N_{R_p}}{2}\right]^2\right\}$$

$$\exp(j2k\tilde{a}_{2_q} m^2\Delta x_q^2)\ , \tag{135}$$

where

$$N_{R_p} = \frac{\tau_p}{\Delta t'_p}\ , \tag{136}$$

and

$$N_{1_q} = 2 \times \underset{\text{PART}}{\text{INTEGER}}\left[\frac{\tilde{r}_{1_q}\lambda}{4\Delta x_q c_a \rho_{az_p} \sin\tilde{\eta}_q} + c_a\left|\cos\eta_{q_{MAX}} - \cos\eta_{q_{MIN}}\right|\right], \tag{137a}$$

The parameters $\tilde{\eta}_q$, $\eta_{q_{MAX}}$ and $\eta_{q_{MIN}}$, in(137a), are found by substituting $\tilde{\alpha}_q$ for α, and $\tilde{r}_{1q}$, $\tilde{r}_{1q_{MAX}}$ and r_{D_q} respectively, for $r_1(0)$, in (106). The values of $r_{1q_{MAX}}$ and r_{D_q} are found by rearrangement of (87) as follows:

$$r_1(0) = r_e\sqrt{c_a^2 + c_b^2 - 2c_a c_b\left(1 - \frac{\sin^2\theta_r}{\sin^2\alpha}\right)}^{\frac{1}{2}} \tag{137b}$$

and solving for the required r_{1_q} with α replaced by $\tilde{\alpha}_q$, and $\sin^2\theta_r$ by $\sin^2\theta_{r_{MAX}}$ and $\sin^2\tilde{\theta}_{r_D}$ respectively. Prior to calculating $r_{1q_{MAX}}$ and r_{D_q}, $\sin^2\theta_{r_{MAX}}$ and

$\sin^2\theta_{r_D}$ must be found by solving (87) with $r_1(0)$ replaced by $r_{1_{MAX}}$ and r_D respectively. The values of $r_{1_{MAX}}$ and r_D are the edges of the valid image data, i.e.

$$r_{1_{MAX}} = \tilde{r}_1 + (N_{R_P} + L_{R_P}) \frac{c\Delta t'_p}{4} \quad , \tag{137c}$$

and

$$r_D = \tilde{r}_1 + (N_{R_P} - L_{R_P}) \frac{c\Delta t'_p}{4} \tag{137d}$$

The reasoning that leads to (137c) and (137d) is explained further in Section 4.4.5. The second term in (137a) is the extra reference function length that must be provided so that the data can slide over the reference function to find the correct linear-phase match (see Section 2.3 and Figure 6). The values of $\Delta t'_p$, Δx_q, and τ_p are calculated, in either J70R01 or J70R00, in such a way that they are compatible with the number of range- and azimuth-looks and the range and azimuth resampling factors. The parameter $\rho_{az_{2q}}$ is the cross-slant range (Doppler) 3-dB resolution, as defined in the .FPM file. The values a_{1_q} and $\tilde{a}_{2_q}$ in (136) are given by (85), (86), and (87) with $r_1(0)$ and α replaced by $\tilde{r}_{1_q}(0)$, and $\tilde{\alpha}_q$.

Figure 26 shows the envelope of $h_{p,q}(n,m)$, and Figure 27 shows how this envelope is mapped into computer memory. The mapping between the eqn. (135) and computer memory is

$$m' = m + \frac{N_{1_q}}{2} \quad , \tag{138}$$

and

$$n' = n - \Delta_{q_{min}} + N_{R_P} \quad , \tag{139}$$

where,

$$\Delta_{q_{min}} = \underset{\text{OVER } m'}{\text{MINIMUM}} \left[\Delta_q \left(m' - \frac{N_{1_q}}{2} \right) \right] \quad , \tag{140}$$

and

$$\Delta_q \left(m' - \frac{N_{1_q}}{2} \right) = \frac{2}{c\Delta t'_p} \left[\tilde{a}_{1_q} \Delta x_q \left(m' - \frac{N_{1_q}}{2} \right) - \tilde{a}_{2_q} \left(m' - \frac{N_{1_q}}{2} \right)^2 \Delta x_q^2 \right] \quad . \tag{141}$$

With the substitutions defined by (138) and (139), (135) can be rewritten as

$$h_{p,q}(n',m') = \text{Rect}\left[- \frac{\left(m' - \frac{N_{1_q}}{2} \right)}{N_{1_q}} \right] \exp\left[j2k\tilde{a}_{2_q} \Delta x_q^2 \left(m' - \frac{N_{1_q}}{2} \right)^2 \right] \text{Rect}\left\{ \frac{1}{N_{R_p}} \left[-n' - \Delta_{q_{min}} + \frac{N_{R_p}}{2} + \Delta_q \left(m' - \frac{N_{1_q}}{2} \right) \right] \right\} \exp\left\{ j \frac{K'}{2} \Delta t'^2 \left[-n' - \Delta_{q_{min}} + \Delta_q \left(m' - \frac{N_{1_q}}{2} \right) + \frac{N_{R_p}}{2} \right]^2 \right\} , \tag{142}$$

where,

$$K' = -K \quad , \tag{143}$$

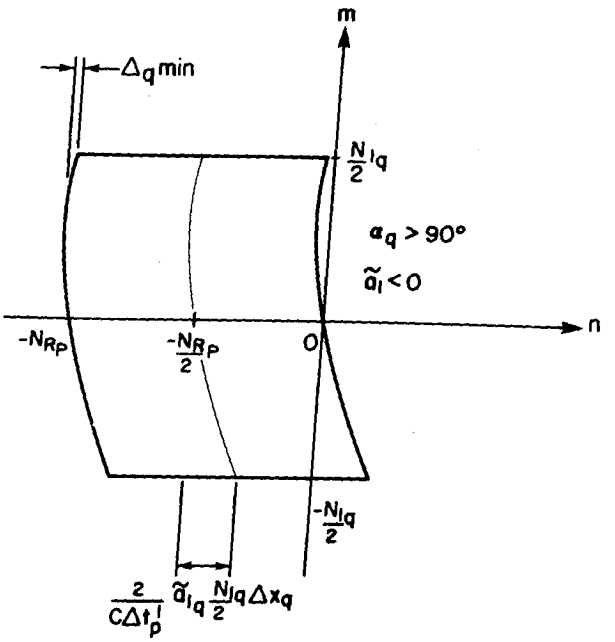

Figure 26. Envelope of compression filter impulse response, $h_{q,p}(m,n)$

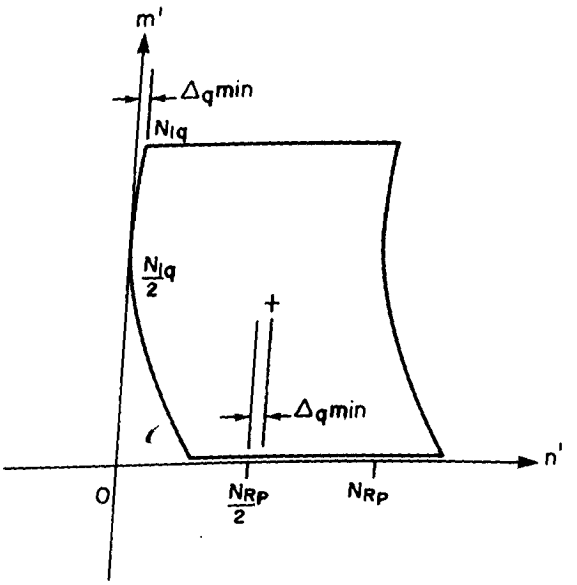

Figure 27. Envelope of $h_{q,p}(m',n')$ stored in computer memory

When implemented in software the filter is calculated in the following way:

(1) N_{LKS_A} files of L_{az}/N_{LKS_A} rows of L_{R_P} complex elements are allocated (note that all of the range-look filters for a given azimuth-look are identical);

(2) for each file a phase function consisting of N_{R_P} complex samples of the form

$$\exp\left\{j\frac{K'}{2}\Delta t_p'^2\left\{-n' - \text{INTEGER PART}\left[-\Delta_{q_{min}} + \Delta_q\left(m' - \frac{N_{1_q}}{2}\right)\right]\right.\right.$$
$$\left.\left. - \Delta_{q_{min}} + \Delta_q\left(m, - \frac{N_{1_q}}{2}\right) + \frac{N_{R_P}}{2}\right\}^2\right\} \exp\left[j2k\tilde{a}_2\Delta x_q^2\left(m' - \frac{N_{1_q}}{2}\right)^2\right] , \qquad (144)$$

is calculated and placed in the file for look 'q'. The row index m' runs from 1 to N_{1_q}, but the column index 'n' starts at $n_s'(m')$, where

$$n_s'(m') = \text{INTEGER PART}\left[-\Delta_{q_{min}} + \Delta_q\left\{m' - \frac{N_{1_q}}{2}\right\}\right] . \qquad (145)$$

This means that starting with row 1 (m'=1), the function is placed in the row starting at position $n_s'(m')$;

(3) the portion of the row not yet occupied by the filter is filled with zeroes;

(4) the process is repeated for N_{1_q} rows, and then the rest of the matrix is filled with zeroes.

If the time-reversed conjugate of $h_{p,q}(n',m')$ is required, as determined by an entry in the context block for J7SE30, the complex conjugate of (144) is calculated and the new phase function is written backwards, i.e., right to left in the computer memory, starting at

$$n_s'(m') = N_{R_P} + \text{INTEGER PART}\left[\Delta_{q_{MAX}} - \Delta_q\left\{m' - \frac{N_{1_q}}{2}\right\}\right] \qquad (146)$$

where $\Delta_{q_{MAX}}$ is found by scanning $\Delta_q(m' - N_{l_q}/2)$, as was done in (140).

In theory, the phase functions required in the $h_{p,q}(n',m')$ matrix could be obtained by calculating a range line (row) of the appropriate FM rate but using the sidelooking geometry. This line could then be placed in the matrix and shifted to the appropriate location in memory so that the envelope in Figure 27 is obtained. Unfortunately, without interpolation these shifts can only be performed to the nearest integer sample number. The approximate phase function that would be obtained using this method would contain phase discontinuities that are unacceptably large and thus this nearest neighbor type shifting technique is inappropriate. Instead, the necessary shift is split into two components: a fractional shift, which is computed as part of the phase term, i.e., the first exp{ } factor in (144); and an integer shift, which is used to locate an address in the $h_{p,q}(n',m')$ matrix. This technique produces a smooth phase function which is identical to the one which would be obtained by computing the entire phase function starting at n'=0, and windowing out an integer number of samples (N_{R_p}), starting at the address corresponding to the integer part of the shift.

4.4.4 2-D FFT of $h_{p,q}(n',m')$

In order to obtain the N_{LKS_A}, $\bar{H}_{q,p}(f_m,f_n)$ filters, the 2-D FFT of each function $h_{p,q}(n',m')$ is computed. This is done by calculating the FFT of each row, i.e.,

$$H_{p,q}(f_n,m') = \sum_{n'=0}^{L_{R_p}-1} h_{p,q}(n',m') e^{-j\frac{2\pi n' f_n}{L_{R_p}}} , \qquad (147)$$

and then transposing each filter to obtain

$$H_{q,p}(m',f_n) = H^T_{p,q}(f_n,m') \quad . \qquad (148)$$

The FFTs of each of the new rows in the files containing the $H_{q,p}(m',f_n)$ functions are then calculated, i.e.,

$$\overline{H_{q,p}}(f_m,f_n) = \sum_{m'=o}^{L_{az_q}-1} H_{q,p}(m',f_n)e^{-j\frac{2\pi m' f_m}{L_{az_q}}} \quad . \qquad (149)$$

These functions are then multiplied, in J7SE01, by the 2-D FFTs of the appropriate data files (see (103)).

An optional frequency-domain $\cos^{(x)}$ window, $W(f_m,f_n)$ can be applied to $\overline{H_{q,p}}(f_m,f_n)$. The application of the window depends upon the selection of a parameter in the J7SE30.CTX file. The window is stored as two vectors $W_{A_q}(f_m)$ and $W_{R_p}(f_n)$ in the .WIN file. The $W_{A_q}(f_m)$ vector is applied as weighting to each row of $H_{q,p}(f_m,f_n)$, and the $W_{R_p}(f_m)$ vector is applied as row-by-row modulation on the $W_{A_q}(f_m)$ weighting. Windows other than $\cos^{(x)}$ can be inserted in the .WIN file by simple code changes, or an optimum FIR filter frequency response can be calculated and placed in .WIN for use as a window.

4.4.5 Calculation of Range and Azimuth Correction Vectors

A set of correction vectors must be computed in J7SE30. They are used as input to J7SE02 in which the following corrections are applied: 1) the range dependent range shifts; and 2) the range-dependent azimuth shifts. The former simultaneously converts the image from slant-range r_1 to side-looking d_o geometry (see Figure 1) and corrects for the range geometric distortions introduced by the two-dimensional filtering operation. The latter simultaneously corrects for the azimuth geometric distortion and writes the data at angle $\tilde{\alpha}_q$ with respect to ground-track. The range shift computation includes a normalization process that ensures that ground-range, which is measured as a ground-range sample count times the ground-range sample width, is always counted along the sidelooking direction from a single ground-range reference line, i.e., zero ground-range. The normalization process ensures that all swaths are imaged on a standardized grid, and thereby simplifies the merging of individual range swaths into a composite image.

An additional normalization process is included in the azimuth shift computation. All azimuth-looks are shifted such that they are on a standard grid in azimuth, counted from an imaginary line on the ground, which would describe the line of intersection of a vertical plane in the centre of the antenna beam and the surface of the earth, if the pointing angle α were $\pi/2$ rad. This normalization ensures that all points to be averaged together fall on integer sample positions. With this provision no interpolation of samples is required during look registration; straightforward integer shifts and additions are all that are required.

As described in Section 4.5, the range shifts are applied first, the matrix is transposed, and then the azimuth shifts applied. The azimuth shifts must therefore be calculated as a function of the resampled range data, i.e., $n_o * \Delta d_{o_q}$, where n_o^* is the normalized, sidelooking ground-range sample number, and Δd_{o_q} is the final sidelooking, ground-range sample spacing.

The samples to be extracted by application of the correction vectors are found by working backwards from the desired image format to the uncorrected data set. The calculation proceeds in the following way:

1) the edge of the image (r_{D_q} in Figure 28) is established in the squinted slant-range plane;

2) the angle θ_{r_D}, which corresponds to r_{D_q} and $\tilde{\alpha}_q$, is computed (see θ_{r_D} in Figure 28);

3) the sidelooking ground-range corresponding to θ_{r_D} is calculated and truncated to an integer number of sidelooking ground-range samples, i.e., $n_o^* \Delta d_o$, as in Figure 29; the normalized near-edge of the swath is at x in Figure 29, i.e., it is $n_o^* \Delta d_{o_q}$ samples from the zero sidelooking, ground-range position;

4) a reference azimuth position, which determines the azimuth-look offset $\Delta az_{2_{q_o}}$ is computed (see Figure 32);

5) the index n_o' is then established; n_o' runs from n_o^* to the end of the image (see Figure 30);

6) n_o' is incremented (note: sample 1 corresponds to n_o^*) and the equivalent squinted ground-range $d_{1_q}(n_o')$ is calculated (see Figure 30);

7) the squinted slant-range $r_{1_q}(n_o')$ is then calculated $d_{1_q}(n_o')$ (see Figure 31);

8) the value of $r_{1_q}(n_o')$ is then used to calculate the azimuth-shifts $\Delta az_{1_q}(n_o')$ and $\Delta az_{2_{qR}}(n_o')$, required for this sample (see Figure 32);

9) the azimuth-shift, required to correct for the $r_{1_q}(n_o')$ versus $\tilde{r}_{1_q}$ mismatch in the compression filter, i.e., $\Delta az_{1_q}(n_o')$, is used to compute the range-shift $\Delta r_q(n_o')$ that also depends on the $r_{1_q}(n_o')$ versus $\tilde{r}_{1_q}$ mismatch, ($\Delta r_q(n_o')$ is the slant-range displacement from E to F in Figure 6);

10) the final corrections for the shift introduced by the reference function definition, i.e., $\Delta_{q_{min}} \neq 0$, and for the invalid data produced by the fast convolution, are applied, and the index $n_q'(n_o')$, into the uncorrected data set, is calculated; and

11) steps 6) to 10) are repeated until the required number of samples have been extracted from the uncorrected data set.

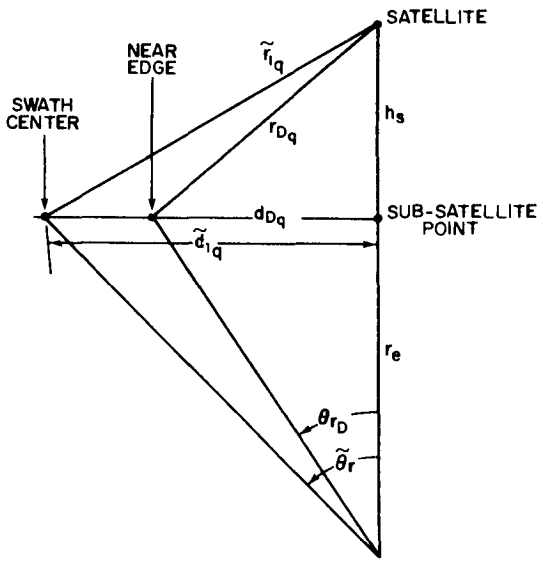

Figure 28. Relationship of 'squinted' slant- and ground-range

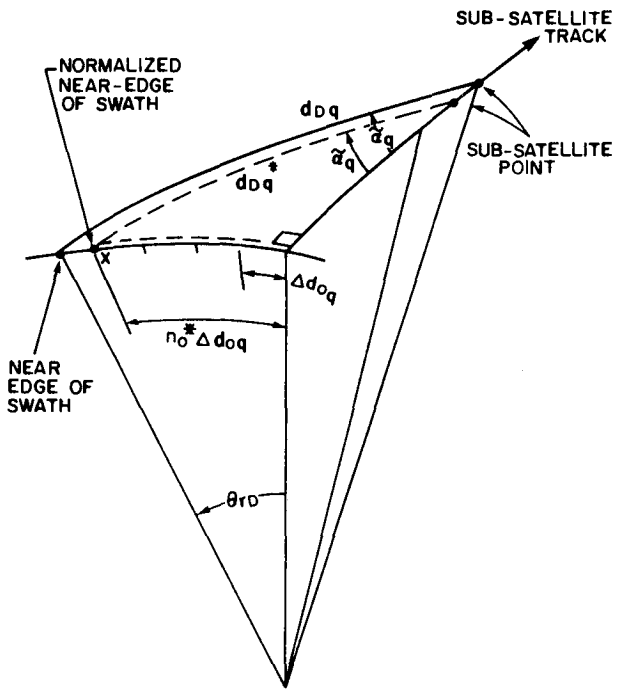

Figure 29. Conversion from 'squinted' ground-range to sidelooking ground range

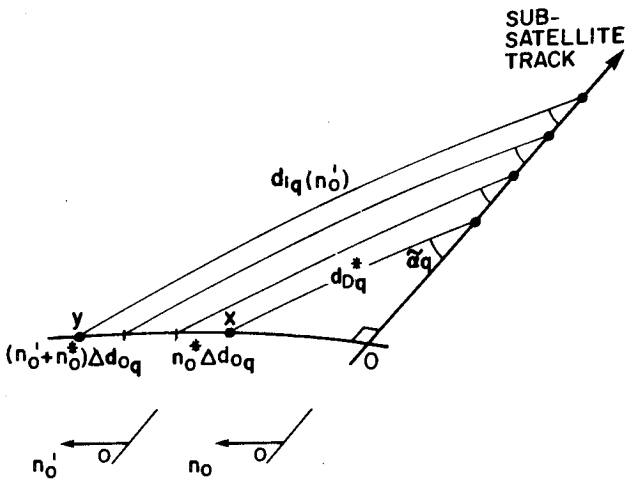

Figure 30. Ground-range sampling

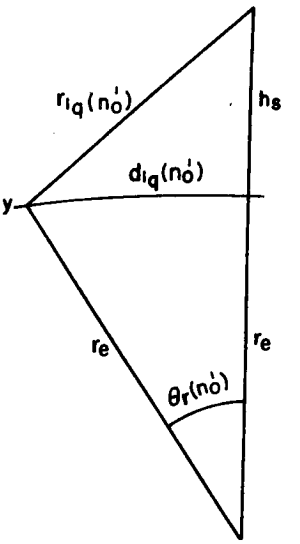

Figure 31. Slant-range corresponding to new ground-range sample

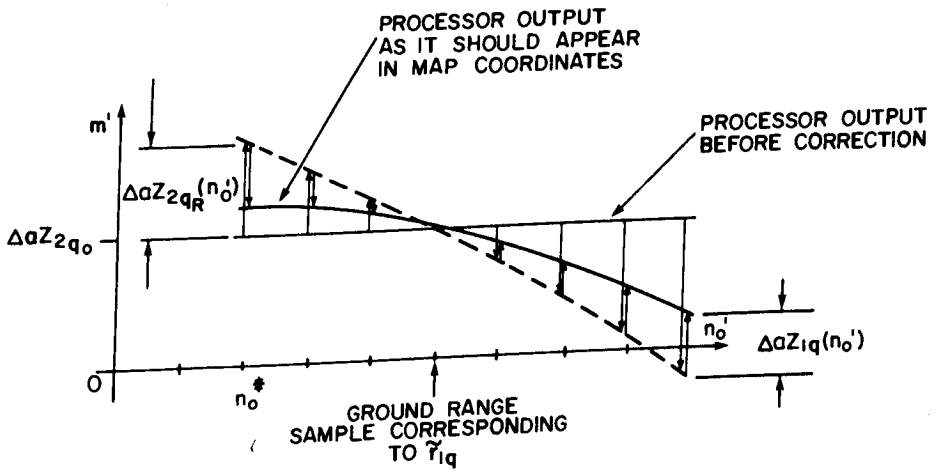

Figure 32. Azimuth-shifts which must be applied to the resampled range data

The output from this procedure consists of: a set of indices $n'_q(n'_o)$, which map the required output for each sample n'_o into the locations in which this output is held; a set of azimuth shifts $\Delta az_{1q}(n'_o)$ and $\Delta az_{2q_R}(n'_o)$; a range normalization value n^*_o; and an azimuth reference position Δaz_{2q_o}.

In order to locate the near edge of the valid range data for the q^{th} azimuth-look in the image, one must first examine what happens when the fast convolution is computed. Thus far in the processor description the azimuth FFT of the product of the 2-D FFTs of the data and the reference function has been calculated. The next step to be performed in J7SE02 is a transpose and IFFT in range. If one examined the data after this step, which completes the fast convolution, one would see that the data has circulated clockwise in range by $N_{R_P}/2$ and in azimuth by $N_{1_q}/2$ (see Figure 33). There is also a strip of invalid data of width N_{R_P} in range and N_{1_q} in azimuth. This invalid data is produced by the matched filter wraparound during the fast convolution (Ref. 18). As already explained in Section 4.4.3, the edge of the valid data in range is r_D, where

$$r_D = \tilde{r}_1 + \left(\frac{N_{R_P}}{2} - \frac{L_{R_P}}{2}\right)\frac{c\Delta t_p}{2} \quad . \tag{150}$$

The angle θ_{r_D} which locates the edge of the data is found using:

$$\sin^2\theta_{r_D} = \sin^2\tilde{\alpha}\left\{1 - \left[\frac{\left(\frac{r_D}{r_e}\right)^2 - c_a^2 - c_b^2}{-2c_a c_b}\right]^2\right\} \quad . \tag{151}$$

The sidelooking ground-range to the edge of the valid range data is common to all looks. It is equal to the arc length subtended by θ_{r_D} on the surface of the Earth. The normalized value of sidelooking, ground-range $n^*_o\Delta d_{o_q}$, to the edge of the valid data, is found by truncating the arc length as follows:

$$n^*_o = \underset{\text{PART}}{\text{INTEGER}}\left\{\frac{r_e}{\Delta d_{o_q}}\theta_{r_D}\right\} \quad , \tag{152}$$

where Δd_{o_q} is the same for all looks. The squint ground-range $d^*_{D_q}$, which locates the normalized edge of the swath, is then

$$d^*_{D_q} = r_e \sin^{-1}\left[\frac{\sin\left(\frac{n^*_o \Delta d_{o_q}}{r_e}\right)}{\sin\tilde{\alpha}_q}\right] . \qquad (153)$$

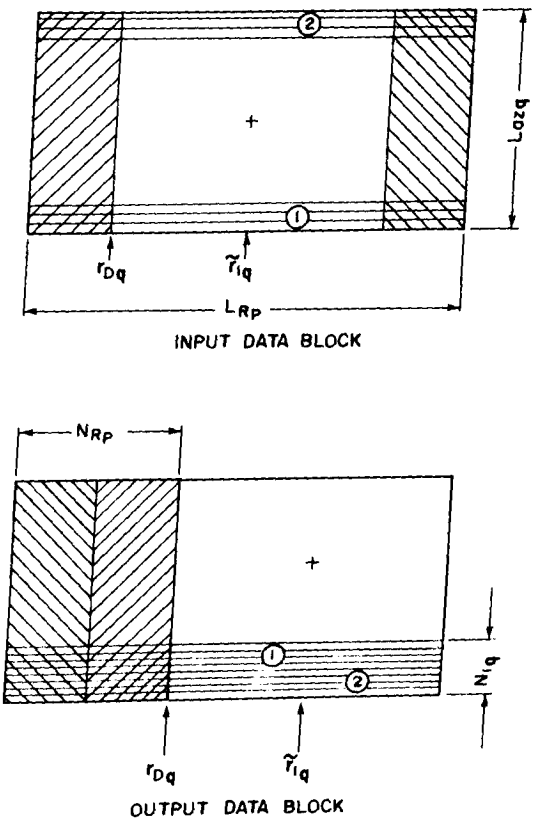

Figure 33. Circulation of data during fast-convolution

The locations of the data points that must be extracted from the data array to form the corrected image are found by solving for the slant-range $r_{1_q}(n'_o)$, which corresponds to the location of each sample n'_o, where n'_o is an index running from one at $n^*_o \Delta d_{o_q}$ to L_{R_q} at the edge of the corrected image. The slant-range $r_{1_q}(n'_o)$ is

$$r_{1_q}(n_o') = r_e \sqrt{-2c_a c_b \cos\left[\frac{d_{1_q}(n_o')}{r_e}\right] + c_a^2 + c_b^2} \quad , \tag{154}$$

where,

$$d_{1_q}(n_o') = d_{D_q}^* + r_e \sin^{-1}\left\{\frac{\sin\left[\frac{(n_o'-1)\Delta d_{o_q}}{r_e}\right]}{\sin\tilde{\alpha}_q}\right\} \quad . \tag{155}$$

The slant-range $r_{1_q}(n_o')$ is used to compute the azimuth corrections to be applied at $d_{1_q}(n_o')$. The azimuth shifts required to correct the geometric distortions caused by the $r_{1_q}(n_o')$ versus $\tilde{r}_{1_q}$ mismatch are given by

$$\Delta az_{1_q}(n_o') = \frac{1}{2\tilde{a}_{2q}\Delta x_q}\left[\frac{r_e}{r_{1_q}(n_o')}\frac{c_a \sin\theta_r(n_o')}{\tan\tilde{\alpha}_q} - \tilde{a}_{1_q}\right] \quad , \tag{156}$$

where,

$$\sin\theta_r(n_o') = \sin\tilde{\alpha}\left\{1 - \left[\frac{\left(\frac{r_{1_q}(n_o')}{r_e}\right)^2 - c_a^2 - c_b^2}{-2c_a c_b}\right]^2\right\}^{\frac{1}{2}} \quad . \tag{157}$$

The azimuth shifts required to write the squinted ground-range data line on the map at the angle $\tilde{\alpha}_q$, i.e., the angle at which it was acquired, are described by the following equations:

$$\Delta az_{2_{q}}(n_o') = \Delta az_{2_{q_0}} + \Delta az_{2_{q_R}}(n_o') \quad , \tag{158}$$

where,

$$\Delta az_{2_{q_0}} = \underset{\text{PART}}{\text{INTEGER}} \left\{ -\frac{r_e}{\Delta x_q} \sin^{-1}\left(\frac{\tan\tilde{\theta}_r}{\tan\tilde{\alpha}_q}\right) \right\} , \tag{159}$$

$$\Delta az_{2_{q_R}}(n_o') = -\frac{r_e}{\Delta x_q} \sin^{-1}\left[\frac{\tan\theta_r(n_o')}{\tan\tilde{\alpha}_q}\right] - \Delta az_{2_{q_0}} \quad , \tag{160}$$

and,

$$\tilde{\theta}_r = \sin^{-1}\left\{\sin\tilde{\alpha}\left\{1 - \left[\frac{\left(\frac{\tilde{r}_1}{r_e}\right)^2 - c_a^2 - c_b^2}{-2c_a c_b}\right]^2\right\}^{\frac{1}{2}}\right\} . \tag{161}$$

The $\Delta az_{2_{q_R}}(n_o')$ and the $\Delta az_{1_q}(n_o')$ terms are summed together to form the exponent of the basic azimuth correction vector $V_{A_q}(n_o')$. The vector $V_{A_q}(n_o')$ is given by

$$V_{A_q}(n_o') = e^{-j\frac{2\pi}{L_{az_o}}\left[\Delta az_{1_q}(n_o') + \Delta az_{2_{q_R}}(n_o')\right]} , \tag{162}$$

where L_{az_o} is the length, in azimuth, of the image to be corrected. The parameter L_{az_o} is always a power of two, however, L_{az_o} can be $\leq L_{az_q}$, e.g., if invalid data has been dropped in J7SE01. The vector $V_{A_q}(n_o')$ is passed to the program J7SE02 by means of the file .AZC.

The $\Delta az_{2_{q_o}}$ term is added to $-N_{1_q}/2$ to obtain the azimuth reference value Δaz_{REF_q}, i.e.,

$$\Delta az_{REF_q} = \Delta az_{2_{q_o}} - \frac{N_{1_q}}{2} \quad . \tag{163}$$

The azimuth reference values are output to the .MRG file to be used during the azimuth-look overlaying (J7SE90) and the range-swath merging programs (J7ME00).

The range shift caused by the $r_{1_q}(n'_o)$ versus $\tilde{r}_{1_q}$ mismatch is calculated as follows:

$$\Delta r_q(n'_o) = - \frac{\left[\tilde{a}_{1_q} \Delta az_{1_q}(n'_o)\Delta x_q + \tilde{a}_{2_q} \Delta az_{1_q}(n'_o)^2 \Delta x_q^2\right]}{\frac{c\Delta t'_p}{2}} \quad . \tag{164}$$

The final address $n'_q(n'_o)$, of the uncorrected data sample to be extracted, is computed using

$$n'_q(n'_o) = \frac{2}{c\Delta t'_p}\left[r_{1_q}(n'_o) - r_D\right] + N_{R_P} + \Delta r_q(n'_o) - \Delta_{q_{min}} \quad . \tag{165}$$

The significance of each of the parts of (165) is as follows: the factor $[r_{1_q}(n'_o) - r_D]$ determines the number of range samples from the edge of the recorded range swath; the term N_{R_P} accounts for the N_{R_P} invalid samples in the output image, which occur between r_D and $r_1(0)$; the $r_q(n'_o)$ is the range positional error caused by the processing; and the $\Delta_{q_{min}}$ term is the number of range samples the reference function $h_{p,q}(n',m')$ was shifted so as to align the first sample with zero range (see Figure 27).

The edges of the corrected image are found next. The integer and fractional parts of the address are computed first,

$$ADD_q(n'_o) = \underset{PART}{INTEGER}\left[n'_q(n'_o)\right] \tag{166}$$

and,

$$FRAC_q(n'_o) = n'_q(n'_o) - ADD_q(n'_o) \quad . \tag{167}$$

The vector $ADD_q(n_o')$ is scanned to find any addresses that are not in the valid data set i.e., addresses that refer to slant-range sample numbers in the range: less than $[N_{R_P} + \Delta r_q(n_o') - \Delta_{q_{min}}]$ or greater than L_{R_q}. The first ground-range sample that refers to a valid slant-range sample in the data set is found and labelled the First Non-Zero Range Correction Vector ($FNZRCV_q$) element. The Last Non-Zero Range Correction Vector ($LNZRCV_q$) element is similarly found and named. When these values are added to n_o' they establish the edges of the final, corrected, ground-range image in the standardized grid. These edges are used during the look registration and swath merging operations. All vector locations before $FNZRCV_q$ and after $LNZRCV_q$ are filled with special flag characters (-1's and -2's). The program J7SE02 sets the image locations, referred to by the flagged vector entries, to zero. The $FNZRCV_q$, $LNZRCV_q$, and n_o^* values are output to the .MRG file to be used by the range-swath merging program (J7ME00).

The fractional part of the address $n'(n_o')$, is used to form the basic range correction vector $V_{R_q}(n_o')$, where

$$V_{R_q}(n_o') = e^{j \frac{2\pi}{NN_R} FRAC_q(n_o')}, \tag{168}$$

and NN_R is the length of the FFT used in the interpolation for each point in the final image (see Section 4.5.3).

The final calculation done in the filter generation program is the determination of how many image lines of wrapped-around picture must be removed from the output data before it can be concatenated with the azimuth blocks. The wrap-around occurs because the corrected image, unlike the file that contains it is not rectangular in shape (see Figure 34). The azimuth shifting process causes data points, shifted off the top of the image, to circulate around to the bottom, and vice versa. As shown in Figure 34, these wrapped-around samples must be removed. The number of samples to be removed is N_{REM}, where

$$N_{REM} = \left| \underset{\text{over } n_o'}{\text{Maximum}} \left[\Delta az_{1_q}(n_o') + \Delta az_{2_{q_R}}(n_o') \right] \right| + \left| \underset{\text{over } n_o'}{\text{Minimum}} \left[\Delta az_{1_q}(n_o') + \Delta az_{2_{q_R}}(n_o') \right] \right| \tag{169}$$

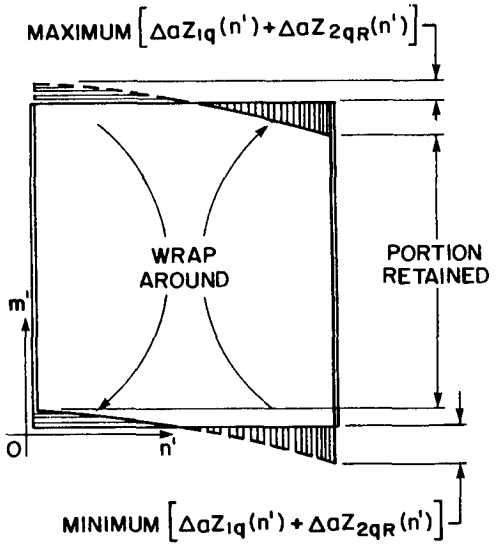

Figure 34. Removal of wrapped-around azimuth data

Both $\Delta az_{1_q}(n'_o)$ and $\Delta az_{2_{q_R}}(n'_o)$ are zero at the swath centre. The value of N_{REM} is calculated for the worst case and entered by hand into J7SE02.CTX.

For radar data that is highly squinted, the azimuth corrections should be applied to the final, full length, range sub-swath, not to the individual blocks that make up the sub-swath. The wrap-around need not be removed then, instead it can be unwrapped, and the corrected sub-swath stored in a file large enough to hold $L_{az_q} + N_{REM}$ azimuth records.

4.5 THE SAR PROCESSOR PART II (J7SE02, J7IG02, J7SE80)

This Section describes the portion of the SAR processor that performs: the transpose required before the range IFFTs, the range IFFTs, the optional range corrections, the second transpose, and the azimuth corrections, (in J7SE02); the optional transpose, done if azimuth corrections are applied, (J7IG02); the optional calculation of the magnitude of the complex data (this step must be performed if multilook imagery is being produced); the removal of invalid data (if any) (in J7SE80); and the look overlay (in J7SE90).

4.5.1 First Transpose in J7SE02

The data block as described by (104) is transposed, such that for each look, $F_{q,p}(m,f_n)$ becomes $F_{p,q}(f_n,m)$. The transpose algorithm used is identical to that described in Section 4.3.3.

4.5.2 Range IFFT in J7SE02

The IFFT of each range line of each of the looks is calculated next. This step completes the fast convolution process. The uncorrected output data block, $f_{p,q}(n,m)$ is

$$f_{p,q}(n,m) = \frac{1}{L_{R_P}} \sum_{f_n=0}^{L_{R_P}-1} F_{p,q}(f_n,m) e^{j\frac{2\pi f_n m}{L_{R_P}}} \quad . \tag{170}$$

4.5.3 Range Correction in J7SE02

The basic range correction vector consists of two parts: the address $ADD_q(n'_o)$, and an exponential $V_{R_q}(n'_o)$ (see (171)), which incorporates the fractional part $FRAC_q(n'_o)$. As discussed in Section 4.4.5 the address and fractional part are combined to form the total address of the desired point, $n'_q(n'_o)$. The address vector $ADD_q(n'_o)$ is used to locate the nearest neighbor to position $n'_q(n'_o)$. For example, for sample $n'_q(n'_o) = 4^3/4$ (see Figure 35), a backwards shift consisting of: an NN_R-point range FFT, centred about position 4 in the $f_{p,q}(n,m)$ data set, a frequency-domain multiply by a linear phase-shift vector, and an inverse NN_R-point range FFT; are performed to move the information from $4^3/4$ to position 4, at which point it can be easily extracted by reading the value in this integer location. If an NN_R point FFT cannot be centred about position 4 without running off the start of the data, set then the FFT is started at position zero. Similarily, if the position to be extracted is too close to the end of the data, set the FFT is performed on the last group of NN_R points in the data set.

The linear phase-shift vector is formed from the basic range correction vector as follows[19]

$$U_{R_{q,n'_o}}(\ell) = \left[V_{R_q}(n'_o)\right]^{\ell}, \quad \ell = 0,1,\ldots,\frac{NN_R}{2}-1 \quad , \tag{171}$$

$$U_{R_{q,n'_o}}(\ell) = \left[V_{R_q}(n'_o)\right]^{0} = 1, \quad \ell = \frac{NN_R}{2} \quad , \tag{172}$$

and,

$$U_{R_{q,n'_o}}(\ell) = \left[V_{R_q}(n'_o)\right]^{(\ell-NN_R)} \qquad \ell = \frac{NN_R}{2} + 1,\ldots,NN_R-1 \ . \tag{173}$$

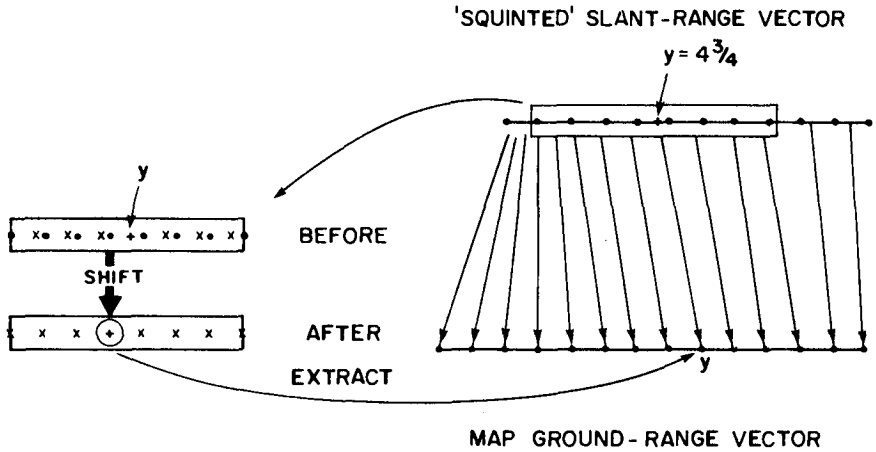

Figure 35. Squinted slant-range to corrected, sidelooking ground-range conversion process

The expanded linear phase-shift vector is multiplied by the NN_R-point FFT of the uncorrected data and then the IFFT is calculated. This sequence of operations accomplishes a backwards shift of $FRAC_q(n'_o)$ samples. The desired sample, which was previously inaccessible, because it lay between the physical samples, can then be extracted and placed in the output range line at position n'_o. If the range correction vector element for point n'_o has been flagged as either -1 or -2 by the filter generation program J7SE30, the location n'_o is filled with a zero.

The value of NN_R is read from the .FPM file, which in turn is created using the .DAT file. The size of NN_R is chosen empirically.

4.5.4 Second Transpose in J7SE02

Once all the range lines have been extracted from $f_{p,q}(n,m)$, the block of range corrected data is transposed using the previously discussed transpose algorithm. Note, if no azimuth corrections are applied this transpose is not performed.

4.5.5 Azimuth Corrections in J7SE02

The azimuth shifts are applied to the range corrected data by means of linear phase-shifts applied to the data in the frequency-domain. For each row (a row now contains azimuth information), an FFT of length L_{az_o} (the full row length) is calculated. The FFT is multiplied by the azimuth linear phase shift vector $U_{A_{q,n'_o}}(\ell)$, where

$$U_{A_{q,n'_o}}(\ell) = \left[V_{A_q}(n'_o)\right]^{\ell}, \quad \ell = 0,1,\ldots,\frac{L_{az_o}}{2} - 1, \tag{174}$$

$$U_{A_{q,n'_o}}(\ell) = \left[V_{A_q}(n'_o)\right]^{0}, \quad \ell = \frac{L_{az_o}}{2}, \tag{175}$$

and

$$U_{A_{q,n'_o}}(\ell) = \left[V_{A_q}(n'_o)\right]^{\ell - L_{az_o}} \quad \ell = \frac{L_{az_o}}{2} + 1,\ldots,L_{az_o} - 1 . \tag{176}$$

The inverse FFT of the product is computed to complete the forward shift of the entire row by $[\Delta az_{1_q}(n'_o) + \Delta az_{2_{q_R}}(n'_o)]$ samples.

4.5.6 Transpose (J7IG02)

The corrected data is transposed once more so that the output rows are range lines. This transpose is not necessary for single data blocks, but if a multiple azimuth-block, multiple range sub-swath image is being produced the transpose must be done so that the blocks can be concaterated, and the sub-swaths merged. This transpose can be omitted if no range and azimuth corrections have been performed.

4.5.7 Optional Magnitude Calculation in J7SE80

For multilook images the magnitude of each look must be computed before the looks can be combined. For single look images the magnitude computation is optional, i.e., the data can be left in complex form. The magnitude is given by:

$$f_{p,q}(n'_o,m') = \left| f_{p,q}(n'_o,m') \right| , \qquad (177)$$

where the (n,m) to (n'_o,m') change in $f_{p,q}$, relative to (170), denotes that the data has been corrected in range and azimuth.

4.5.8 Removal of Invalid Azimuth Data in J7SE80

As explained in Section 4.4.5 a number of complete corrected range lines, which have been corrupted by the wrap-around of the data during the azimuth corrections and the two-dimensional fast convolution, must be removed at the top and bottom of each image (see Figure 34). The number of lines to be removed N_{REM} is set in the J7SE80.CTX file. This step may be skipped if only a single azimuth block is being produced.

4.5.9 Range Sub-Swath Copy Operation

If more than one azimuth block is to be produced per range sub-swath the portion of the processor from J7SE00 to J7SE80 must be repeated once per block. The present hardware configuration has a limited amount of disc storage available, therefore if several azimuth blocks are to be processed, the output from some of the blocks, or sets of blocks, must be stored on magnetic tape prior to subsequent executions of J7SE00. For modes which require the processing of more than one azimuth block, the azimuth blocks are usually combined into sets of blocks. e.g., 4 blocks per set, and these sets are stored on tape or disc as one per output volume.

4.6 THE SAR PROCESSOR PART III (J7SE90)

The last steps in the SAR processing per se are the concatenation of the azimuth blocks, orsets of blocks, for each of the range sub-swaths; and the overlaying of the range-and azimuth-looks. The range-look overlay feature was not implemented in the processor, as of August 1980. When and if it is included, it will be run as a separate program following J7SE90.

Immediately prior to the execution of J7SE90, the azimuth blocks that were stored on tape are copied to disc. It is now possible to place the files on disc because certain files that were used in J7SE00 to J7SE90 have been deleted.

The concatenation of the azimuth blocks is combined with the azimuth-look overlay process. The azimuth-looks are delayed with respect to each other and then the respective rows from each look are added together to form an azimuth multilook row. The names of the files that specify the rows and azimuth blocks for each azimuth-look are contained in the .LKO file. It also contains the length of the rows, the number of rows in each file and the number of records to skip, if any, at the beginning of each file. the .MRG file contains the azimuth reference values Δaz_{REF_q}, which determine the integer

number of samples delay between the azimuth-looks. The azimuth multilook image row number, at which to start adding rows from look 'q' to the rows from looks 1 to 'q', is determined by the following calculation:

$$\text{offset}_q = \Delta az_{REF_q} - \Delta az_{REF_4}, \quad \alpha \leq \frac{\pi}{2} \text{ rad.} \quad , \tag{178}$$

or

$$\text{offset}_q = \Delta az_{REF_q} - \Delta az_{REF_1}, \quad \alpha > \frac{\pi}{2} \text{ rad.} \quad . \tag{179}$$

The edges of the rows, for which no data exists in a given look, have already been zero-filled during the range correction procedure, and therefore pose no problem here. Also, the range-dependent fractional part of the delay between the looks, $\Delta az_{2_{q_R}}(n_o')$ has been removed during the azimuth correction process, so that of all the azimuth samples, in all of the azimuth-looks, lie on integer sample numbers, counted from the sidelooking position. Thus a simple integer delay is sufficient to align the looks.

Figure 36 shows how the azimuth-looks overlay for the case $\alpha < \pi/2$ rad.. The first (offset_1 - offset_2) records are composed entirely of data from look 1. Starting at record offset_1, rows from look 2 are added to the rows already read from look 1. The first and last non-zero values, (FNZRCV) and (LNZRCV), in each look are also indicated. The average intensity of the multi-look image will change from the zero-filled to single-look, to two-look sections of the image, in a staircase-like pattern. This pattern is indicated by the shading in Figure 36.

As previously mentioned, the capability for range multilook images has not been implemented. In order to implement range multilooking, it would be necessary to add, in a straightforward manner, corresponding samples of the azimuth multilook images produced by J7SE90. The range-looks, of a given point on the ground, are all produced simultaneously, i.e., one look results from each section of the transmitted range bandwidth; the looks are therefore registered with respect to one another. By contrast, the azimuth-looks of a given point on the ground are produced sequentially, separated temporally by the time it takes to acquire (offset_q - offset_{q-1}) records, and hence they must first be registered before they can be summed.

4.7 THE MERGE SUPPORT AND RANGE SUB-SWATH MERGE PROGRAMS (J7MS00 and J7ME00)

If the final image is to be several range sub-swaths wide, the completed multilook sub-swaths must be merged as the last step in the processing. Prior to merging the sub-swaths several parameters must be computed from the data in the .MRG files and the CSATMS.OLP file. The values of $\text{offset}_q(i)$,

$FNZRCV_q(i)$, $LNZRCV_q(i)$ and $n'_o(i)$ are read from the .MRG file for each swath 'i', and the standard right and left overlaps $N_{OVS_{R_{MODE}}}$ and $N_{OVS_{L_{MODE}}}$ are read from from the CSATMS.OLP file.

In order to merge the sub-swaths and not produce gaps or repeated data, the edges of the non-zero imagery containing all the looks must be accurately located. The maximum differences between the individual $FNZRCV_q$'s, and the individual $LNZRCV_q$'s for the extreme azimuth-looks are calculated for the worst combinations of squint-angle and slant-range that are encountered with the radar from which the data is being processed. These differences in $FNZRCV_q$ and $LNZRCV_q$ are used to calculate a set of standard left overlap values ($N_{OVS_{L_{MODE}}}$) and standard right overlap values ($N_{OVS_{R_{MODE}}}$) for this mode. The member of the set of overlaps to be chosen in a particular case is determined by the slant-range to the scene centre. For SEASAT three slant-range intervals were used. The $N_{OVS_{L_{MODE}}}$ and $N_{OVS_{R_{MODE}}}$ determine the number of ground-range samples to be removed at each edge of the image.

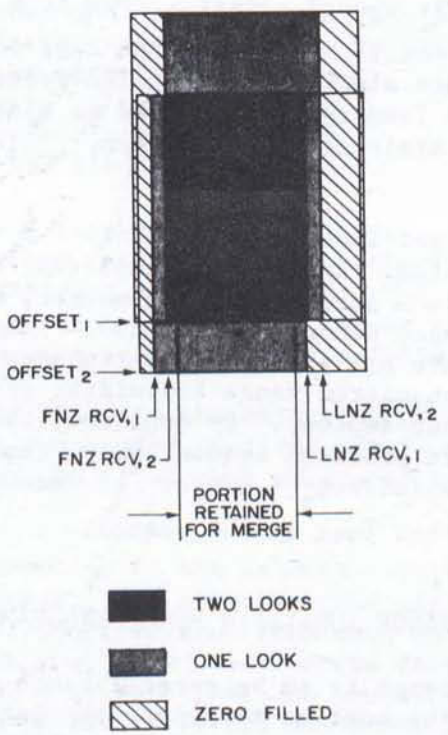

Figure 36. Azimuth-look overlay

These standard overlaps are used in conjunction with the $FNZRCV_q(i)$ and $LNZRCV_q(i)$ to find the intraswath starting and ending positions, RELSTART(i) and RELEND(i). As a first step, for each sub-swath 'i', the $FNZRCV_q(i)$ and $LNZRCV_q(i)$ are scanned to find the minimum $FNZRCV_q(i)$ ($FNZRCV_{MIN}(i)$) and the maximum $LNZRCV_q(i)$ ($LNZRCV_{MAX}(i)$). Then, the values RELSTART(i) and RELEND(i) are calculated from

$$RELSTART(i) = N_{OVS_{L_{MODE}}} + FNZRCV_{MIN}(i) \ , \tag{180}$$

and,

$$RELEND(i) = LNZRCV_{MAX}(i) - N_{OVS_{R_{MODE}}} \ . \tag{181}$$

The intraswath starting and ending positions as given by (180) and (181) must be converted to positions on the normalized grid (see Section 4.4.5) so that the edges of the data segment that can be extracted from each swath can be determined. The normalized grid locations, corresponding to RELSTART(i) and RELEND(i), are

$$LHEDGE(i) = n_o'(i) + RELSTART(i) \ , \tag{182}$$

and,

$$RHEDGE(i) = n_o'(i) + RELEND(i) \ . \tag{183}$$

The edges of the sub-swaths will in general overlap. The width of these overlaps must be computed and then used, together with the RELSTART(i), to find the the sample numbers in each sub-swath at which to start extracting data for the final merged image. The first samples to be extracted from each sub-swath are

$$START(1) = RELSTART(1) \ , \quad i=1 \ , \tag{184}$$

and

$$START(i) = RELSTART(i) + [RHEDGE(i-1) - LHEDGE(i)] + 1, \quad i=2,N_{SSW}. \tag{185}$$

The last sample extracted from each sub-swath is RELEND(i).

The range sub-swaths must also be delayed in azimuth with respect to each other (see Figure 37). The offset relative to the first sub-swath is

$$STARSW(i) = offset_1(i) - offset_{1_{MIN}}, \tag{186}$$

where only the offsets from look 1 are used.

With the parameters, START(i), RELEND(i) and STARSW(i) established, the sub-swaths can be merged. In the merge program, data record segments START(i) to RELEND(i), are read from each of the sub-swath files and combined into a single merged output record. Records are read from sub-swath 'i' beginning at record STARSW(i) in the merged image. If no segments are extracted from a particular sub-swath such as in the cross-hatched areas in Figure 37, a string of zeroes of length (START(i) - RELEND(i) + 1) is appended to the merged record in place of the missing data.

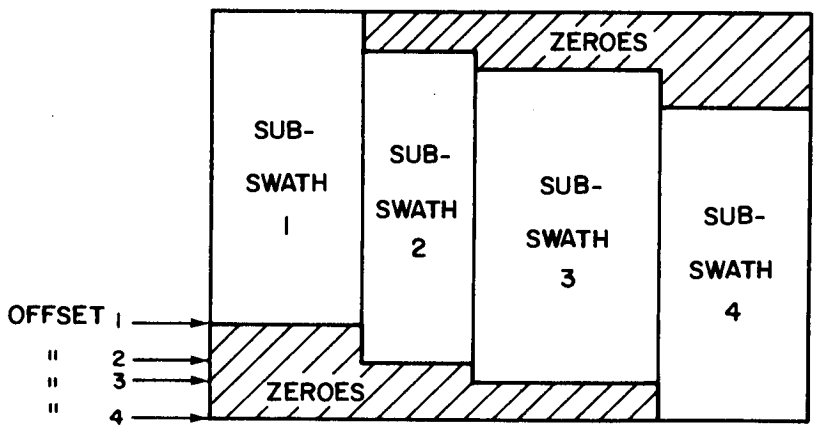

Figure 37. Merging of range sub-swaths

4.8 THE DOPPLER CENTROID ESTIMATION PROGRAMS (J7CE0X, J7CE01, J7CE02X, J71G02, J7CE03)

The description contained in this Section is reorganized from information provided by Gravdal[7].

The Doppler centroid estimation (DCE) programs are used with the SEASAT data to obtain a refined estimate of the complement of the squint angle $\tilde{\alpha}$. The calculated value of $\tilde{\alpha}$, $\tilde{\alpha}_{yp}$, given by (29), is sufficiently accurate for the processing of the SEASAT Survey-Mode data and for checking on the value produced by the DCE programs. An approximate value of $\tilde{\alpha}$ is required because the DCE program is capable of measuring $\tilde{\alpha}$ only within a limited spread of values bracketing the approximate value. The reason for this is that the $\tilde{\alpha}$ measurement of the Doppler frequency centroid f_D, as discussed in Section 4.3.1, can contain an ambiguity equal to a multiple of the PRF. This ambiguity can only be resolved by using an independent estimate of $\tilde{\alpha}_{yp}$.

The Doppler frequency centroid f_D is calculated from the range compressed azimuth spectrum. The term "range compression" is used to denote a one-dimensional convolution with the impulse response of a filter matched to the range coding, in this case linear FM. The impulse response of the matched filter is

$$h(n) = \exp j\left\{-\frac{K}{2}\left(\frac{\tau}{2} - n2T\right)^2 + \omega_o(\tau - n2T)\right\}, \quad n = 1,2,\ldots,N_R \ , \tag{187}$$

where, for SEASAT, the values of ω_o, N_R, k, τ and T are fixed at:

ω_o = 11.382407 x 10^6 x 2π rad/s (the range offset frequency ÷ 2);

NR = 768 (the filter length in complex samples);

K = 3.53586 rad/s^2 (the FM rate);

τ = 33.8 μs (the pulse length);

and T = 21.96372 ns (the sampling period).

4.8.1 Calculation of Impulse Response (J7CE0X)

The impulse response (187) is calculated in J7CE0X. The function h(n) is augmented with zeroes to length L_R, where for SEASAT L_R = 2048. The complex-to-complex FFT of the augmented impulse response is computed and the result is stored in disc file FILT.

4.8.2 Unpacking of Raw Data (J7CE01)

The packed SAR data is read from the tape and converted into floating-point format. Sections of the floating-point data, $2L_R$ range-offset samples long, are stored in a disc file until L_{az} rows are accumulated; for SEASAT $L_{az} = 2048$. The operator must specify: $n_{1_{ST}}$, the position of the first sample (real) of interest in the unpacked records; $2L_R$, the number of samples to be unpacked per record; m_{ST}, the record on the tape at which to start unpacking; and L_{az}, the number of records in the data block.

4.8.3 Range Compression (J7CE02X)

The purpose of the J7CE02X program module is to compress the linear FM coded signal of the SEASAT-A radar. This is done by convolving each range record with a reference-function (187) which is matched to the linear FM pulse. The range compression is done by fast-convolution.

The recorded signal is on the range-offset carrier, $2\omega_o$. This program converts the recorded real, range-offset signal into quadrature components, i.e., the complex envelope of the signal. The complex signal is then convolved with the augmented reference function. The processing consists of the following steps:

1) read a sub-block of data from the disc;

2) perform a real-to-complex FFT on each row of sub-block;

3) read the FFT of the augmented reference function from file FILT;

4) multiply each term in the FFT of the augmented reference function by each term in the frequency spectrum of the received signal;

5) perform a complex IFFT on the record (the combination of real-to-complex FFT and complex IFFT has the effect that the $2L_R$ real input samples are converted to L_R complex samples on output);

6) repeat 1) to 5) for all the sub-blocks in the block.

Since the range compression is a fast-convolution process there will be (N_R-1) invalid data records at the beginning of the output block. These records are skipped during the DCE process.

4.8.4 Transpose (J7IG02)

After the range-compression has been completed the data block is transposed using the technique described in Section 4.3.3.

4.8.5 Estimation of the Complement of the Squint Angle (J7CE03)

The purpose of this module is to estimate the angle $\tilde{\alpha}$ from the azimuth spectrum. In order to reduce the effect of non-uniform reflectivity of the ground, a considerable amount of averaging is performed. Five averaged spectra are extracted from the data block. In order to reduce the effect of strong point targets on the azimuth spectra a thresholding process is implemented. The averaged and smoothed azimuth spectra are cross-correlated with the derivative of the antenna power spectrum. The zero-crossings, from negative to positive, of the cross-correlation products identify the centre frequencies of the spectra. The angles $\tilde{\alpha}$, are then calculated from the centre frequencies.

The following parameters are required by the program and must be entered by the operator:

1. PRF (Hz),
2. λ (m),
3. f_{SR}(Hz),
4. V_{eq} (m/s).
5. h_s (m),
6. $r_{l_{edge}}$ (m),
7. r_e (m),
8. $n_{l_{ST}}$, (as per J7CE01),
9. Is $\alpha_{yp} > 0$ or < 0?
10. In which ambiguity interval does α_{yp} lie?

The first step in finding $\tilde{\alpha}$ is the computation of a set of highly averaged azimuth power spectra, $P_{aw}(i,k)$, where 'i' is the power spectrum component number and 'k' is the spectrum number. For SEASAT, 'k' has a maximum value (k_{max}) of 5, and 'i' has a maximum value (i_{max}) of 64. The spectrum is calculated by averaging adjacent spectral components together to reduce the number of spectral lines from L_{az} to i_{max}; adjacent spectra are added together to form a sub-block average; several records are skipped; and a new sub-block average is formed. This process is repeated for several sub-blocks and the sub-block averages are averaged to form one of the k_{max} smoothed spectra. The entire process is repeated k_{max} times. For each k^{th} spectrum an average slant-range $r_{l_{MID}}$ is calculated. These

$r_{1_{MID}}$ values are used to relate the frequencies measured to the angles $\tilde{\alpha}$

The i^{th} component of the k^{th} spectrum is calculated as follows:

$$P_{aw}(i,k) = \sum_{\ell=1}^{N_{SBLK}} \left\{ \sum_{n=N_A}^{N_B} \left[\frac{i_{max}}{L_{az}} \sum_{m=(i-1)\frac{L_{az}}{i_{max}}+1}^{i\left[\frac{L_{az}}{i_{max}}\right]} P_w(m) \right] \right\} , \tag{188}$$

where

$$P_w(m) = \left\{ Re[V(m)] \right\}^2 + \left\{ Im[V(m)] \right\}^2 , \tag{189}$$

$$N_A = N_{SBLK}(N_{REC/SBLK} + N_{SKP})(k-1)$$

$$+ (N_{SKP} + N_{REC/SBLK})(\ell-1) + 1 , \tag{190}$$

$$N_B = N_{SBLK}(N_{REC/SBLK} + N_{SKP})(k-1)$$

$$+ (N_{SKP} + N_{REC/BLK})(\ell-1) + N_{REC/BLK} , \tag{191}$$

and V(m) is the azimuth FFT vector, $N_{REC/SBLK}$ is the number of spectra to be averaged per sub-block, N_{SKP} is the number of records to be skipped between sub-blocks, and N_{SBLK} is the number of sub-blocks to be averaged for the k^{th} spectrum. $N_{REC/SBLK}$, and N_{SKP} refer to complex range cells.

The next step is to threshold the averaged spectra $P_{aw}(i,k)$ to remove the large discrete lines. The threshold spectrum is given by:

$$\overline{P_{aw}}(i,k) = \frac{bias}{16}\left[\frac{1}{4}P_{aw}(i-3,k) + \frac{1}{2}P_{aw}(i-2,k) + \frac{3}{4}P_{aw}(i-1,k) + P_{aw}(i,k) + \frac{3}{4}P_{aw}(i+1,k) + \frac{1}{2}P_{aw}(i+2,k) + \frac{1}{4}P_{aw}(i+3,k)\right] , \quad (192)$$

where bias is a parameter input by the operator. For the values $P_{aw}(i-3,k)$, $P_{aw}(i-2,k)$, $P_{aw}(i-1,k)$ (with i=1,2, and 3), and $P_{aw}(i+1,k)$, $P_{aw}(i+2,k)$ and $P_{aw}(i+3,k)$ (with $i=i_{max}-2$, $i=i_{max}-1$, and $i=i_{max}$), the spectral lines at the opposite end of the spectrum are used, i.e., the spectrum is wrapped around by three points at each end. The thresholding procedure works in the following way. If $\overline{P}_{aw}(i,k) \geq P_{aw}(i,k)$,

then

$$P_{aw_F}(i,k) = P_{aw}(i,k) \quad ; \quad (193)$$

and if $\overline{P}_{aw}(i,k) < P_{aw}(i,k)$,

then

$$P_{aw_F}(i,k) = P_{aw}(i,k)/bias \ , \quad (194)$$

where the $P_{aw_F}(i,k)$ are the spectra which are used to find the k_{max} centroid estimates.

The slant-range to the middle of the range swath, over which the averaged spectrum was computed, is calculated next:

$$r_{1_{MID}}(k) = r_{1_{edge}} + \frac{n_{1_{ST}} c}{2f_{SR}} + \left\{\frac{1}{2}\left[N_{SBLK}(N_{REC/SBLK} + N_{SKP}) - N_{SKP} - 1\right] + (k-1)(N_{REC/SBLK} + N_{SKP})N_{SBLK}\right\}\frac{c}{f_{SR}} \ , \quad (195)$$

The $r_{1_{MID}}(k)$ and $P_{aw_F}(i,k)$ form the set of values used to compute the k_{max} spectrum centroids.

The derivative of the two-way antenna pattern is correlated with the spectra $P_{aw}(i,k)$ to find the zero-crossing point. The zero-crossing point indicates the estimated centroid. For SEASAT-A, the one-way azimuth antenna pattern is of the form

$$P_A = \left(\frac{\sin f_m}{f_m}\right) , \tag{196}$$

where f_m is the azimuth frequency and $f_{m_o}=0$ is at the centre of the aperture. The formula for the derivative of the two-way antenna power spectrum, as a function of azimuth frequency, is:

$$P_A(f_m,k) = \sum_{Q=-R}^{R} \frac{-4K_o D}{1-D^2(f_m+Q\ PRF)^2} \left(\frac{\sin U}{U}\right)^4 \left(\cot U - \frac{1}{U}\right) , \tag{197}$$

where,

$$U = AK_o \cos^{-1}\left[D(f_m+Q.PRF)-\cos^{-1}(D.f_{m_o})\right] , \tag{198}$$

$$A = \frac{r_e \sin\theta}{r_{1_{MID}}(k)} , \tag{199}$$

$$k_o = 142.37 \text{ (an antenna constant)}, \tag{200}$$

$$D = \frac{-\lambda\, r_{1_{MID}}(k)}{2V_{eq}\, c_a\, r_e \sin\theta} , \tag{201}$$

$$\theta(k) = \cos^{-1}\left\{\frac{r_e^2 + (r_e+h_s)^2 - r_{1_{MID}}^2(k)}{2r_e[r_{1_{MID}}(k)+h_s]}\right\} \tag{202}$$

$$c_a = 1 + \frac{h_s}{r_e} . \tag{203}$$

Q is the order of spectrum from which the foldover is calculated and $\pm R$ is the number of aliased spectra included in the calculation of the derivative. In this case 2R=3, and $f_{m_o}=0$.

The formula in (197) gives a continuous spectrum. In order to calculate spectral lines, the continuous frequency f_D is replaced by

$$f_m(m) = m\Delta f_m \quad , \tag{204}$$

where m is the line number and Δf_m is the azimuth frequency line spacing. The value of Δf_m is

$$\Delta f_m = \frac{PRF}{L_{az}} \quad . \tag{205}$$

If the portion of (197) to the right side of the Σ sign is represented by $B[(f_m+QPRF),k]$, then $P_A(i,k)$ averaged over L_{az}/i_{max} spectral lines becomes

$$P_A(i,k) = \sum_{m=1}^{L_{az}/i_{max}} \sum_{Q=-R}^{+R} B\left\{\left[\frac{L_{az}}{i_{max}}(i-m) + m\right]\Delta f_m + Q\cdot PRF, k\right\} . \tag{206}$$

The derivative of the two-way antenna pattern, given by (206), is cross-correlated with each of the smoothed spectra $P_{aw_F}(i,k)$ to obtain a zero-crossing estimate, and thus an estimate of the Doppler frequency centroid. The cross-correlation between an azimuth spectrum and the corresponding reference function is performed in the time-domain. Two periods of $P_{aw_F}(i,k)$ are stored in an array to facilitate the cross-correlation. The cross-correlation output is

$$C(j) = \frac{1}{i_{max}} \sum_{i=1}^{i_{max}} P_{aw_F}(i+j-1,k)P_A(i,k).$$

$$j=1,2,\ldots,i_{max} \tag{207}$$

The position of the centroid is found by searching for the zero crossing in C(j). A new vector $C_w(j)$ is formed, where

$$C_w(j) = C(j), \quad j=1,2,\ldots,i_{max}$$

$$C_w(i_{max}+1) = C(1) \ . \tag{208}$$

The vector $C_w(j)$ is scanned from the first entry to the last, but only every N_{SKP_2} th entry is checked, i.e., $C_w(1)$, $C_w(1+N_{SKP_2})$, etc.. When a negative value is detected the above process continues in increments of N_{SKP_2} until a positive value is found. The scanning is then stopped and a linear regression analysis is performed, between the two end-points, to find the zero-crossing. It is assumed that the two end-points are separated by N_{SKP_2} points. The first step in the linear regression analysis is the calculation of the mean frequency line number,

$$m_{MID} = i + \frac{N_{SKP_2}}{2} \ , \tag{209}$$

and the mean amplitude,

$$C_{w_{MID}} = \frac{1}{(N_{SKP_2}+1)} \sum_{n=0}^{N_{SKP_2}} C_w(i+n) \ . \tag{210}$$

The slope of the straight line through the points between $C_w(i)$ and $C_w(i+N_{SKP_2})$ is

$$\frac{\Delta C_w}{\Delta m} = \sum_{\ell=1}^{i+N_{SKP_2}} \frac{(\ell-m_{MID})[C_w(\ell)-C_{w_{MID}}]}{(\ell-m_{MID})^2 \frac{L_{az}}{i_{max}} \Delta f_m} \ . \tag{211}$$

If the slope is negative the zero-crossing is 'false' and the program seeks for a new zero-crossing from negative to positive.

The centre frequency f_D, which identifies the zero-crossing, is calculated from

$$f_D = m_{MID} \cdot \frac{L_{az}}{i_{max}} \cdot \Delta f_m - \left(\frac{L_{az}}{i_{max}} + \frac{1}{2}\right) \cdot \Delta f_m - \frac{C_{w_{MID}}}{\left(\frac{\Delta C_w}{\Delta m}\right)} \quad . \tag{212}$$

If no zero-crossing is found, the process must be repeated with a new set of data.

The complement of the squint angle $\tilde{\alpha}$, is calculated from f_D. The k_{max} estimates of f_D must be checked to see if they all lie in the same ambiguity interval. If the estimates do not monotonically increase or decrease with 'k' it indicates that some of the estimates are wrapped around the spectrum. The program checks for a difference of PRF/2 between successive f_D estimates. Depending on the sign of the difference, the PRF is added to, or subtracted from, f_D. Note that this adjustment process does not determine the number of ambiguity intervals that f_D lies from its true position, it only places all of the estimates within the same interval. The operator must supply, using his knowledge of α_{yp}, the estimated ambiguity interval, and whether $\alpha_{yp} \geq 0$ or $\alpha_{yp} < 0$. Then, the individual values of $\tilde{\alpha}(k)$ are calculated using the formula

$$\tilde{\alpha}(k) = \frac{180}{\pi} \cos^{-1}\left\{\frac{-f'_D r_{1_{MID}}(k) \cdot \lambda}{4\pi V_{eq}(r_e+h_s)\sin[\theta(k)]}\right\} \quad . \tag{213}$$

where f'_D is f_D adjusted for the correct ambiguity interval, and $r_{1_{MID}}(k)$ and $\theta(k)$ are given by (195) and (202) respectively. As a final step, the mean and the standard error of the $\tilde{\alpha}(k)$ are calculated:

$$\bar{\alpha} = \frac{1}{k_{MAX}} \sum_{k=1}^{k_{MAX}} \tilde{\alpha}(k) \quad , \tag{214}$$

and,

$$\sigma_\alpha = \frac{\{[\alpha(k)-\alpha]^2\}^{\frac{1}{2}}}{k_{MAX}-1} \quad . \tag{215}$$

The $\tilde{\alpha}(k)$, $r_{1_{MID}}(k)$, $\bar{\alpha}$ and σ_α values are output to the operator's console and stored as part of the operator's log for this production run. The mean value $\bar{\alpha}$ is input as $\tilde{\alpha}$ to the J70R00 program.

5. PROCESSING HARDWARE

The processor described in Section 4 has been implemented using the equipment shown in Figure 38. The main computational units are: a 32-bit word-length host computer, (an Interdata 8/32) equipped with 1 MByte of directly addressable core memory; and an array processor (Floating Point System AP-120) with 64K (38 bit) words of memory. The array processor is interfaced to the 8/32 computer by means of a high speed direct-memory-access (DMA) Input/Output (I/O) bus. Two 80 MByte disc drives, used for file storage during processing, and two 75 inch per second, 1600 BPI, 9-track tape drives used for input and output, are interfaced to the host computer through a second, independent, high speed DMA I/O bus. The system also includes a 512x512x8 bit Raster Graphics Processor (RGP) Imaging System. The RGP system provides the capability for displaying portions (512x512 pixels) of the processed SAR images on a high resolution colour television monitor.

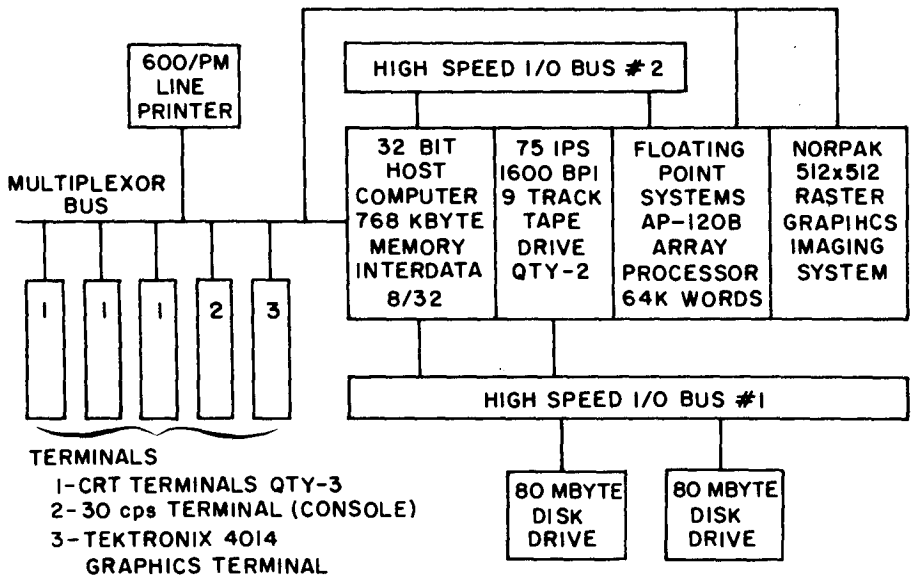

Figure 38. The hardware used for the two-dimensional SAR processor

The use of two high speed I/O channels allows simultaneous transfers of data from the host (8/32) to and from the array processor, and from the host to and from the disc. Each transfer occurs on its own channel.

6. BLOCK AND SCENE TIMINGS

The processor can be configured in various ways to process data from different SARs. Thus far data has been processed from the Environmental Research Institute of Michigan X and L-band radars, and from the SEASAT-A L-band

radar. Four data products have been produced from the SEASAT data:

- 100m x 100m resolution, single-look images, 100 km x 100 km;
- 25m x 25m resolution, four-look images of various widths and lengths;
- 12.2m azimuth x 25m range resolution, two-look images;
- 7.4m azimuth x 25m range resolution, single-look images.

Table 1 gives typical block and scene timings. The block is the basic processing unit. In order to form larger pictures many blocks must be processed and concatenated to form a swath. The widths of some representative swaths are shown in the Table. These swaths can be merged to form wider images.

TABLE 1

SAR Processor Timing Tables

Block Timing Table

Block Size Input			Block Size Output				Processor Time
Range	Azimuth	Type	Range	Azimuth	No. Looks	Res. (m)	(min)
2048	2048	ANY	--------	--------	--	-------	50*
1024	1024	ANY	--------	--------	--	-------	10
2048	2048	SEASAT	1080	240	4	25	31.5*
1024	4096	SEASAT	256	768	1	7.4	29
1024	4096	SEASAT	256	1024	2	12.2	30

Scene Timing Table

Scene Size						Maximum
Range (km)	Azimuth	Type	No. Looks	Res. (m)	Processor Time (hours)	Elapsed Time (hours)
21	47.5	SEASAT	4	25	8.9	10.5
21	47.5	SEASAT	4	25	6.3	7.5**
100	100	SEASAT	1	100	-----	5.0
21	47.5	SEASAT	4	25	5.6	7.0***
4.2	14.8	SEASAT	1	7.4	3.7	4.5
4.2	49.7	SEASAT	2	12.2	3.7	4.5

NOTES: — *All times are for the minimum configuration (Figure 38) unless otherwise indicated.*

* *This is an example of the savings in time possible by configuring the processor for a particular data type.*

** *This entry is for the next scene at the same range delay as the previous scene.*

*** *Estimated time for the minimum configuration plus a 300 MB disc drive.*

The efficiency of the processing greatly depends on the number of valid output points obtained from the input data block. The valid output block size is obtained by subtracting a number of samples equal to the respective matched filter length from each dimension of the input block[4]. The matched filter length increases inversely as the square of the resolution cell size; thus the matched filter for 7.4m azimuth resolution is 11.4 times longer in azimuth than the matched filter for 25m azimuth resolution. The net effect of this increased length is, that for equal quantities of the data, e.g., a block size of 2048 x 2048 data versus one of 1024 x 4096 data, the block processing efficiency drops dramatically. For the 25m x 25m, 4-look case, with an input data block size of 2048 x 2048, four azimuth looks of length 240, i.e., 960 points, are produced from the 2048 azimuth lines input. In contrast, for the 7.4m azimuth x 25m range, single-look case, with an input block size of 1024 range x 4096 azimuth data, only 768 points are produced from the 4096 azimuth lines input. The processing efficiency can be greatly improved by increasing the block length in azimuth. The hardware configuration in Figure 38 does not contain enough disc storage to allow larger blocks to be processed. However, if a 300 MByte disc were added to the system, the scene timings for the 25m x 25m resolution, 4-look case could be reduced by approximately 37%. Likewise, for the 7.4m azimuth x 25m range resolution, single-look case the scene timings could be reduced by approximately 66%.

7. EXAMPLES OF IMAGERY

Figures 39-43 show examples of SEASAT-A SAR imagery produced by the CRC processor. Two of the images are 25m x 25m resolution, 4-look, and the other three images are 7m azimuth x 25m range resolution, 1-look. The orientation of the images depends on whether the satellite orbit was ascending or descending.

The images were created on an Optronics P1500 film recorder from 8-bit data originally produced as 32-bit floating point numbers. The maximum and minimum of the scene were found, then the data were linearly rescaled to 16 bit integers, over the range -32768 to +32767. A portion of the linear scale was then selected. Typically -32767 to -24000 was used, and the data were rescaled again so that all values above -24000 were set to the maximum (white), and all values between -32767 to -24000 were linearly spread over 8 bits (0-255).

8. NOTES ON PROCESSOR IMPLEMENTATION

8.1 REMARKS ON PROCESSOR AS PRESENTLY IMPLEMENTED

As of August 1980, certain discrepancies exist between some of the equations documented here and those actually used in the processor. In particular, the present processor does not have the extensions for range multi-look processing, and for azimuth-offset data. It is planned that these features will be added in the future. In addition certain minor differences exist:

1. for ERIM data the Δd_o value is not transferred directly from the .DAT file to the .FPM file, see (9);

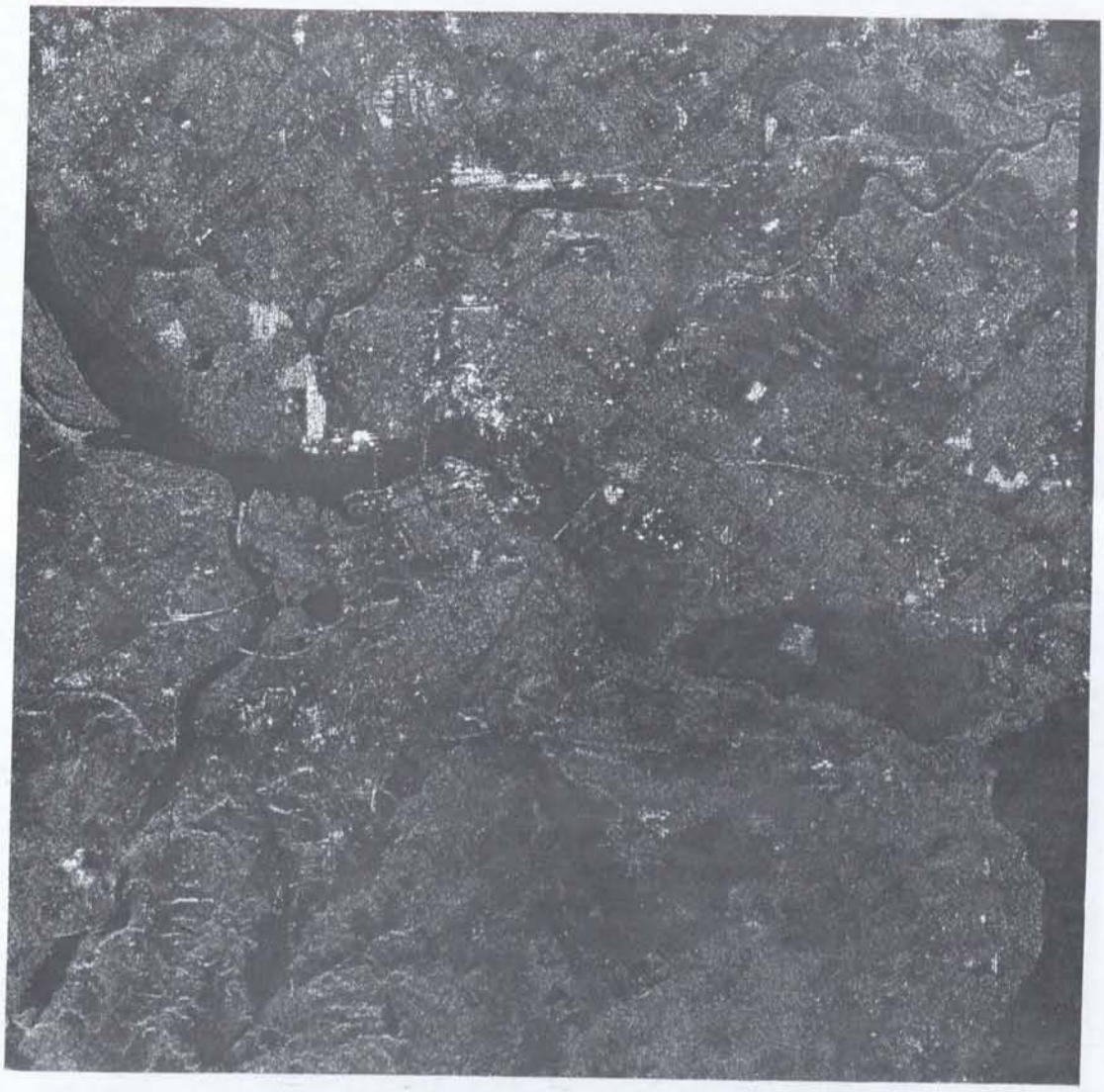

Figure 39. SEASAT SAR image Ottawa, 7m azimuth x 25m range resolution

Figure 40. SEASAT SAR image Ottawa, 25m azimuth x 25m range resolution

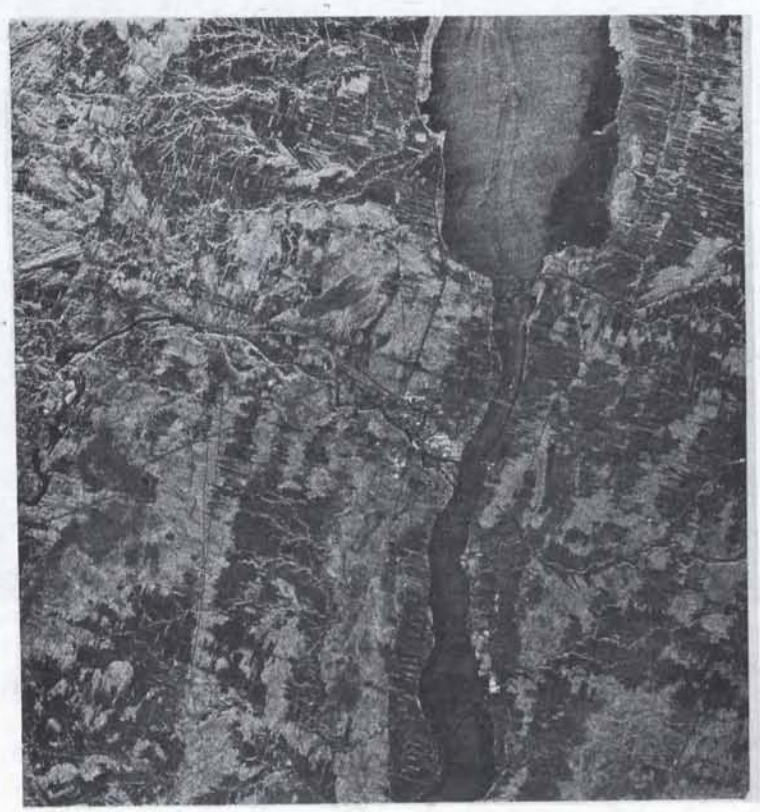

Figure 41. SEASAT SAR image Trois Rivieres, 25m x 25m range resolution

Figure 42. SEASAT SAR image Cambridge Bay,
7m azimuth x 25m range resolution

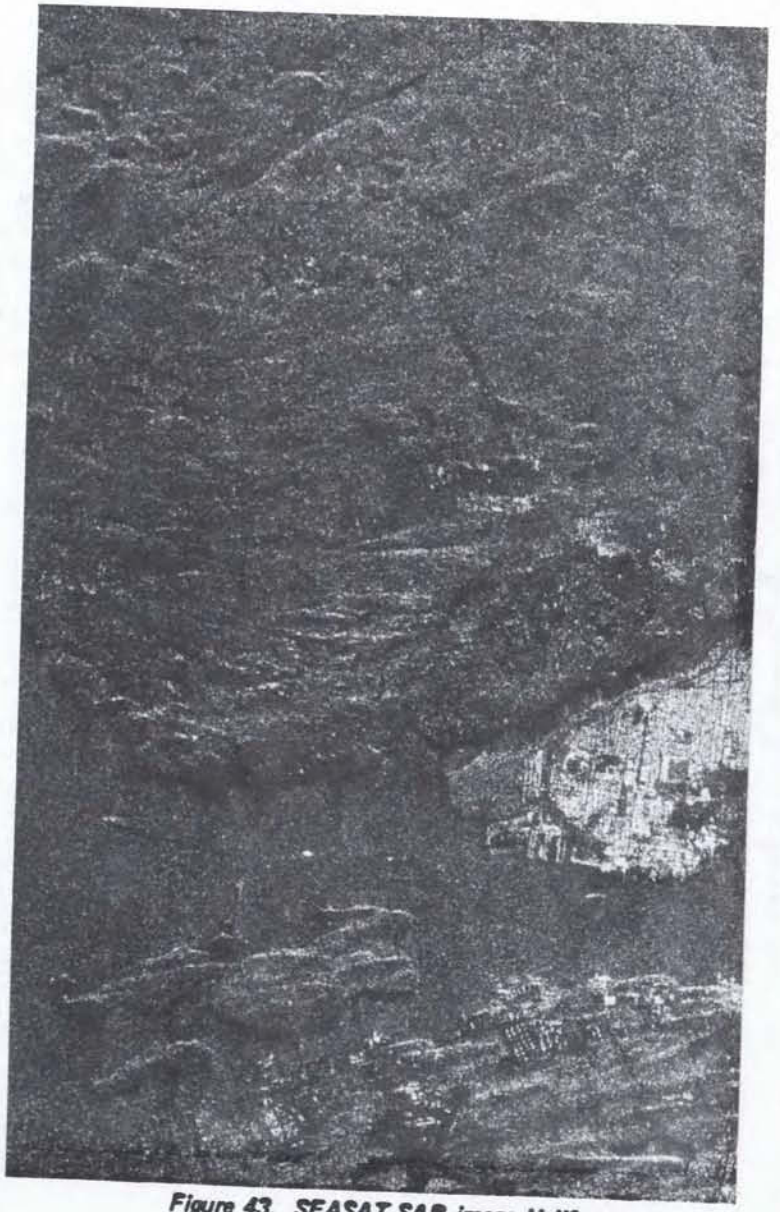

Figure 43. SEASAT SAR image Halifax,
7m azimuth x 25m range resolution

2. the equation for azimuth filter length (137) is different; the present formula is based on a sidelooking antenna which was judged adequate for the SEASAT and SAR-580 radars;

3. the azimuth-look spacing equations 113-123 are different; the present equations are based on evenly spaced looks in angle $\tilde{\alpha}$, not in Doppler frequency f_D;

4. equation 110 that corrects f_D for azimuth resampled data (Survey-Mode SEASAT) is not implemented; instead, the angle $\tilde{\alpha}$, inserted in the .FPM file by J70R00, is changed by J70R00 to 90° to compensate for the f_D shift that occurs during azimuth resampling (J7RE00). Unfortunately the present system does not apply the azimuth corrections to SEASAT Survey-Mode. Since the SEASAT Survey-Mode is used to locate scenes, eqn. 52, must also be changed to compensate for the lack of azimuth corrections.

The previous equation for the azimuth filter length is as follows:

$$N_{1_q} = 2 \begin{matrix}\text{INTEGER} \\ \text{PART}\end{matrix} \left(\frac{\lambda \tilde{r}_{1_q}}{4\rho_{az_{2q}} \Delta x_q} \right). \tag{216}$$

In the present software the look-angles are determined by calculating $\Delta\alpha$, the beamwidth, for a sidelooking SAR of a given resolution, and then spacing the looks equally across $\Delta\alpha$. The slant ranges $\tilde{r}_{1_q}$ are then calculated from the $\tilde{\alpha}_q$. The beamwidth $\Delta\alpha$ is

$$\Delta\alpha = \cos^{-1}\left\{1 - \left[\frac{1 - \cos\left(\frac{\lambda N_{LKS_A}}{2\rho az_{1_q}}\right)}{\sin^2\gamma}\right]\right\}, \tag{217}$$

where

$$\gamma = \cos^{-1}\left(\frac{h_s}{\tilde{r}_1}\right). \tag{218}$$

The look-angle, for the 'q^{th}', look is

$$\tilde{\alpha}_q = \tilde{\alpha} + \frac{\Delta\alpha}{2}\left(\frac{2q-1}{N_{LKS_A}} - 1\right), \tag{219}$$

and the slant-range $\tilde{r}_{1_q}$, to the centre of the sub-swath, for the 'q^{th}' look is

$$\tilde{r}_{1_q} = r_e\left[c_a^2+c_b^2-2c_a c_b\left(1 - \frac{\sin^2\tilde{\theta}_r}{\sin^2\tilde{\alpha}_q}\right)^{\frac{1}{2}}\right]^{\frac{1}{2}} . \qquad (220)$$

These angles and ranges are adjusted so that the $LNOM_{A_q}$ are integers. The $LNOM_{A_q}$ values are calculated using eqns. 113 and 114. The new values of f_{D_q} are then calculated using eqns. 116 and 117. The revised look-angles are

$$\alpha'_q = \alpha_q + \delta\alpha_q , \qquad (221)$$

where

$$\delta\alpha_q = \frac{1}{\left(\frac{\partial f_{D_q}}{\partial\alpha_q}\right)} (f'_{D_q} - f_{D_q}) , \qquad (222)$$

$$\frac{\partial f_{D_q}}{\partial\alpha_q} = C_o\left[\frac{-\sin\tilde{\alpha}_q}{\tilde{r}_{1_q}} + \frac{c_a c_b^2 r_e^2 \sin^2\tilde{\theta}_r \cos^2\tilde{\alpha}_q}{\tilde{r}_{1_q}^3 \sin^3\tilde{\alpha}_q} \cdot \frac{1}{\left(1 - \frac{\sin^2\tilde{\theta}_r}{\sin^2\tilde{\alpha}_q}\right)^{\frac{1}{2}}}\right] , \qquad (223)$$

and

$$C_o = \left(\frac{-2V_{eq} r_e c_a \sin\tilde{\theta}_r}{\lambda}\right) . \qquad (224)$$

The new ranges are

$$r'_{1_q} = r_e\left[c_a^2+c_b^2-2c_a c_b\left(1 - \frac{\sin^2\tilde{\theta}_r}{\sin^2\tilde{\alpha}_q}\right)^{\frac{1}{2}}\right]^{\frac{1}{2}} . \qquad (225)$$

The only major discrepancy in the SEASAT location program is in eqn. 52; the equation for Δm is presently implemented as

$$\Delta m = -\frac{r_e}{\Delta x_o}\left\{\sin^{-1}\frac{\tan\left\{\cos^{-1}\left[\frac{\left(\frac{r_{1x}}{r_e}\right)^2 - c_a^2 - c_b^2}{-2c_a c_b}\right]\right\}}{\tan\tilde{\alpha}}\right\}$$

$$-\sin^{-1}\left\{\frac{\tan\left\{\left(\frac{\tilde{r}_{1_{SUR}}}{r_e}\right)^2 - c_a^2 - c_b^2}{-2c_a c_b}\right\}}{\tan\alpha_{yp}}\right\} \qquad (226)$$

This compensates for the Δaz_{2q}-type corrections but does nothing to compensate for the error introduced by the lack of Δaz_{1q} corrections.

8.2 MODIFICATIONS REQUIRED FOR ADDITION OF RANGE MULTILOOKING

In order to add the range multilook feature to the processor the following equations must be added or changed:

- equations 30 and 31, for $\Delta t'_p$ and τ_p, in J70R00; and

- equations 124 - 127 in J7SE30.

In addition, an entry for N_{LKS_R} must be added to the .DAT files, and the J7SE30.CTX file, and entries for $LNOM_{R_P}$ must be added to the .LNO files. Software changes must also be made to accomplish the actual look extraction. Two approaches are possible:

1) J7SE00 can be changed to extract N_{LKS_R} files from the range spectrum as per Section 4.3.2.5. The $LNOM_{RP}$ entries must be read from the .LNO file to control the look extraction. In addition, the N_{LKS_R} entry must be added to the J7SE00.CTX file. After the range looks are extracted, they are each processed as per the single range-look case;

or

2) the program J7SE00 can be run N_{LKS_R} times and the J7SE00.CTX entry, which controls the range-offset demodulation, can be changed each run so that a different range-look is extracted each time. The .LN0 file would have be input to the J7DC00 (Data Control Program) and it would be used to update the frequency about which to demodulate for each range-look. This technique has the advantage that no major software changes are required to the processor; it is however, not as efficient in execution as method 1).

8.3 MODIFICATIONS REQUIRED FOR ADDITION OF PROCESSING CAPABILITY FOR AZIMUTH-OFFSET DATA

In order to add the capability for processing azimuth-offset data, the following equations must be added or changed:

- equations 4 and 34 for Δx_q,
- equation 37 for f_α,
- equation 99 for $\overline{G}_{A0_{S_P}}(f_{m_{A0}}, f_n)$,
- equation 100 for $\Psi_{A0_P}(f_{m_{A0}}, f_n)$,
- equation 110 for f_D,
- equation 115 for N_q,
- equations 118-125 for $\tilde{r}_{1q}$, and $\tilde{\alpha}_q$ (these equations must be changed anyway, see Section 8.1).

In addition, new entries must be added to J7SE30.CTX and J7SE01.CTX to allow the choice of the azimuth-offset mode. A new entry must also be added to the .FPM and .DAT files so that the f_{0A} frequency can be passed to both J7SE30 and J70R0Ø.

The addition of a processing capability for azimuth-offset data implies the necessity to make most of the modifications required for the addition of a processing capability for a new radar. As will be explained in Section 8.4, this necessitates a new J70R0Ø program to handle the radar-specific details of the converstion.

If an input data azimuth-resampling program, such as J7RE00, is required for azimuth-offset data, the existing J7RE00 will have to be extended to provide this capability.

8.4 MODIFICATIONS REQUIRED TO ADD PROCESSING CAPABILITY FOR A NEW SAR

If it is required to process data from other SARs, changes must be made to the production system.

If the new SAR uses Linear FM (LFM) range coding, the only software change required in the processor itself is a new unpacking sub-routine in J7SE00. If LFM coding is not used, but the coding is invariant from pulse-to-pulse, then the filter generation program J7SE30 must be rewritten. If the range coding is not constant from pulse-to-pulse this processor cannot be used.

If the new SAR parameters indicate that different processing block sizes or different numbers of looks, than in one of the present production modes, are required, then new .CTX files must be set up for J7SE00, J7SE01, J7SE02, J71G02, J7SE80 and J7SE30. In addition, the production procedures, controlled by the sub-task monitor J7SEA0 and generated the Data Control Program J7DC00, must be changed.

For new data types the program J70R00, or J70R01, whichever is appropriate, must be modified. It will depend on the SAR just what changes will be required, e.g., is a Survey-Mode capability required and is a Doppler centroid estimator required?

If an ERIM-type, sub-swath location capability is required for a squinted, airborne or satellite-borne system, the ERIM sub-swath location program in J7DC00 will have to be rewritten.

8.5 COMMENT ON ASPECT-RATIO OF PRESENT DATA PRODUCTS

The present production system produces data products with a 1:1, azimuth: range, aspect ratio. If new data products such as ERIM, azimuth-multilook, are introduced, the aspect ratio will be N_{LKS_A}:1 where N_{LKS_A} is the number of azimuth-looks. To maintain a 1:1 aspect ratio a new program must be introduced after J7SE90 to increase the azimuth sampling rate. Without this addition the number of range- and azimuth-looks would have to be balanced so as to maintain a 1:1 aspect ratio.

9. SUMMARY

A novel software-based SAR processor is described. The processor is capable of routinely producing the following data products from data acquired by the SEASAT-A satellite-borne SAR:

- 7m azimuth x 25m range resolution, single-look imagery,
- 25m azimuth x 25m range resolution, four azimuth-look imagery,
- 12.2m azimuth x 25m range resolution, two azimuth-look imagery; and
- 100m azimuth x 100m range resolution, single-look imagery;

In addition, it can produce the following data products from the ERIM(SAR 580) airborne SAR:

- X-band, 2.1m azimuth x 1.5m range resolution, single-look imagery; and

- L-band, 2.1m azimuth x 2.3m range resolution, single-look imagery.

The SAR processor is adaptable in that it can be configured to process imagery from any SAR system that maintains the range coding constant from pulse-to-pulse.

A description of the equations that were used to implement the software-based CRC SAR processor is given, as are details the processor configuration. The two main processor subsystems: the SAR processing subsystem, and the support subsystem are described. The SAR processing subsystem, which is very general in nature, is reconfigured by changes to context, or parameter, files. The support subsystem is less general, in that it must provide the software interface between the different SAR data types and formats and the SAR processor. Certain parts of the support subsystem must be replaced for each new data type.

A block diagram and description of the processor are given. The individual elements are described separately and it is shown how the individual programs communicate with each other through a data file structure.

The hardware upon which the processor was programmed is briefly described and timings for the various production products, generated using this hardware, are given. Examples of the image data products are also included in the description.

Finally, specific comments are made with respect to including a processing capability for range-multilook images, and azimuth-offset data. Specific discrepancies between this description and the present implementation are listed and it is described how these discrepancies will be resolved.

10. ACKNOWLEDGEMENTS

The software comprising the CRC SAR processor was developed by W.E. Thorp and Y. Bellemare. The Doppler centroid estimator was designed and programmed by B. Gravdal. The author would like to acknowledge with appreciation the contributions of the above individuals. He would also like to thank Mr. G.E. Haslam who had many helpful discussions with the author during the development of the processor.

This work is supported by the Department of National Defence, Research and Development Branch.

11. REFERENCES

1. Vant, M.R. and G.E. Haslam, *A Theory of 'Squinted' Synthetic-Aperture Radar*, CRC Report 1339, Ottawa, November 1980.

2. Vant, M.R., G.E. Haslam and G.M. Royer, *A Digital Signal Processing Approach for Satellite Synthetic-Aperture Radar(SAR)*, Proceedings International Conference on Radar, Paris, pp. 252-256, December 1978.

3. Vant, M.R., G.E. Haslam and W.E. Thorp, *The CRC Digital Processor*, Proceedings of the Second SEASAT Synthetic-Aperture Radar Processing Workshop, ESRIN, Frascati, Italy, 10-12 December 1979.

4. Mersereau, R.M. and D.E. Dudgeon, *Two-Dimensional Digital Filtering*, Proc. IEEE, Vol. 63, pp. 610-623, April 1975.

5. Turin, G.L., *An Introduction to Matched Filters*, IRE Trans. Inf. Theory, Vol. IT-6, pp. 311-329, June 1960.

6. Helms, H.D., *Fast Fourier Transform Method of Computing Difference Equations and Simultaneous Filters*, IEEE Trans. Audio Electroacoust., Vol. AU-15, pp. 85-90, June 1967.

7. Gravdal, B., Private Communications, Communications Research Centre, Ottawa, Ontario, Canada.

8. MacDonald, Dettwiler and Assoc. Ltd., *Specification of SEASAT HDDT to CCT Tape Translation System*, prepared for Dept. of Supply and Services, April 1978, Revision 1, 26 May 1978, unpublished.

9. Weast, R.C. (ed), *CRC Handbook of Chemistry and Physics*, 49th Edition, The Chemical Rubber Co., Cleveland, Ohio, 1968-1969.

10. Thorp, W.E., *J7DC00, Data Control Program for General SAR Processor Production System, Program Documentation*, Private Communications, Communications Research Centre, Ottawa, Ontario, Canada, 1980.

11. Thorp, W.E., *General SAR Processor Production System, Naming Conventions for Imagery, and Files, Production System File Listings*, Private Communications, Communications Research Centre, Ottawa, Ontario, Canada, 1980.

12. Franks, L.E., *Signal Theory*, Englewood Cliffs: Prentice-Hall, 1969, pp. 79-83.

13. Twogood, R.E. and M.P. Ekstrom, *An Extension of Eklundh's Matrix Transposition Algorithm and its Application in Digital Image Processing*, IEEE Trans. Comput., Vol. C-25, pp. 950-952, September 1976.

14. Eklundh, J.O., *A Fast Computer Method for Matrix Transposing*, IEEE Trans. Comput., Vol. C-21, pp. 801-803, July 1972.

15. Thorp, W.E., *J7IG01, J7IG02 Matrix Transpose, Program Documentation*, Private Communications, Communications Research Centre, Ottawa, Ontario, Canada.

16. Thorp, W.E., *General SAR Processor User's Manual for J7SE00, J7SE01, J7SE02, J7SE30, J7SE80*, Vols. I, II, III, Private Communications, Communications Research Centre, Ottawa, Ontario, Canada.

17. Skolnik, M.I. (ed), *Radar Handbook*, New York:McGraw-Hill, 1970, p. 16-3.

18. Oppenheim, A.V. and R.W. Schafer, *Digital Signal Processing*, Englewood Cliffs: Prentice-Hall, 1975, pp. 110-115.

19. Rabiner, L.R. and B. Gold, *Theory and Application of Digital Signal Processing*, Englewood Cliffs:Prentice-Hall, 1975, pp. 113-115.